Cellulose Based Lithium Ion Polymer Electrolytes for Lithium Batteries

Dissertation

zur Erlangung des Grades

“Doktor der Naturwissenschaften”

am Fachbereich Chemie und Pharmazie

der Johannes-Gutenberg-Universität in Mainz

Marcin Chelmecki

Born in Jaworzno, Poland

Mainz 2004

Madzi

i naszym Rodzicom

Contents

Abbreviations:

AC	-	alternating current
CV	-	cyclovoltammetry
DC	-	direct current
DMA	-	dynamic mechanical analysis
DMF	-	N,N-dimethylformamide
DRS	-	dielectric relaxation spectroscopy
DS	-	degree of substitution
DSC	-	differential thermal analysis
EIS	-	electrical impedance spectroscopy
emf	-	electromotive force
ERS	-	electrical relaxation spectroscopy
GPC	-	gel permeation chromatography
HPC	-	hydroxypropylcellulose
IR	-	infrared spectroscopy
IS	-	impedance spectroscopy
LS	-	laser light scattering
MS	-	degree of molar substitution
NMR	-	nuclear magnetic resonance
PEO	-	poly(ethylene oxide
PEO-HPC	-	(w-ethoxy-tris(oxyethylen))-2-oxypropylcellulose
PS	-	polystyrene
SHE	-	standard hydrogen electrode
SPE	-	solid polymer electrolyte
TGA	-	thermogravimetric analysis
TGA-MS	-	coupled thermogravimetry – mass spectrometry
THF	-	tetrahydrofuran
TTS	-	time-temperature superposition
UV	-	ultraviolet
VTF	-	Vogel-Tamman-Fulcher equation
WLF	-	Williams-Landel-Ferry equation

1. Introduction

One of the most remarkable discoveries in the last 400 years has been electricity. But the practical use of electricity has only been at our disposal since the mid-to late 1800s, and in a limited way at the beginning. Nowadays humanity became dependent on electricity, a product without which our technological advancements would not have been possible. With the increased need for mobility, people moved to portable power sources - for automobile applications (e.g. car batteries), computing (e.g. notebook), entertainment (e.g. walkman), telecommunication (mobile phones) and others. Applications include stationary storage, vehicle traction and remote power sources, as well as industrial and domestic cordless devices such as electric shaver or toothbrush [1-6].

First primitive batteries were used in Iraq and Egypt as early as 200 BC for electroplating and precious metal gilding. In 1748, Benjamin Franklin coined the term battery to describe an array of charged glass plates. However, most historians date the invention of batteries to about 1800 when experiments by Alessandro Volta resulted in the generation of electrical current from chemical reactions between dissimilar metals. Experiments with different combinations of metals and electrolytes continued over the next 60 years. In the 1860s, Georges Leclanche of France developed a carbon-zinc wet cell; nonrechargeable, it was rugged, manufactured easily, and had a reasonable shelf life. Also in the 1860s, Raymond Gaston Plant invented the lead-acid battery. It had a short shelf life, and about 1881 Émile Alphonse Faure developed batteries using a mixture of lead oxides for the positive plate electrolyte with faster reactions and higher efficiency. In 1900, Thomas Alva Edison developed the nickel storage battery, and in 1905 the nickel-iron battery. During World War II the mercury cell was produced. The small alkaline battery was introduced in 1949. In the 1950s the improved alkaline-manganese battery was developed. In 1954 the first solar battery or solar cell and in 1956 the hydrogen-oxygen fuel cell were introduced. The 1960s saw the invention of the gel-type electrolyte lead-acid battery. Lithium-ion batteries, wafer thin and powering portable computers and cell phones were introduced in the 1990s. Computer chips and sensors now help to prolong battery life and speed up the charging cycle. Sensors monitor the temperature inside a battery as chemical reactions during the recharging cause it to heat up; microchips control the power flow during recharging so that current flows in rapidly when the batteries are drained and then increasingly slowly as the batteries become fully charged.

Another source of technical progress is nanotechnology; research indicates that batteries employing carbon nanotubes will have twice the life of traditional batteries.

During the last few decades advanced batteries have a potentially important role to play in the development of many areas of technology. Compared with the fast advancements in areas such as microelectronics, the lack of progress in battery technology is apparent.

The consumer market demands high energy densities and small sizes. Lithium secondary batteries are the most promising to fulfil such needs. Pioneer work with the lithium battery began in 1912 under G.N. Lewis but the first commercial non-rechargeable battery become available in early 1970. Attempts to develop rechargeable lithium batteries followed in the 1980s, but failed due to safety problems [1].

In the first commercial ´´lithium ion battery`` lithium ions swing between anode and the cathode through an organic liquid electrolyte in which an inorganic lithium salt is dissolved [2]. Replacement of the liquid electrolyte system by a solid one enables to create cells with very slim geometry. It caused studies of solid polymer electrolytes (SPE) which are actively pursued as a major contribution to the development of high energy density batteries [3][4].

1.1 Fundamentals of Electrochemistry

One of the basic quantities in electrochemistry is the electrical potential ϕ. The electrical potential of a point in space is defined as the work W expended in bringing a unit positive charge q from infinity, where the electric potential is zero, to the point in question. The electric potential can be calculated from equation 1:

$$f = \frac{W}{q} \qquad \text{Equation 1}$$

The difference in electrical potential ϕ_1 and ϕ_2 between two points 1 and 2 within the conservative electric field is the work W_{12} expended in taking a unit positive charge q from point 1 to point 2 (equation 2):

$$f_2 - f_1 = \frac{W_{12}}{q} \qquad \text{Equation 2}$$

Writing E for the potential difference $f_2 - f_1$ and dW_{el} for the work to transfer an infinitesimal quantity of charge one obtains equation 3:

$$W_{12} = -dW_{el} = E * dq \qquad \text{Equation 3}$$

If the charge transfer is reversible then the work dW_{el} is equal to the decrease in Gibbs energy of the system (equation 4):

$$dW_{el} = -dG \qquad \text{Equation 4}$$

The escaping tendency of a charged particle, an ion or an electron, in a phase depends on the electric potential of that phase. The relation between the electric potential and the escaping tendency is the chemical potential $\tilde{m}_i$ of a charged species (equation 5):

$$\tilde{m}_i = m_i + z_i * Ff \qquad \text{Equation 5}$$

where F is the charge per mole of electrons, F = 96 484.56 C/mol and z_i is the charge per species. Coulomb C is the unit of electric charge and corresponds to the amount of charge transferred in 1 second by a current of 1 ampere.

Equation 5 divides the chemical potential into two terms. The first term m_i, is the chemical contribution to the escaping tendency. The chemical contribution is produced by the chemical environment in which the charged species exists, and is the same in two phases of the same chemical composition since it is a function only of T, P and composition. The second term,

$z_i * Ff$, is the electrical contribution to the escaping tendency; it depends on the electrical parameters of the phase [7].

An electrochemical cell consist of two electrochemically active electrodes in contact with an electrolyte, which may be a solution or a solid. The electrodes are also in contact with a current collectors which are part of an electronic circuit. The physical structure containing the electrodes is called an electrode compartment. The two electrodes may share the same compartment. If the electrolytes are different, then the two compartments may be joined by a salt bridge, which is an electrolyte solution that completes the electrical circuit by permitting ions to move between the electrodes. Alternatively, the two solutions may be in direct physical contact (for example, through a porous membrane) and form a liquid junction. A galvanic cell (voltaic cell) is an electrochemical cell that produces electricity as a result of a spontaneous electrochemical reaction. An electrolytic cell is an electrochemical cell in which a non-spontaneous reaction is driven by an external power source with direct current [8].

In the electrochemical cell the work expended on the system to move the electrons from one electrode to the other is $-W_{el}$ (equation 6):

$$-W_{el} = q(f_2 - f_1) = -2FE \qquad \text{Equation 6}$$

where f_1 and f_2 are the potentials of the electrodes.

Based on equation 4 and knowing that the change of Gibbs energy ΔG for the electrochemical cell reactions are (equation 7):

$$\Delta G = \Delta G^\circ + RT \ln \frac{a_2}{a_1} \qquad \text{Equation 7}$$

one obtains (equation 8):

$$nFE = -\Delta G^\circ - RT \ln \frac{a_2}{a_1} \qquad \text{Equation 8}$$

If both electrodes are in their standard states $a_1 = 1$ and $a_2 = 1$, the cell potential is the standard cell potential E°. Based on that one obtains the Nernst equation for the cell (equation 9):

$$E = E^\circ - \frac{RT}{nF} \ln Q \qquad \text{Equation 9}$$

where n is the number of electrons involved in the cell reaction and $Q = \frac{a_2}{a_1}$ is the proper quotient of activities.

The Nernst equation relates the cell potential to a standard value and the proper quotient of activities of the substances involved in the cell reaction. Knowing the values of E° and the activities, we can calculate the cell potential.

The fundamental relation between the cell potential and the Gibbs energy change accompanying the cell reaction is equation 10, meaning that the spontaneous electrochemical reaction only occurs, when nFE is:

$$nFE \leq -\Delta G \qquad \text{Equation 10}$$

The value of E depends on the current drawn in the external circuit. The limiting value of E measured as the current goes to zero is called the electromotive force (emf) of the cell or zero current cell potential (equation11):

$$\lim_{I \to 0} E = emf \qquad \text{Equation 11}$$

The cell emf is proportional to $(-\Delta G/n)$, the decrease in Gibbs energy of the cell reaction per electron transferred. The cell emf is therefore an intensive property of the system.

Different electrode systems have its own characteristic electrical potential but it is not possible to measure those potentials directly. To solve this problem one electrode was assigned as standard potential and the others are assigned relative to that basis. The system selected as standard is the standard hydrogen electrode (SHE) build up from a piece of platinum in contact with hydrogen gas at unit fugacity and an acid solution in which the protons have unit activity (Figure 1).

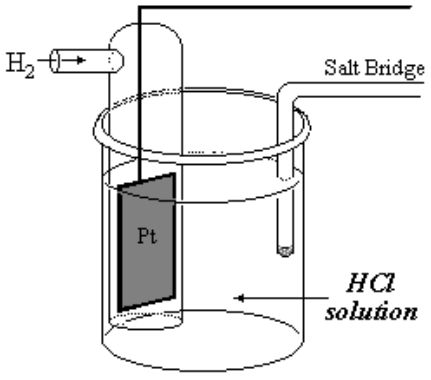

Figure 1. Standard hydrogen electrode (SHE).

The electrical potential of the SHE is set to the conventional value zero (equation 12):

$$f^\circ_{H^+,H_2} = f_{SHE} = 0 \qquad \text{Equation 12}$$

The Nernst equation for the hydrogen electrode is (equation 13):

$$f_{H^+,H_2} = f^{\circ}_{H^+,H_2} - \frac{RT}{F}\ln\frac{f^{1/2}}{a_{H^+}} \qquad \text{Equation 13}$$

where f is the fugacity of H_2 and a_{H^+} is the activity of the protons in the aqueous solution. The argument of the logarithm is a proper quotient of fugacity and activity for the electrode reaction if the presence of the electrons is ignored in constructing the quotient. From equation 11 one can calculate the potential, relative to SHE, of a hydrogen electrode at which f_{H_2} and a_{H^+} have arbitrary values [7].

Having SHE as reference electrode one can compare the potentials of all other electrode (half cell) systems to that of the standard hydrogen electrode. The standard potential of half cell is the value of the standard emf of a cell in which molecular hydrogen under standard pressure is oxidized to solvated protons at the left-hand electrode [10]. The standard potential of half cells are tabulated. Such a table of electrode potentials is equivalent to a table of standard Gibbs energies from which one can calculate values of equilibrium constants for chemical reactions in solution based on the equation 14 [7]:

$$\Delta G^{\circ} = -RT\ln K \qquad \text{Equation 14}$$

and equation 15:

$$nFE^{\circ} = -\Delta G^{\circ} \qquad \text{Equation 15}$$

The current produced by a galvanic cell arises from the spontaneous reaction taking place inside it. This redox reaction is the outcome of the loss of electrons from one species and their gain by another species. The loss of electrons is identified as oxidation (increase in oxidation number) and the gain of electrons is called reduction (decrease in oxidation number). Any redox reaction may be expressed as the difference of two reduction half-reactions. Half-reactions are conceptual i.e. the mechanism of such reactions is more complex without free electrons involved.

In an electrochemical cell oxidation takes place at the anode and reduction takes place at the cathode during the spontaneous reaction (discharging). As the reaction proceeds in a galvanic cell, the electrons released at the anode travel through the external circuit, re-enter the cell at the cathode, where they bring about reduction. In an electrolytic cell electrons must be withdrawn from the species in the anode compartment and must pass from the cathode to the species undergoing reduction [6]. Whether an electrode is a cathode or anode depends on the direction of the current flow (Table 1):

Plate	Discharge	Charge
Positive	Cathode	Anode
Negative	Anode	Cathode

Table 1. Electrode name - current flow direction dependence.

The time, current, and concentration of the electrolysis bath is controlled scientifically by using the laws of electrolysis which established the stoichiometry of such process. Faraday's law stating that the number of moles of substance produced at an electrode during electrolysis is directly proportional to the number of moles of electrons transferred at that electrode.

The cell reaction is the reaction in the cell written on the assumption that the right hand electrode is the cathode, and hence that reduction is taking place in the right hand compartment.

1.2 Batteries

The battery is an electrical device that converts chemical energy into electrical energy, consisting of a group of electric cells that are connected in series and/or in parallel to provide the required voltage and capacity, respectively, and acts as a source of direct current. The term is also now commonly used for a single cell, but strictly speaking batteries are made up of connected cells encased in a container and fitted with terminals to provide a source of direct electric current at a given voltage. Each cell consists of a positive and negative plate separated by an electrolyte which enables ion transfer between the two half cells. An electrochemical cell interfaces the external world through current collectors: one contacts a oxidising half cell (the anode) and the other a reducing half cell (the cathode). The compartments contain the electrochemically active material which changes oxidation state upon charging and discharging [3]. The voltage, or electromotive force, depends on the chemical properties of the substances used, but is not affected by the size of the compartments or the amount of electrolyte.

Electrical cells that provide electrical energy are classified into two general types. Castellan [7] defined it as following:

Primary cells. These are constructed of high-energy materials which react chemically and produce electrical power spontaneously. The cell reaction is not reversible, and when the materials are consumed the device must be discarded.

Secondary cells. These devices function like a primary cell, but are reversible. After providing power, the high-energy materials can be reconstituted by imposing a current from an exterior power source in the reverse direction. The cell reaction is thus reversed and the device is recharged.

Common chemical systems for primary batteries include zinc-carbon, zinc chloride, magnesium, alkaline-manganese dioxide, mercuric oxide, silver oxide, zinc / air, and lithium.

Typical examples of the secondary cell are the lead-acid battery used in automobiles, the nickel: -cadmium, -zinc or -iron batteries, silver oxide batteries, sealed nickel hydrogen batteries, nickel-metal hydride batteries, lithium -manganese dioxide, -titanium disulfide, -iron sulphide, -manganese titanium, -nickel oxide and -manganese oxide batteries.

The most important performance parameters for batteries are energy density, capacity and power density. Tarascon and Armand define the energy density as the amount of electrical

energy expressed either per unit of weight ($\frac{W*h}{kg}$) or per unit of volume ($\frac{W*h}{l}$) that a battery is able to deliver. It is the product of the cell potential times capacity ($\frac{A*h}{kg}$), both of which are linked directly to the chemistry of the system [6]. The power density ($\frac{W}{l}$) is related to the energy density at a given discharge rate, and indicates how rapidly the cell can be discharged and how much energy is generated in a given time. A cell with high energy density may exhibit a significant voltage and capacity drop at higher discharge rates and therefore have a low power density. The power density is usually discussed in terms of the cell mass ($\frac{W}{kg}$). The rechargeable batteries are also described by their cycling, which describes how many times the cell can be charged and discharged. Other parameters used for battery characterization are the discharge profile, self discharge rate and total service life [9]. The discharge profile is a plot of battery voltage as a function of time, simulating a constant load of the battery, used to indicate the cell performance under controlled conditions. The self discharge rate describes how fast the battery discharges itself upon storage. The total service life (or lifetime) is a time how long the battery works. The memory effect was firstly observed in NiCd batteries and occurs when part of the active material that has not been cycled changes its physical characteristics and shows an increase in resistance. The change can be either a crystal growth with reduction of the active surface area, or a formation of an intermetallic compound. Both result in a voltage depression and a loss of capacity [3].

It is proved that parameters like the cell potential, capacity and energy density of the battery are related to the intrinsic properties of the materials that form the half cell compartments. The cycle-life and lifetime are also depending on the nature of the interfaces between the electrodes and electrolyte. Safety is a function of the stability of the electrode materials, interfaces and electrolyte [6][11]. Common types of commercial batteries and some of their characteristics and comments are summarized in the following Table 2 [12].

Material	Voltage (V)	Energy density per volume $(\frac{W*h}{l})$	Energy density per weight $(\frac{W*h}{kg})$	Number of cycles	Comments
Lead-Acid	2	65	35	50-100	inexpensive, robust
Ni-Cd	1.2	130	40	1000-5000	high current densities, memory effects
Ni-metal-Hydride	1.2	190	60	500-5000	large self-discharge, memory effects
Alkali-Mn	1.5			<500	Expensive
Li-Ion[1)]	3.6	270	100	300	No memory effects, safety electronics
Li-Polymer[2)]	3.6	240	150	300	Adaptable to all geometries, less hazardous

[1)] liquid organic electrolyte; [2)] polymer as electrolyte

Table 2. Characteristic of batteries.

The highest energy densities and single cell voltages from all presented cell types are observed for lithium based systems. The only disadvantage is relatively low cycle number. The cycle number presented in Table 2 is based on deep discharge measurements. Shallow discharges of lithium batteries provide more cycles than deep discharges what allows for an increase of the total number of cycles [1].

1.2.1 Lithium Batteries

The most promising results in the research of power sources so far have been with electrochemical systems using a lithium anode, lithium ion conducting electrolyte and a lithium ion accepting cathode material [13]. Since high-energy density batteries are the target, lithium is a material of great interest for application. Lithium is the lightest of all metals (equivalent weight M=6,94 $\frac{g}{mol}$), has the largest electrochemical standard potential (-3,04 V versus SHE) and provides the largest specific energy density. Stable passivation products on the surface of other metals like magnesium or aluminium disqualify those materials for battery construction. Passivated lithium surfaces stay still electrochemically active [1].

Present days lithium batteries use a solid reductant as the anode and a solid oxidant as the cathode. On discharge the anode supplies Li^+ ions to the electrolyte and electrons to the external circuit. The cathode is a component into which Li^+ ions are inserted from the electrolyte and charge compensated by electrons from external circuit [3][5][14]. A schematic view of the battery is presented in Figure 2.

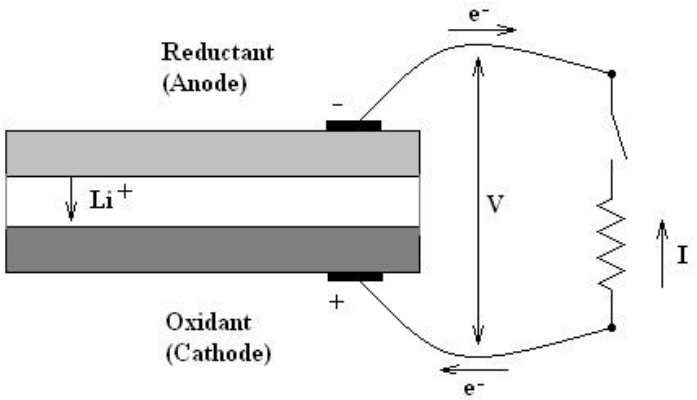

Figure 2. Elements of an electrochemical lithium cell during discharge

The cells with lithium metal as the reduction compartment were formerly the most extensively investigated. However, such cells were withdrawn from the market because of safety problems. The electrochemical potential of Li metal lies above the LUMO of almost all known electrolytes and the reaction with the electrolyte results in the formation of a passivating surface layer. Although Li^+ ions pass through the layer, on charging Li tends to

form dendrites. The uneven lithium growth at the anode was repeated during each subsequent discharge-recharge cycle and lead to short cuts of the electrical circle, in some cases to explosion hazards. Such instability of the lithium metal cells caused the shift of the research to cells using lithium composites compartments. The lithium composite materials are an insertion hosts for Li^+ and have a slightly lower electrochemical standard potential than Li metal. The commercial example of such anode is the Li – graphite composite LiC_6 [15] . Although lower in energy density than comparable lithium metal systems (usually ~20%), such cells are much more safe. The Li-ion battery is a cell with no memory effect and no scheduled cycling is required to prolong the battery's life.

The high cell voltage of Li-ion batteries allows to manufacture batteries consisting only of one cell [1].

1.3 Electrolytes

Substances that dissociate into ions when dissolved in water or other polar solvents are called electrolytes. They can be divided into acids, bases and salts, because they all provide ions when dissolved in water. Their solutions conduct electricity due to the mobility of the cations (positive) and anions (negative). Strong electrolytes completely ionize when dissolved, and no neutral molecules are left in the solution.

Besides the electrodes, the electrolyte constitutes the third key component of a battery. Although the role of electrolyte is often considered trivial, its choice is actually crucial. There are numerous liquid solvents available, each with different dielectric constants and viscosity, and we can select specific solvents to favour the ionic conductivity of the electrolyte. The use of a polymer rather than a liquid electrolyte adds further selection criteria linked to the electrochemical stability of the polymer and its thermal properties [6].

The Li-ion battery type offers high energy densities, but for high-power applications or use in extreme conditions more conducting and more durable electrolytes are needed. The choice of electrolyte is crucial and is based on criteria that differ depending on whether we are dealing with polymer or liquid-based lithium ion rechargeable batteries. The polymer electrolyte resembles a plastic film that allows an exchange of ions [1][6][16]. Unlike inorganic glasses or ceramic electrolytes, the polymer electrolytes are compliant and this property makes it possible to construct solid state batteries in which the polymer conforms to the volume changes of the electrodes. The latter usually undergo a 4-10% volume-change upon charging/discharging and that could result in a loss of contact at the electrode – electrolyte interface [17][18][19].

Another advantage of polymer-based electrolytes is their reduced reactivity in comparison to liquid electrolytes. It is generally accepted that no solvent system is thermodynamically stable towards the lithium anode. Furthermore, solid-state constructed batteries are more tolerant to shock, vibration, and mechanical deformation [17]. The potential utility of polymer electrolytes has stimulated the synthesis of new polymer systems, physical studies of their structure and charge transport as well as theoretical modelling of the charge transport processes. Possible applications of such electrolytes are not only all solid-state rechargeable lithium ion batteries, but also application for other electrochemical devices such as supercapacitors, electrochromic windows and sensors [20][19].

An important research objective is to identify an electrolyte with the desired combination of mechanical properties, electrical conductivity and stability against powerful oxidizing and reducing electrodes. Among the most promising materials are highly conducting but brittle superionic glassy electrolytes like Li_2S-SiS_2-P_2S_5 [21] or ethylmethylimidazolium tetrafluoroborate/$LiN(SO_2CF_3)$ [22] and rubbery ´salt-in-polymer` electrolytes [23].

1.3.1 Polymer Electrolytes

Bruce and Vincent defined polymer electrolytes as ionically conducting solid phases formed by the dissolution of salts in ion-coordinating macromolecules [24]. The research on solid polymer electrolytes has begun with the discovery of ion conductivity in a poly(ethylene oxide)-alkaline metal ion complex made by P.Wright in 1975 [25][26]. First suggestions to use such a system for batteries came from M.Armand in 1978 [27]. Since then studies of solid polymer electrolytes have been steadily increasing. Detailed overviews of the solid polymer electrolytes development were published by several authors [28][29][30][17]. The general goal of these efforts is to achieve materials which satisfy certain requirements for battery application. To reach the conductivity level of liquid electrolytes, polymer electrolytes should possess conductivities approaching or exceeding 10^{-3} S cm^{-1} at ambient temperature. A large transference number for Li^+ needs to be achieved because it relates to higher power densities. Furthermore, whole salt-in-polymer system must have an electrochemical stability window extending from 0 V to 4,5 V vs. Li/Li^+ to be compatible with lithium and cathode materials [17]. The electrochemical stability window of a substance is expressed as potential window in Volts [V] as unit and determined by cyclovoltammetry (CV). The broader and higher the stability window, the more stable the corresponding material are against oxidation or reduction processes (anodic and cathodic decomposition processes) [31].

A material that conducts electricity with ions as charge carriers is an ionic conductor. The phenomenon of ionic conductivity in solid materials are of great importance for new technologies. It is most interesting for energy storage like rechargeable batteries and conversion systems like fuel cells. The inorganic ion conductors like AgI, $Na_xAl_2O_3$, ZrO_2 [116], $Rb_4Cu_{11}I_7Cl_3$ [117][118], Li_2SO_4, $RbAg_4I_5$ [126] are already widely characterized. Laskar and Chandra affirm that high ionic conductivity in solids requires that certain structural and energetic conditions have to be fulfilled. The major rule is that the conductivity is the product of the free ion concentration with the ion mobility and charge number [118]. Normally, pure salt-free polymers exhibit a very low electrical conductivity. Polymer materials find generally applications as insulators because of their good dielectric properties. However, a considerable number of polymeric materials are known to conduct electricity by the migration of ions. There are several techniques used to ensure a high free ion concentration in polymers. The most trivial method of introducing ions is to wet a fibrous or porous polymer with a liquid electrolyte. A typical example of such a gel polymer electrolytes

like poly(vinylidene fluoride) plasticized with a solution of lithium perchlorate in propylene carbonate [128]. Gel electrolytes are currently of great interest commercially as they are seen as an attractive alternative to the solvent-free system. They are formed by dissolving the salt in a polar liquid and adding a polymer network to give the material mechanical stability. Two distinct methods can be used to achieve macroscopic immobilization of the liquid solvent:

- increase the viscosity of the liquid electrolyte by adding a soluble polymer e.g. PEO, poly(methyl methacrylate) (PMMA), polyacrylonitrile (PAN), until a gel consistency is achieved;
- load the liquid electrolyte into a microporous matrix e.g. porous polyethylene.

The addition of a plasticizing solvent to a polymer-salt system modifies the electrolyte by lowering T_g through an isothermal increase in the system's configurational entropy and this consequently increases the mobility of all particles. A suitable choice of organic solvent can lead to very high conductivities ($10^{-3} – 10^{-2}$ [S/cm]) while still retaining the rubbery character of the material [151]. Sekhon has found the role of polymer in gel electrolytes to depend upon the nature of salt used. In the case of lithium ion conducting polymer gel electrolytes containing various lithium salts - which are nearly fully dissociated - the addition of polymer results in an increase in viscosity which lowers mobility and conductivity decreases [152]. The second possibility are polymeric salts in which free ions may be accommodated within polymer molecules as counterions to charged groups covalently bound to the polymer. When repeat unit of the polymer contains an ionisable group, the material is commonly named polyelectrolyte. In Figure 3 the general formula of polyelectrolyte is presented.

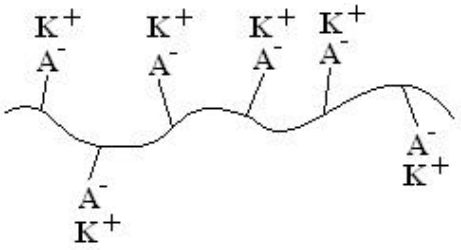

Figure 3. General formula of polyelectrolyte where:

A^- could be $-CO_2^-$, $-SO_3^-$, $-PO_3^{2-}$, $-COO^-$

K^+ could be Na^+, K^+, Li^+

The potentially mobile ions distributed within a more or less fixed superstructure of opposite charge, makes these polymers similar to the inorganic ion conductors. The conductivity of

most of those materials has been found to be much lower than in inorganic analogues and lower than in blends of salts with polymers, the polymer segments playing the role of a solvent for the salts. The biggest differences in conductivity between the blends of salts with polymers and the polyelectrolyte salts have been found for lithium ion based systems. The high melting and glass transition temperatures of polyelectrolytes are a consequence of the strong Coulombic interactions between the ions. For the same reason only weak dissociation in dipolar aprotic medium was observed [153][131]. The ionic mobility can substantially be increased by using strongly electronegative counterions. Solvent addition influences the structural mobility and breaks the Coulombic bounds resulting in a swollen material [118].
The newest class of the polymer electrolytes are the ones in which both salt and solvent are polymeric. Two approaches have been used: in one, poly(ethylene oxide) has been blended with a polymeric salt, and in the other, both solvent and salt functions are attached as side chains to the same backbone. McIntyre and coworkers synthesized lithium salts of two polyanionic addition polymers containing alkyl sulphonic acid and perfluoroalkyl carboxylic acid side groups. Blends of these polymers were formed with PEO [131]. Poly[lithium methacrylate-co-oligo(oxyethylene)methacrylate] film prepared as a polymeric solid electrolyte were reported by Tsuchida et al. [154].

In this work the blends of salts with polymers (polymer-in-salt) class of electrolyte is investigated. The polymeric matrix has a high molecular mass enough to be elastomeric above the glass transition temperature and the chemical character allows to dissolve lithium salts. It is proved that the ionic mobility in such polymer electrolyte systems is better when the lithium salt possesses strong electronegative and polarisable anions like - SO_3CF_3, -$N(SO_2CF_3)_2$, -BF_4, -ClO_4, -PF_6, -AsF_6.
In this work PEO-HPC was blended with:

1. Lithium trifluoromethanesulfonate $LiSO_3CF_3$
2. Lithium bis(trifluorosulfone) imide $LiN(SO_2CF_3)_2$
3. Lithium tetrafluoroborate $LiBF_4$

with different molar concentrations in the range 0,02–0,2 [Li]/[O]. The salts were introduced with the aid of a volatile solvent (THF), which dissolves both the salt and the polymer.
Removal of the co-solvent results in the elastomeric polymer electrolyte blend.

The solid polymer electrolytes act as an ion conducting medium and are used as separator membranes between the electrodes. Li^+ ion conductivity is observed in polymers that are good solvents for lithium salts and have low glass transition temperatures. Due to the

solvation power and complexing ability of poly(ethylene oxide) (PEO) to alkali metal ions, the majority of polymer electrolyte systems reported in literature as yet have been based on systems consisting or including of PEO like structures [4][32-40]. Since the migration of ions is perceived to take place in the amorphous phase of PEO [41] the research concentrated on new systems with low cristallinity. Killis et al. [42] proposed the reaction of isocyanates with a functionality higher than two with the OH end groups of glycols and obtained networks in which cristallinity is reduced and comparable to the oligomeric aducts. A similar result was obtained with the use of PEO-triols [43]. The conductivity of other systems without PEO, like polyesters [44-47] or the nitrogen EO homologue, poly(ethyleneimine) [48], proved to be quite disappointing.

The major property improvements were achieved for systems based on low molecular weight PEO grafted to a high glass transition temperature (T_g) polymer backbone that imparts mechanical stability to the material [4][18][37-40][49-52]. The polymers with short solvating chains attached to a high molecular weight main chain provides materials with no or reduced crystallinity, and adds degrees of freedom to the solvating side chain units which have a free end. The first report of such materials was of a polyphosphazene with two side arms linked to the phosphorus and containing two ether oxygens [49]. Other poly(phosphazene-ethylene oxide)s were reported as well [53][54][55]. A similar approach was successfully applied to siloxane-based polymers [50]. The drawbacks of such materials are their complex and difficult chemistry and the lack of mechanical properties, even after crosslinking. First promising conductivities were obtained with architectures [51] based on polymethacrylate with longer (8 and 22 EO) side chains. Better mechanical strength with similar reasonable conductivity was achieved in later work using poly(p-phenylene) / oligo(oxyethylene) (up to 10^{-3} [S/cm]) [4][52] and poly(amide-elthylene oxide) (up to 10^{-4} [S/cm]) [56]. Although a large number of polymer electrolyte systems have been prepared and characterized the need of cheap, mechanically stabile materials with conductivities approaching 10^{-3} S cm^{-1} at ambient temperature was still not fulfilled. One of the possible solution is the use of cellulose. Several attempts were tried like grafting of hydroxyethylcellulose and carboxymethylcellulose with mono- and diisocyanates and poly(propylene oxide) [57] or synthesis of cellulose esters with poly(ethylene oxide) side chains [58][59][60]. An overviews of the solid polymer electrolytes is presented in Table 3.

Name	Monomer unit	Conduc. at 20°C [S/cm]	Conduc. at 100°C [S/cm]	Ref.
Poly(ethylene oxide)	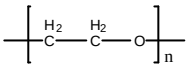	~10^{-9}	~10^{-4}	[25] [26] [53]
Poly(propylene oxide)	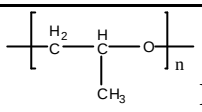 M_n=1500	$3*10^{-9}$	$4*10^{-5}$	[42] [46] [53]
Poly(ethylene imine)	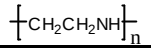	-	$2,5*10^{-7}$	[48]
Polyether	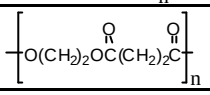	>10^{-10}	$4*10^{-6}$	[47]
Poly(ß-propiolactone)	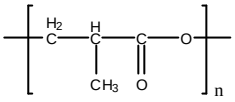	$3,2*10^{-7}$	$1,9*10^{-6}$	[43]
Poly(ethylene sulfide)	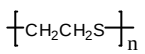	10^{-11} at 40°C	$3*10^{-5}$ at 70°C	[163]
a-(p-Toluenesulfonyl)- ? -methoxy-oligo(oxyethylene)	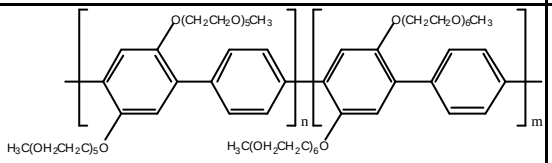	$4,3*10^{-5}$	~$1,7*10^{-4}$	[4]
Poly[? -methoxyhexa(oxyethylene)ethoxy]methyl siloxane	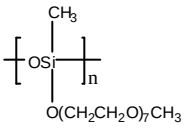	$1,1*10^{-5}$	~10^{-4}	[50]
Poly-[bis((methoxyethoxy)ethoxy)phosphazene]	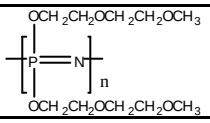	$1,1*10^{-5}$	$1,2*10^{-4}$	[53-55]
Hydroxyethyl cellulose grafted with diisocyanates of poly(ethylene oxide)	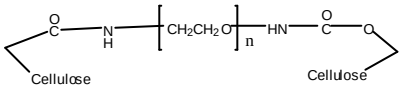	10^{-7}-10^{-6}	$7*10^{-4}$	[57]
Hydroxypopyl cellulose ester with poly(ethylene oxide) side chains	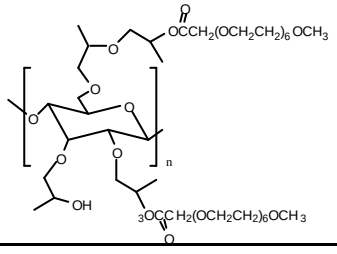	$3*10^{-6}$	$8*10^{-4}$	[58] [60]

Table 3. Some polymers which have been used as solid solvents for polymer electrolytes and its conductivities.

1.3.2 Theory of Ionic Transport in Polymer Electrolytes

Ion conduction in polymers takes place for three reasons:

1. polymer materials are swollen with a liquid electrolyte, in which the ions are mobile,
2. polyelectrolytes contain mobile conterions,
3. a solution of a salt in an ion-solvating polymer contains mobile ions.

The (ω-ethoxy-tris(oxyethylen))-2-oxypropylcellulose (PEO-HPC) synthesized and characterized in this work belongs to the latter group of polymer ion conductors.

The ionic conductivity in solids is described in terms of the number of charges per carrier q_i, the number of carriers per volume unit n_i and the average mobility μ_i in an electric field of unit strength [61]. The expression for the conductivity is the sum of all i carriers contribution:

$$s(T) = \sum_i q_i n_i(T) m_i(T) \qquad \text{Equation 16}$$

Ohmic conductivity in polymers is regarded as a perturbation of the self diffusion of the ions. In a solid structure at absolute zero temperature ions are trapped at their preferred sites in a potential well formed by the surrounding atoms. At higher temperatures self-diffusion is observed which means random hopping of the ions over the potential barriers between the wells. With the assumption that empty sites exist in the material, the average direction of the hopping will be biased by the applied field or the potential wells are deformed by the applied electric field. In analogy to diffusion of non-charged species in homogenous materials, the ion conductivity is related to the self-diffusion coefficient D by the Nernst-Einstein equation:

$$s = \frac{nq^2}{kT} D \qquad \text{Equation 17}$$

Based on the equations number 16 and 17 the average velocity μ in a field of unit strength is defined as:

$$m = \frac{qD}{kT} \qquad \text{Equation 18}$$

The temperature dependence of the ion hopping based conductivity in solid materials is described with the Arrhenius equation:

$$s(T) = s_0 e^{\left(\frac{-E_A}{kT}\right)} \qquad \text{Equation 19}$$

where E_A is the energy barrier height and kT is the thermal energy.

The Arrhenius type behaviour is typical for systems like:

- amorphous systems at temperatures lower than glass transition temperature

and

- crystal systems, especially at high salt concentrations and in systems with the tendency to form polymer/salt complexes.

In the Arrhenius type behaviour the energy barrier height E_A is a rate determining factor of the conductivity process. The motion of ions through the polymer matrix is a thermally activated process based on the jumping over an energy barrier of ions possessing enough energy. With increasing temperature the average energy of ions grows and more charged species posses sufficient energy to overcome the energy barrier E_A, in consequence the overall ion conductivity increases. The preexponential factor s_0 is the limiting conductivity of the material at temperature $T \to \infty$.

In order to develop a molecular understanding of the transport properties in amorphous polymer electrolytes, several models of ion transport in amorphous polymers were developed. One of the simplest ways of understanding polymer segmental mobility are the Free Volume based models. The Free Volume may be regarded as the volume in which each molecule of a liquid moves in an average potential field due to its neighbours. However, theoretical estimates of Free Volume depend on postulates regarding the compressibilities of the molecules and the nature of their packing in the liquid state. A definition of Free Volume used in polymer studies is based on equation 20:

$$v = v_0 + v_f \qquad \text{Equation 20}$$

were v is the measured specific volume of the polymer and v_f is the free volume at a given temperature. v_0 is the Van der Waals volume of the constituent molecules.

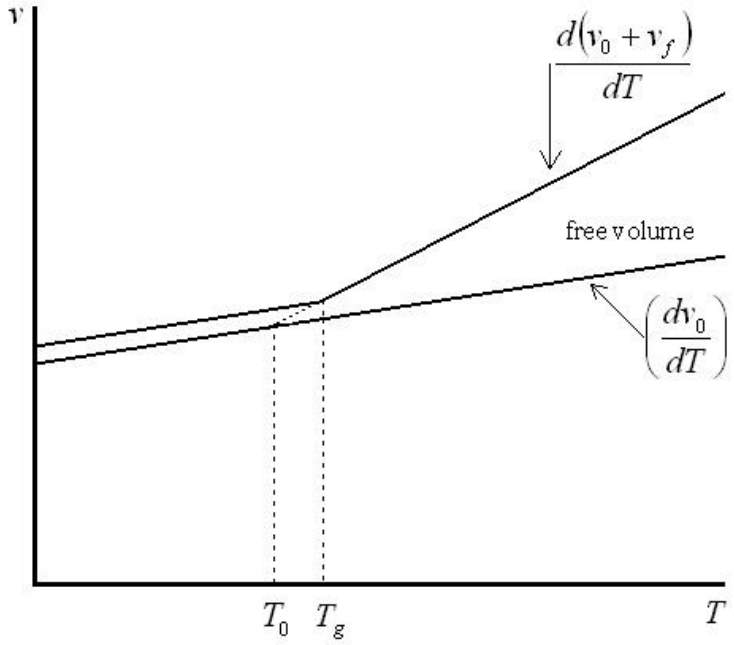

Figure 4. Schematic representation of the temperature dependences of the Free Volume and the overall volume, that is the thermal expansion coefficient.

When the polymer is a liquid or rubber-like the increase of temperature causes the increasing of the Free Volume in the system v_f. With decreasing temperature up to the glass transition temperature T_g, the Free Volume v_f diminishes. At T_g the mobility of chain segments is not possible any more and below T_g the Free Volume of the system v_f is constant. The Van der Waals volume v_0 changes with temperature independently from the condensation state (glass, rubber or liquid) because the amplitude of the thermal oscillations remain independent. This change is approximately linear with temperature. Knowing the relation of the volume-temperature dependence of a system, it is possible to determine the Vogel temperature T_0. The temperature dependence of the $\frac{d(v_0 + v_f)}{dT}$ function above T_g extrapolated up to the crossing point with the $\left(\frac{dv_0}{dT}\right)$ function determines the Vogel temperature T_0 (Figure 4), defined as equilibrium glass transition temperature at which the Free Volume disappears.

The basic idea underlying the Free Volume approach to ion conducting phenomena in solid polymer electrolyte (SPE) is that the molecular mobility at any temperature is dependent on the available Free Volume at that temperature. As temperature increases the Free Volume increases and molecular motions become more rapid. A few molecular theories based on this Free Volume concept have been proposed, with the aim of relating dynamic quantities such as

the diffusion coefficient and viscosity [62]. In homogeneous amorphous polymer-salt blends and polyelectrolytes the ion transport strongly depends on the ion diffusion, which may be linked to a cooperative rearrangement of the polymer segments. The latter is governed by the energy interval $T-T_0$ and associated with a local Free Volume of the material. Thus, the temperature dependence of the ion conductivity derives from the thermal dependence of the Free Volume. The viscosity can be written as an empirical relationship in terms of the Vogel-Tamman-Fulcher (VTF equation):

$$h = Ce^{\left(\frac{-B}{k(T-T_0)}\right)} \qquad \text{Equation 21}$$

where $C \propto T^{\frac{1}{2}}$ [63][64]. The temperature dependence of Free Volume relates to the h viscosity of the material as a material characteristic parameter. h is expressed in the empirical Doolittle equation [65][66]:

$$h = Ae^{\left(\frac{b_0 v_0}{v_f}\right)} \qquad \text{Equation 22}$$

where: - b_0 is a dimensionless constant,

- v_0 is the van der Waals volume and

- v_f is average free volume.

Equation 21 combined with the Stokes-Einstein relationship [67][68]:

$$D = \frac{kT}{6prh} \qquad \text{Equation 23}$$

(k - constant, r - Van der Waals radius for the ions), and the Nernst-Einstein equation (Equation 17) turn the VTF equation into the form to predict the temperature dependence of conductivity as related to a characteristic temperature T_0:

$$s(T) = Ae^{\left(\frac{-B}{k(T-T_0)}\right)} \qquad \text{Equation 24}$$

where T_0 is the Vogel temperature generally placed ~50 K below the experimentally observed glass transition temperature. T_0 is idealized as the temperature at which all free volume vanishes or all polymer segmental motions disappear or the configurational entropy of the material is zero. The parameter A is mathematically considered as scaling factor in the ordinate direction. In case of conductivity it contains the charge carrier density and charge number [69]. The parameter B is proportional to a characteristic hard sphere volume of the moving polymer chain segment or to the inverse, the expansivity of the material [63][61][70].

In a other words, B determines how fast the conductivity increases and, respectively, the diffusion with increasing temperature, over the glass transition temperature and converges to its limiting value $A^{*}T^{-\frac{1}{2}}$ [69].

Williams, Landel and Ferry (WLF) gave a formulation of the relaxation processes which characterizes any glass-forming material. The WLF theory considers a quantity named shift factor a_T. The quantity a_T is the ratio of any mechanical relaxation process at temperature T to its value at reference temperature T_r. The WLF theory can also be used to describe ion diffusion processes. The function $\log a_T$ versus $T - T_r$ is an universal curve for all polymers as long as for each material a specific T_r and a_T are found. The WLF equation is:

$$\log a_T = \frac{-C_1(T - T_r)}{(C_2 + T - T_r)} \qquad \text{Equation 25}$$

where C_1 and C_2[K] are dimensionless constants.

It was found that $T_r - T_g \approx 50K$ and based on VTF $C_2 = T_r - T_0$, where T_0 is the Vogel temperature. Based on experimental data it is known that on average $C_2 \approx 102$ [K] and $C_1 \approx 8{,}9$, what allows to rewrite the WLF equation using T_g:

$$\log a_T = \frac{-17{,}44(T - T_g)}{(51{,}6 + T - T_g)} \qquad \text{Equation 26}$$

WLF behaviour is found to be universal for many disordered systems, including glasses and polymers. It is based on:

- empirical observations of polymer relaxation times, which implied a universal form for $a_T(T\text{-}T_r)$
- viscosity measurements and on the VTF form for the viscosity, which allowed the analytical expression of that form.

It is not based on any sort of Free Volume formulation but is consistent with them [63][71].

The conductivity form of Williams- Landel-Ferry equation is:

$$s(T) = s(T_{ref}) \exp\left[\frac{C_1(T - T_r)}{C_2 + T - T_r}\right]. \qquad \text{Equation 27}$$

1.4 Purpose and Preview

To overcome the disadvantage of currently used polymer electrolytes the goal of this thesis is to develop a new type of solid polymer electrolytes with a rigid backbone and a "soft" side chain structure with Li^+-ion solvating properties. The rigid backbone will provide improved mechanical stability while the soft side chains form a liquid like matrix in which lithium ion conduction takes place. Moreover the novel material should be based on cheap substrates and its synthesis should not be complicated aiming at low overall costs. The solid polymer electrolyte should satisfy following requirements:

- thermal stability window at least up 100 °C,
- sufficient ionic conductivity (more 10^{-5} S/cm at room temperature),
- mechanical stability,
- electrochemical stability in the window of Li-ion cell operation
- applicability to real lithium batteries.

Cellulose was chosen as stiff, rod like macromolecule for the backbone while flexible oligo-oxyethylenes are chosen as side chains. The new materials have been synthesized through the reaction between hydroxypropylcellulose (HPC) and oligoethyleneoxide derivatives. The products have been investigated using nuclear magnetic resonance (NMR), gel permeation chromatography (GPC), laser light scattering (LS) in order to characterize their degree of substitution and molecular weight.

Blends of the products with lithium salts have been prepared and the effects of salt concentration on ionic conductivity (σ_{ion}), thermal stability and glass transition temperature (T_g) have been investigated. Because of the relatively poor mechanical properties of the polymer-salt blends two crosslinking methods were employed. The improvement of mechanical properties after the crosslinking reaction was recognized with dynamic mechanical analysis (DMA). The change in ionic conductivity level upon crosslinking was found to be slight and as such can be ignored. The applicability of the best product have been tested in a real battery. The self-assembled lithium battery has been discharged and charged several times. The discharge/charge curves have been recorded.

This work is part of an European Project entitled ``Complex Macromolecular Structures as Elements of Functional Devices`` (CODE).

2. Synthesis

The first part of this work concentrates on the synthesis of the cellulose ether derivatives with well-defined structure. The optimal structure involves a maximum degree of substitution of the cellulose and a unique side chain structure and length. All oligoethyleneoxide chains used for grafting have the same length. High degrees of substitution and a regular distribution of the side chains are expected. Because of difficulties related to the solubility of the cellulose as starting material for all experiments 2-hydroxypropylcellulose (HPC) have been used. HPC with average molecular weight of M_W=80.000 g/mol, M_W=100.000 g/mol, M_W=360.000 g/mol and M_W=1.000.000 g/mol have been used. However, only the product obtained from HPC M_W=80.000 g/mol was employed for all subsequent experiments.

2.1 Cellulose and Hydroxypropylcellulose

Although cellulose is the most common naturally occurring organic substance, Anselm Payen first recognized its existence as the common material of plant cell walls in 1838. It exists in almost pure form in cotton fiber (98%) and in combination with other materials, such as lignin and hemicelluloses, in flax (80%), wood (40-50%), plant leaves and stalks, etc. Some bacteria also produce cellulose. This polymer in plants forms microfibrils with an average diameter of 2-20 nm and length 100 - 40 000 nm [72][73].

Cellulose is a linear homopolymer of β-D-glucopyranose. The lowest energy conformation for β-D-glucopyranose is the chair formation and in this shape it appears in the cellulose chain. The glucose base unit are linked together by the C1 and C4 carbon atoms of subsequent monomer units and consecutive units along the chain are symmetry related by a screw axis. The monomer unit and consequently the whole chain has a polar axis (C1? C4). The hydroxyl groups on the ends of the cellulose chain have a different nature. At one end the C1 hydroxyl is an hemiacetal group with reducing activity and at the other end the C4 hydroxyl is an alcoholic non-reducing group (Figure 5).

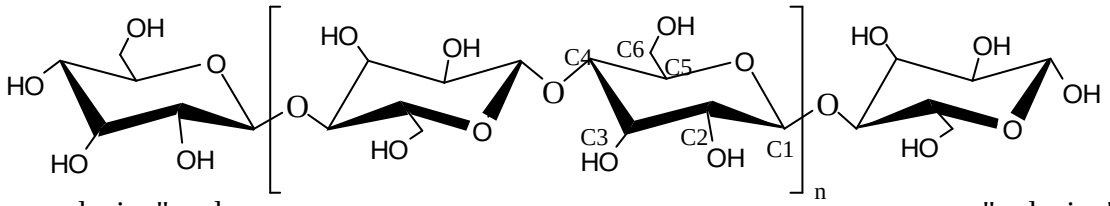

Figure 5. Cellulose chain structure

The chemical character of the cellulose is determined by the presence of three hydroxyl groups per repeat unit. The positioning of the hydroxyls along the extended molecule makes them readily available for hydrogen bonding. Intramolecular hydrogen bonds are formed between the hydroxyl groups at the C3 carbon of one glucose unit and the ring oxygen of the next monomer in the same chain. Additionally there are possibilities to build intermolecular hydrogen bonds mostly based on C6 and C2 hydroxyl groups. These hydrogen bonds cause the chains to group together in highly ordered, crystal structures and give arise for a considerable main chain stiffness of the cellulose. Cellulose usually consists of a mixture of highly crystalline and amorphous regions. The crystalline parts display one chain

conformation but many possible packing arrangements, with either antiparallel (Figure 6a) chains or parallel chains (Figure 6b) [74].

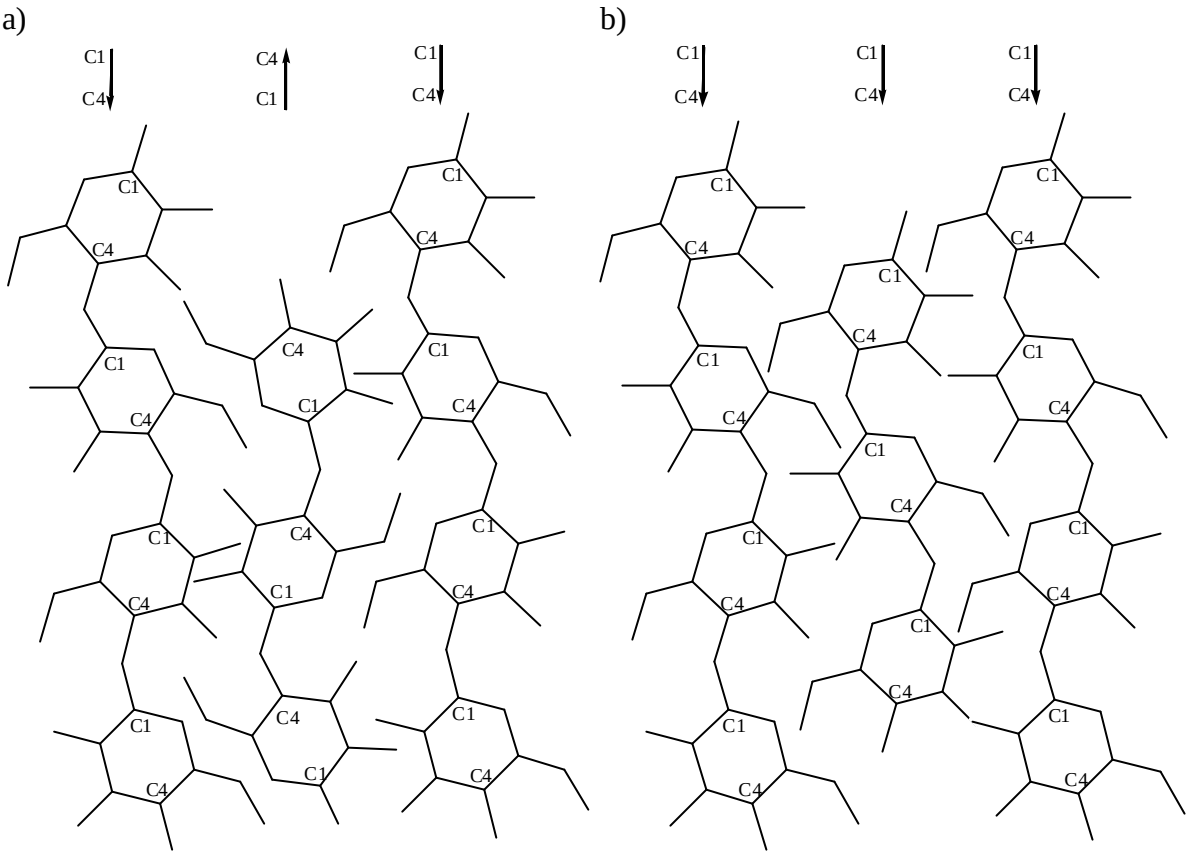

Figure 6. Possible cellulose structures:

a) antiparallel chain packing arrangement of cellulose,

b) parallel chain packing arrangement of cellulose,

The chains are usually longer than the crystalline regions and they pass through several different crystalline regions, with areas of disorder in between. In the less ordered regions the chains are more available for hydrogen bonding to other molecules like water what makes cellulose highly hygroscopic but not soluble in water. Strength and insolubility in most solvents are the effects of intermolecular hydrogen bonding. However the primary C6 and secondary C2, C3 hydroxyl groups are able to undergo reactions typical for corresponding alcohols [59][72-77].

One of commonly used modifications are reactions in heterogeneous systems. The reaction takes place on a solid swollen cellulose substrate while the original fibre structure is maintained. Products of such processes are not homogeneous and the distributions of degree of substitution (DS) are broad. The DS corresponds to the average number of hydroxyl groups

substituted per glucose ring and therefore cannot exceed a value of 3. When the sequential addition of moieties during the cellulose derivatization is possible the product must be characterized additionally by a degree of molar substitution (MS). The MS in the present case is the average number of oxyethylene moieties per repeat unit. In order to achieve homogeneous cellulose derivatives, reaction conditions that disrupt the crystalline regions and force the chains apart are needed. The obtained cellulose derivatives then are soluble in common solvents, and thus capable for further modification [78][79][80].

Several systems which enable reactions in solution have been found. Cellulose is sufficiently stable toward hydrolysis under neutral or basic conditions but it is susceptible to hydrolysis by acids. One of the first method of derivatization was based on inorganic acids (e.g. nitration with a mixture of nitric and sulfuric acid) and acetic acid (acetylation with glacial acetic acid or acetic anhydride). Similarly the cellulose lattice can be destroyed by alkalis, like quaternary alkyl ammonium hydrides [81]. Products of higher degree of substitution have been achieved using mixtures of sulfurdioxide, diethylamine and dimethyl sulfoxide (SO_2-DEA-DMSO) [82][83], N_2O_6 and dimethyl sulfoxide [82] or N,N-dimethylacetamide with lithium chloride [82][84][85]. Many partially substituted cellulose derivatives (usually with DS 0.5 – 2.0) are important materials for further modifications. The most widely used are methylcellulose and cellulose acetate [59][86]. The substituted polymeric materials are soluble in common organic solvents e.g. dimethyl sulfoxide. That enables activation of the residual hydroxyl groups and reactions resulting in highly substituted cellulose derivatives.

The group of cellulose derivatives which has gained substantial practical importance is the class of cellulose ethers. Among several possible ways of cellulose etherification, for this work particularly important is the formation of hydroxypropyl cellulose. The formation of HPC by the reaction of alkali cellulose with propylene oxide in the presence of alkali occurs by an addition reaction initiated by the sodium hydroxide cellulose oxonium complex. The displacement action on the epoxide group generates a new reactive site at the end of the introduced substituent. By the same mechanism further epoxide molecules can be added, leading to alkoxy side chains [73]. The course of these interactions is illustrated by the following reaction scheme (Figure 7):

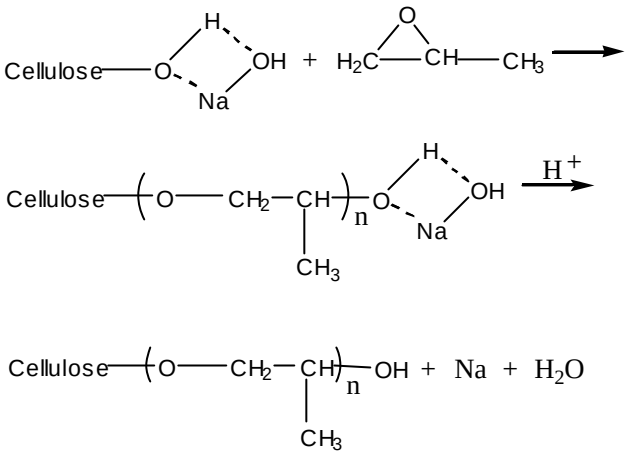

Figure 7. Preparation of HPC - reaction scheme

Subsequent reaction of activated cellulose with propylene oxide (or other epoxides) yields hydroxypropyl cellulose (or other hydroxyalkyl derivatives), which has a number of useful properties, depending on DS (and the length of the hydroxyalkyl side chains). This sequential addition of propylene oxide makes it necessary that the products must be characterized by the degree of substitution DS and the degree of molar substitution MS. DS can not be higher than 3, what corresponds to the number of hydroxyl groups per glucose ring. The MS is the average number of substituents per cellulose repeat unit and can extend 3 [72][73][87].

The most important attribute of HPC and other cellulose ethers is its characteristic solubility. Solubility of cellulose ethers depends on the type of substituent, the degree of substitution and the distribution of the substituents along the cellulose chain. Elaborated synthesize methods allow to produce hydroxypropyl cellulose on a commercial scale with well defined distribution of the substituents, maximum degree of substitution (DS = 3) and molar substitution on a level not higher than 4. Hydroxypropyl cellulose with DS = 3 and MS = 4 has found many commercial application mostly as food and drug additive. On the list of additives currently permitted in food within the European Union, the HPC associated E number is E463.

It is used mostly as bulking agent (types of products used to prevent or treat constipation) and emulsifier (a surface-active agent that promotes the formation of an emulsion and prevent separation of product components to ensure consistency). The others application are: coating agent, film former, foaming agent, glaze, polish, stabilizer, surface-finishing agent, suspending agent, thickener and whipping agent stabilizer. HPC belongs to the group of medicines known as artificial tears. It is inserted in the eye to relieve dryness and irritation caused by reduced tear flow that occurs in certain eye diseases.

A number of studies of solid polymer electrolytes based on cellulose decorated with polyethyleneoxide side chains have already been reported. Preliminary investigations reported by LeNest et al. [88] of structures based on polysaccharides crosslinked with polyethylene oxide and grafted with polyether chains were followed by Schoenenberger's et al. [89] investigation of the structures involving cellulose on which oligoethers were grafted and crosslinked in various stoechiometries through urethane chemistry. Those structures had been achieved from hydroxyethyl cellulose. Esterification reactions were used to prepare cellulose based polymer-in-salt electrolytes first by Nishaburi [59] and later by Cowie et al. [60]. Esters were synthesized from cellulose acetate employing an acid anhydride with a catalyst or acid chloride in the presence of a tertiary base. Cowie et al. [58][60] have suggested hydroxypropyl cellulose as an alternative substrate. Reactions of acetylcellulose with p-toluenesulfonylated side chains were used successfully with different oligoethylene side chains in Nishaburi's dissertation [59]. Gel polymer electrolytes based on cellulose ester derivatives were studied as mixtures with propylene carbonate or propylene carbonate with ethylene carbonate and lithium salts [58]. Systems were characterized in terms of glass transition temperature, ionic conductivity and dynamic mechanical properties.

Cellulose ethers are another interesting group of cellulose derivatives. Several sorts of cellulose ether derivatives have been investigated in which alkyl side chain are involved [76][87][90-93]. The most often used method of synthesis starts from cellulose acetate and alkyl bromides in NaOH/DMSO like reported by Basque et al. [91]. Alternatively the group of Ritcey [87][93] have used hydroxypropyl cellulose activated either in anhydrous ethanol with NaOH or in a tetrahydrofuran - potassium tert-butoxide system. In both cases brominated side chain reagents have been used. Cellulose alkyl ethers were recognized as stable and homogenous ultrathin film forming materials when subject to the Langmuir-Blodgett technique.

In this work cellulose derivatives with oligoethyleneoxide side chains have been synthesized. Because of difficulties related to the solubility of raw cellulose, oligoethyleneoxide chains were grafted onto commercial hydroxypropyl cellulose from Aldrich. Besides good solubility another advantage of HPC is that all hydroxyl groups are secondary and thus of equal character. In the other cellulose derivatives the extent of substitution of hydroxyl groups may differ due to the different reactivity of primary and secondary hydroxyls.

The first part of this work concentrates on the synthesis of the cellulose ether derivatives with well-defined structure.

2.2 Hydroxypropylcellulose Derivatization

The grafting of the oligoethyleneoxide side chains was achieved via two synthetic methods. One starts from a bromide derivative (compound 2, Figure 8) and another makes use of the tosyl residue as a leaving group (compound 3, Figure 8). The side chain reagents were prepared form tri(ethylene glycol) monoethyl ether (compound 1, Figure 8) following the synthetic route presented in Figure 8:

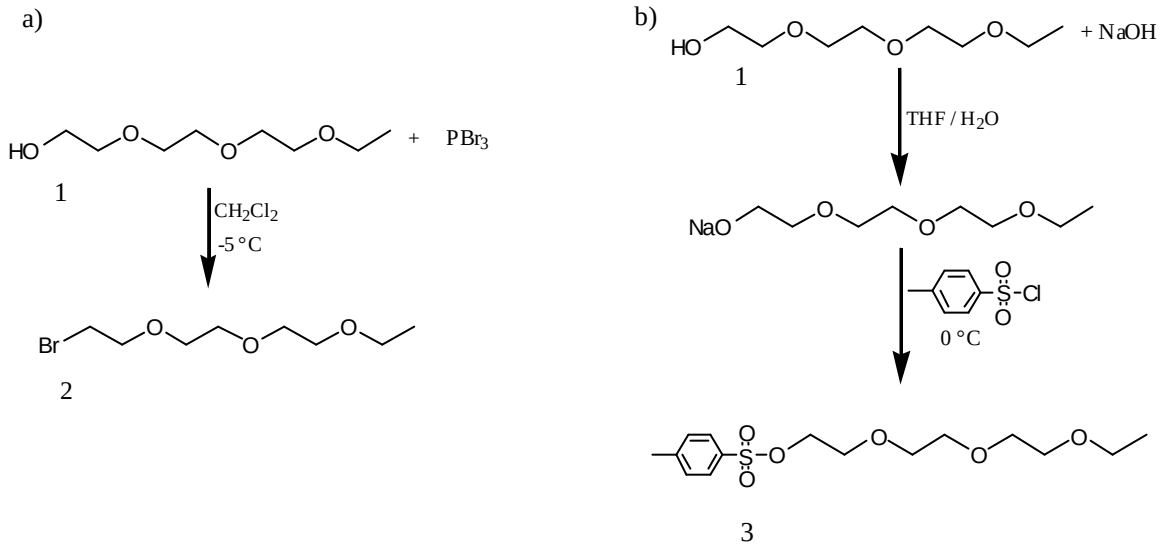

Figure 8. Preparation of oligoethyleneoxide chains
a) with PBr_3
b) with tosyl chloride

The possibility to employ α-epoxide compounds was ruled out, since the reaction of the epoxy group generates a new reactive site and further epoxide may be added at the same position. The resulting products possibly will have strongly irregular structures. The successful synthetic strategy was based on the following scheme (Figure 9):

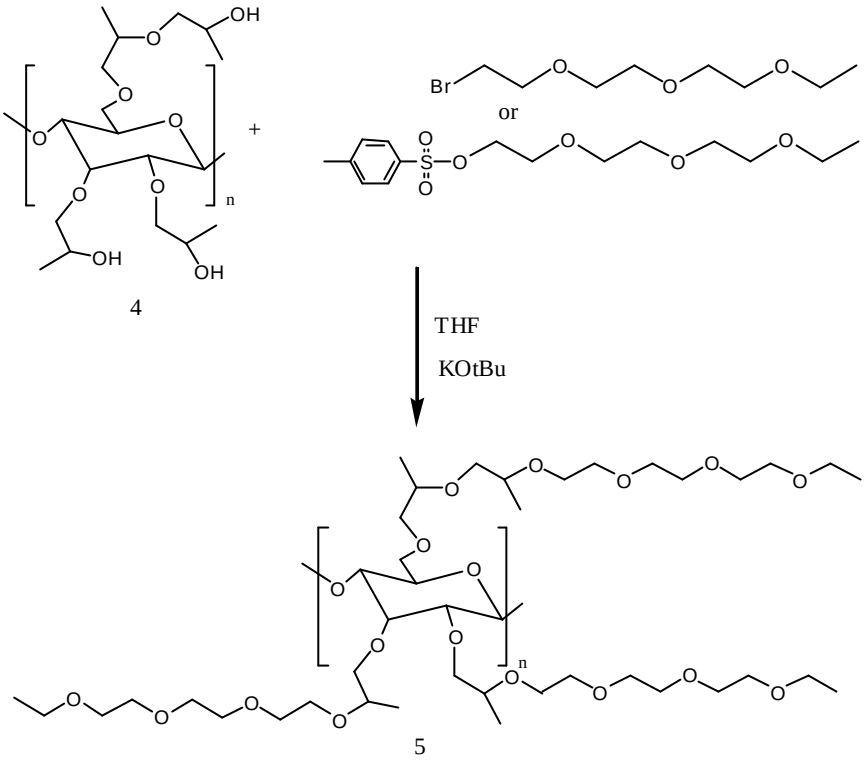

Figure 9. Hydroxylpropylcellulose derivatization reaction scheme.

The reaction mechanisms are similar for both cases. An oxonium ion is formed by the treatment of a functional secondary hydroxylpropyl group with the help of potassium cations, followed by substitution with ω-ethoxy-tris(oxyethylen). Similar reported recipes worked out by Nishaburi [59] and Ritcey [87] allowed to optimize the synthesis conditions. A four-molar excess of each reactant with respect to the hydroxyl groups was used. The products of the respective reactions were purified and the degree of substitution was determined. Higher efficiency of the substitution reaction, faster and easier side chain preparation methods entailed that for further studies the synthetic approach based on α-tosyl-ω-ethoxy-tris(oxyethylen) (compound 3, Figure 8) was chosen. A series of experiments have been done varying the conditions in order to minimize the reaction time, reagent excess, side reactions and to maximize the degree of substitution. The time of reaction, concentrations of the reactants, temperature and solvent were then varied to determine the best reaction procedure. It was found that the best parameters to reach the maximum degree of substitution of 2-hydroxypropylcellulose HPC (compound 4, Figure 9) are:

- reaction temperature:
    a) 25°C in the first step of the reaction
    b) 0°C in the second step

- sufficient excess of the side chain reagent equal to the excess of base: 110% in comparison to OH groups in HPC
- about 3 days reaction time.

The degree of substitution of the products varies between 2,8 and 3,0 as determined by NMR. The optimized synthesis economizes the use of the reagent, reduces the overall reaction time and facilitates the work up procedure.

A reduction of the reactant excess causes a lower degree of substitution and allows to synthesize ω-ethoxy-tris(oxyethylen) grafted 2-hydroxypropylcellulose, "PEO-HPC" (compound 5, Figure 9), with a known amount of unsubstituted hydroxyl groups. This attribute was made use of for the crosslinking reaction which is the content of the next chapter.

2.3 Crosslinking Methods

In order to crosslink the lithium ion conducting cellulose derivatives, the PEO-HPC (compound 5, Figure 9) with a degree of substitution of 2,8 was synthesised. The residual hydroxyl groups were used either directly for a crosslinking reaction with a modified diisocyanate or were used to attach the photocrosslinkable sites.

2.3.1 Thermally Inducted Crosslinking

The aptitude of isocyanates to undergo reactions with hydroxyl groups makes them very attractive for reactions with 2-hydroxypropylcellulose. The urethane chemistry was used for crosslinking in a large variety of cases. Petrovic et al. [94] reported in 1987 the work about networks obtained by cross-linking poly(propylene glycol) chains with a triisocyanate cross-linker. Gandini et al. [95] reported synthesis and characterization of the oxipropylated chitosan and their reaction with oligoether-based mono and di-isocyanate. The resulting networks, containing lithium salt, were investigated as polymer electrolyte. LeNest et al. used a similar approach reporting reactions of polysaccharides [88] and hydroxyethyl cellulose [89] with oligomeric polypropylene oxide monoisocyanates and polyethylene oxide diisocyanates. The products were tested in terms of film forming properties, three-dimensional topology, conductivity, mechanical and thermal properties. Gandini [96] studied the surface modification of various cellulose materials under heterogeneous conditions using different grafting agents bearing anhydride or isocyanate reactive groups. LeNest, Gandini and Pawlicka reported in 2000 and 2001 [57][97][98] the characterisation of polymer electrolyte obtained by a grafting reaction of hydroxyethyl cellulose with diisocyanates.

There are two ways to achieve isocyanate-terminated polyethers. The first one presented by LeNest, Gandini and Armand [96][99][100] leads to an diisocyanate by reacting the terminal primary amino group of a difunctional polyether (e.g. commercial Jeff amine) with bis(trichloromethyl)carbonate (commercial triphosgene). The reaction product is a corresponding polyether terminated with a -NCO group with the chain-extension in accordance to the chain-extension of the initial polyether. The second possibility is the reaction of polyether glycol with two molar excess of diisocyanate. In this work a THF solution of tri(ethylene glycol) was reacted with toluene-di-isocyanate (compound 6, Figure

10) in the presence of catalytic amounts of 1,4-diazabicyclo[2.2.2]octane (DABCO) (Figure 10).

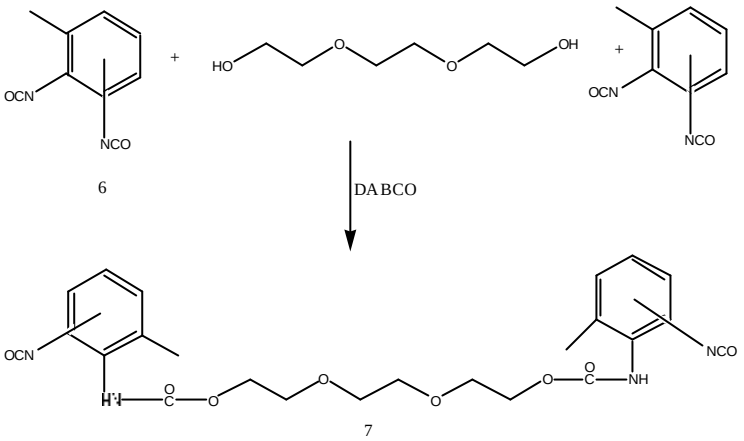

Figure 10. Diisocyanate crosslinking agent preparation

The diisocyanate crosslinking agent (compound 7, Figure 10) was added to a water free solution of PEO-HPC DS=2,8 (compound 5, Figure 9) in different ratios of the isocyanate group to unsubstituted hydroxyls. The crosslinking reaction is described in Figure 11.

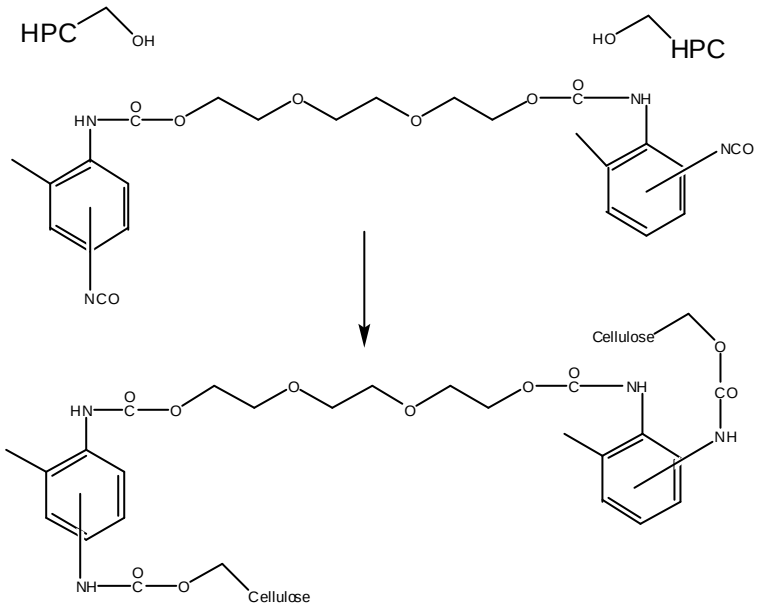

Figure 11. PEO-HPC DS=2,8 crosslinking with a diisocyanate reagent

2.3.2 Photo Inducted Crosslinking

The concept of using photosensitive moieties to crosslink polymeric materials was realized with N-substituted 3,4-dimethyl-pyrrole-2,5-dione (dimethylmaleimide; compound 8, Figure 12). Meier in his dissertation [77] successfully examined similar systems with cellulose ethers containing short alkyl (isopentyl) chains. Alternatively, useful photosensitive reactive groups like the cinnamoyl group or anthracene undergo some undesired and uncontrolled radical reactions, for instance photo initiated radical polymerisation and conversion with oxygen [101][102]. Moreover, cis / trans isomerisation reactions of the cinnamoyl residue influences the yield of the dimerisation reaction [77]. Coumarin reported by Lattes et al. [103] and Ramamurthy et al. [104] as well as cyclopropene derivatives reported by DeBoer [105][106] do not exhibit those disadvantages but their multistep synthesis makes them unattractive for applications. The possibility of crosslinking via thermally initiated Diels-Alder reactions in which an alkene adds to a 1,3-diene to form a 6-membered ring [107-110] was excluded because of much lower reactivity and reversibility in some cases [111]. The 3,4-dimethyl-pyrrole-2,5-dione group (compound 8, Figure 12) undergoes irreversible [2+2] cycloaddition reactions with high yield without side reactions (Figure 12). It is assumed that the response of the 3,4-dimethyl-pyrrole-2,5-dione group attached to a polymer does not differ from the behaviour of its low molecular counterparts [77][112-115]. The stereochemistry of the reaction is dependent on the environment (solution / bulk; type of solvent etc.) but the cis-anti-cis configuration in the product is preferred (compound 9, Figure 12). The N-substituted 3,4-dimethyl-pyrrole-2,5-dione group photodimerization is induced by UV light coming from e.g. a low-pressure mercury lamp.

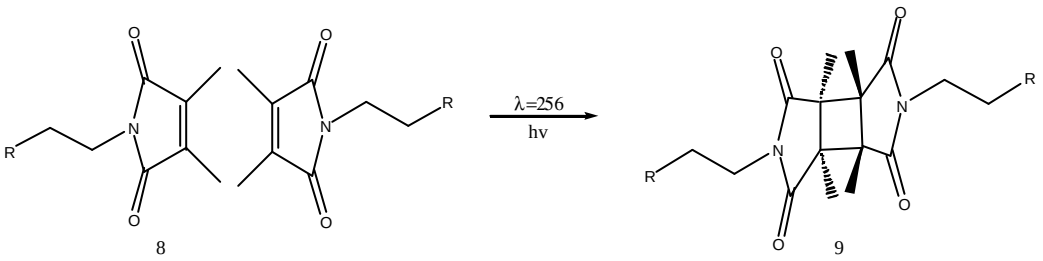

Figure 12. Photodimerization of N-substituted 3,4-dimethyl-pyrrole-2,5-dione

In order to combine the photosensitive moieties (compound 8, Figure 12) with a cellulose backbone the PEO-HPC (compound 5, Figure 9) with DS=2,8 were synthesized. The residual

free hydroxyl groups were used to introduce the 3,4-dimethyl-pyrrole-2,5-dione via N-attached spacers: propyl and ethoxyethyl. The alkyl substituents were synthesized from 3-aminopropyl-bromide hydrobromide (compound 10, Figure 13) and 2,3-dimethylmaleic anhydride (compound 11, Figure 13) resulting in 1-(3-bromo-propyl)-3,4-dimethyl-pyrrole-2,5-dione (compound 12, Figure 13).

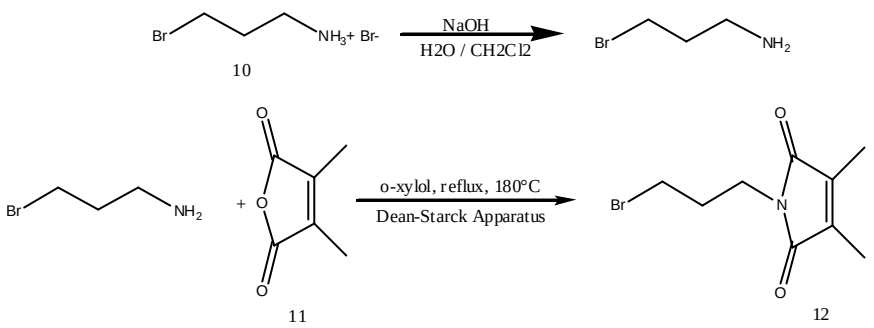

Figure 13. 1-(3-bromo-propyl)-3,4-dimethyl-pyrrole-2,5-dione preparation way.

The ethoxyethyl spacer was introduced starting from 2-ethoxyethanol. The two step synthesis starts with the preparation of 1-(2-ethoxyethanol)-3,4-dimethyl-pyrrole-2,5-dione (compound 14, Figure 14) from 2-(2-aminoethoxy)-ethanol (compound 13, Figure 14) and 2,3-dimethylmaleic anhydride in o-xylene. A Dean-Starck apparatus was used in order to remove the reaction water. The yield of this reaction was up to 100%. Afterwards, 1-(2-ethoxyethanol)-3,4-dimethyl-pyrrole-2,5-dione was converted in to 1-[2-(2-Bromo-ethoxy)ethyl]-3,4-dimethyl-pyrrole-2,5-dione (compound 15, Figure 14) by the reaction with phosphorus tribromide. (Figure 14).

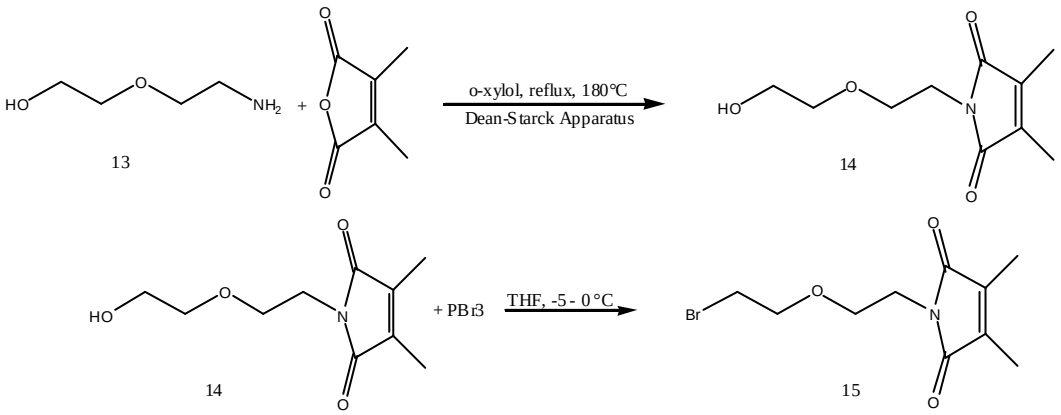

Figure 14. Synthesis of 1-[2-(2-Bromo-ethoxy)ethyl]-3,4-dimethyl-pyrrole-2,5-dione.

Compounds 12 and 15 (Figure 15) were further reacted under the conditions of Williams-ether synthesis with PEO-HPC DS=2,8. In the Williams ether synthesis, an alkoxide reacts with an alkyl halide to give an ether (Figure 15).

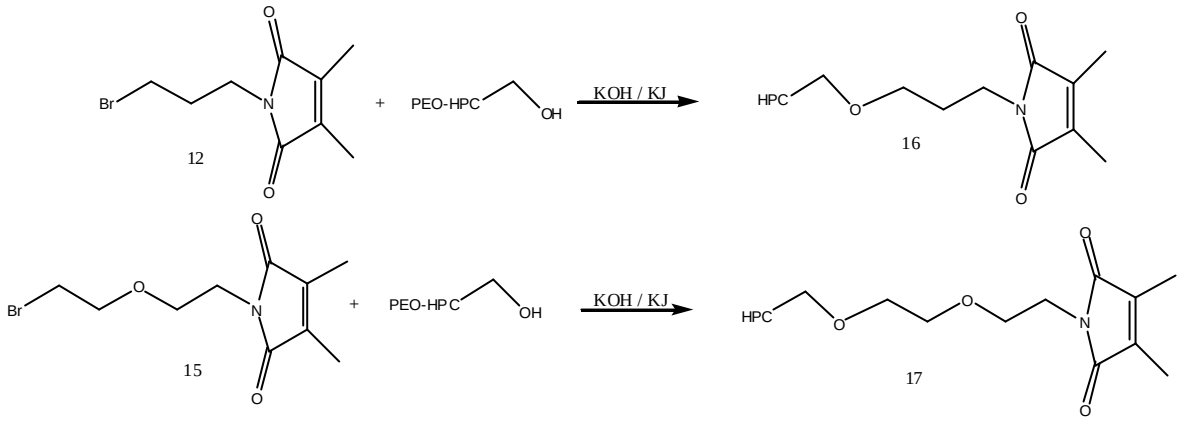

Figure 15. Cellulose grafting with crosslinking species

The crosslinking reaction takes place when the sample is exposed to UV light. In order to monitor the photocrosslinking reaction the compound 17 (Figure 15) was spin coated as a thin film and exposed to the low-pressure mercury lamp light (254 nm). The change in UV absorbance as depending on irradiation time is recorded in Figure 16.

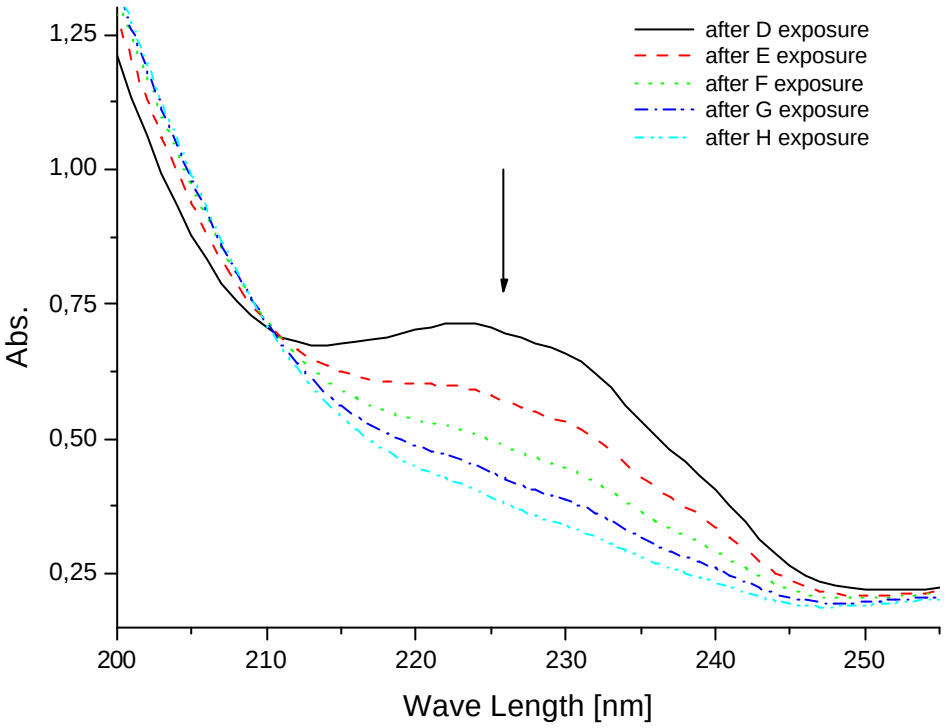

Figure 16. Change of the UV spectra of a spin coated film of sample 17 if exposed to the light of a low pressure mercury lamp as depending on irradiation time.

The absorption of the 3,4-dimethyl-pyrrole-2,5-dione group occurs between 210 and 240 nm. Notably visible in Figure 16 is the depletion of the peak intensity with irradiation time. The slight adsorption increase on the spectra margin (region 200 nm – 210 nm) comes from the photodimerization product. At 211 nm an isosbestic point appears. The appearance of an isosbestic point during a chemical reaction is evidence that there are only two absorbing species present at a constant total concentration. Moreover the isosbestic point proves that the reaction goes directly from educt to product from the 3,4-dimethyl-pyrrole-2,5-dione group to the photodimerization product. The change in absorption intensity of the peak in the region 210 nm – 250 nm is presented in terms of peak integration decrease (Figure 17).

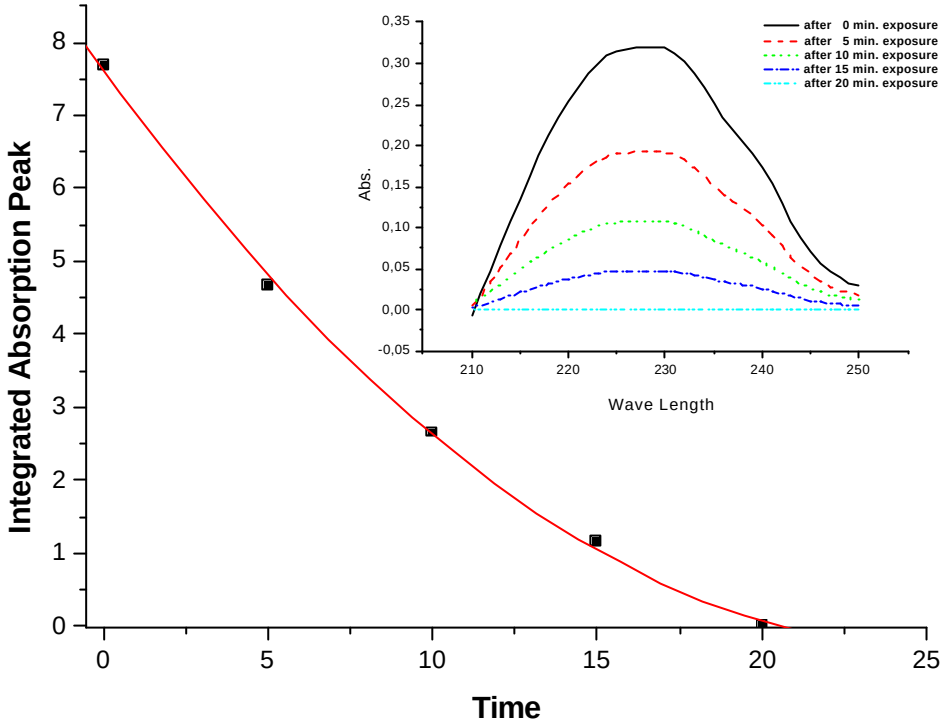

Figure 17. Change of the peak integration (210 nm – 250 nm) in UV spectra of a spin coated film of sample 17 if exposed to the light of a low pressure mercury lamp as depending on irradiation time.

The reaction rate deducted from the absorption peak area changes, and seems to be the highest in the first 5 minutes of UV light curing and decreases with time. The concentration of the dimethylmaleimide end-capped substituents is highest on the beginning and decreases with the reaction progress. With increasing irradiation time and decreasing concentration of the reactant the reaction speed decreases. Because of immobilization of the photoactive reactants, though attached to PEO-HPC, the complete conversion is impossible.

3. Characterization of ω-Ethoxy-tris(oxyethylen) Grafted 2-Hydroxypropylcellulose

3.1 Structure Characterization

Since the substituent distribution in addition to the total degree of substitution (DS) or the molar substitution (MS) is expected to influence the properties of the resulting cellulose derivatives, it is of a great importance to develop an analytical method to provide for precise information on the substituent distribution by means of a facile and reliable procedure. The ether derivative of HPC investigated in this work was synthesized with the Williamson reaction in a way which does not allow to attach more than one substituent to the same hydroxyl group. Therefore PEO-HPC MS is equal to DC and can not overcome 3. The average degree of substitution has a large effect on the properties of PEO-HPC and therefore is the factor of paramount importance to be characterized.

3.1.1 Chemical methods

Several attempts have been made to evaluate DS in cellulose derivatives. The first efforts have been based on the chemical activity of the cellulose hydroxyl groups. Rickert in 1978 [116] developed a chemical method generally based on the reactivity of the remaining hydroxyl groups of cellulose derivative with respect to tosylation with p-toluenesulfonyl chloride, followed by iodination with sodium iodide. Takahashi [117] reported tritylation of hydroxyl groups with trityl chloride in the presence of pyridine. These chemical methods are laborious, time-consuming and relative in contrast to the absolute methods based on nuclear magnetic resonance (NMR) [75][118].

3.1.2 NMR

The NMR has been established as an element-selective quantitative method suitable to study the polymer electrolytes. Vincent [119] applied NMR technique to study crystallinity, Stevens et al. [120], Scrosati et al. [121] and Armand et al. [122] investigated the ionic dynamics, Armand et al. [123] [124] qualify diffusion coefficients, Johansson [125] measured polymer chain mobility within the SPEs. NMR is an effective technique for obtaining information about ionic motions (thorough the ^{7}Li [97][126] and ^{19}F [126] resonance) and polymer chain dynamics (thorough the ^{1}H [97][98][126] resonance) since it is sensitive to the effects that such motions have on the nuclear spin-relaxation rates. Stevens et al. [120], Scrosati et al. [121] and Armand et al. [122] measurements of these relaxation rates as a function of temperature have been used to study the correlation between the cationic and the polymer chain segmental motions in SPEs.

For NMR studies on cellulose and cellulose derivatives ^{1}H-NMR and ^{13}C-NMR spectroscopy have been used [73][127]. In this work all nuclear magnetic resonance measurements have been carried in solution. In ^{1}H–NMR spectroscopy the intensity of the resonance signal corresponds to the number of hydrogen nuclei in the sample giving rise to that signal. The position of a specific resonance signal in the spectrum is determined by the type of the chemical binding, position and environment of the hydrogens in the chemical compound. Experience has shown that, due to relatively small energy differences, the resonance

frequencies of all differently bound hydrogens are positioned in a relatively narrow range of 20 ppm [73][128]. Nehls et al. [129] reviewed the use of ^{13}C-NMR to investigate cellulose and its derivatives in the liquid phase. They discussed the advantages of the use of ^{13}C rather than ^{1}H-NMR spectroscopy for the characterization of soluble cellulose derivatives. In principle, the two techniques should yield equivalent information but in practice the ^{1}H-NMR spectra of polymers often consist of broad overlapping peaks owing to enhanced dipolar interactions resulting from hindered isotropic motion within the molecule. The effect is much less in the case of ^{13}C-NMR and, in addition, the chemical shift is greater [130]. ^{13}C-NMR spectroscopy allow the same information for the ^{13}C nuclei of the investigated compound to be deduced from the signal intensity and signal position. The information coming from signal intensity has to be considered differently from the ^{1}H analogue because the intensity depends on several factors which influence the relaxation process. The reduced natural occurrence of carbon and reduced sensitivity causes that differences are much bigger in the ^{13}C than in case of ^{1}H resonances. The chemical shift signals registered in ^{13}C-NMR experiments are reaching up to 230 ppm.

The application of NMR techniques to cellulose and its derivatives often gives rise to specific difficulties. The most common is the poor solubility of the cellulose in solvents conventionally used in NMR investigations. This is not true for the cellulose ethers discussed here. HPC itself and the derivatives received from there are easily soluble in most common solvents. The relatively high viscosity of solutions of cellulose derivatives even at low concentration limits the free molecular motion and gives rise to broader resonance signals and limited resolution. Moreover, the protons in the cellulose molecules either being part of hydroxyl or acetal functions or bound to carbinol carbons are quite similar in their response and thus show similar chemical shifts [73]. In spite of such difficulties NMR analysis of 2-hydroxypropylcellulose has been reported by Bannister, Davies, Ward and MacIntyre [131]. Information about the degree of substitution was obtained on the basis of $^{13}CH_3$ and $C^{1}H_3$ chemical shifts. Similarly, in this work NMR was used for determining the degree of substitution of PEO-HPC. The position of the resonance signal in a ^{1}H–NMR spectrum is determined by the type of the chemical binding, the position and the environment of the protons in a chemical compound. The measured area under the signal curve, allows the number of hydrogen nuclei in resonance to be deduced. Knowing that, the DS determination of PEO-HPC is based on the intensities of the resonance signals ratio of -CH_3 (Number 1 and 2, Figure 18) and all other hydrogens in the ^{1}H-NMR spectra. The molecular structure and ^{1}H–NMR spectrum of the PEO-HPC measured in deuterated chloroform are presented in

Figure 18. The numbers of resonance signals correspond to the proton numbers as marked on the molecular structure below.

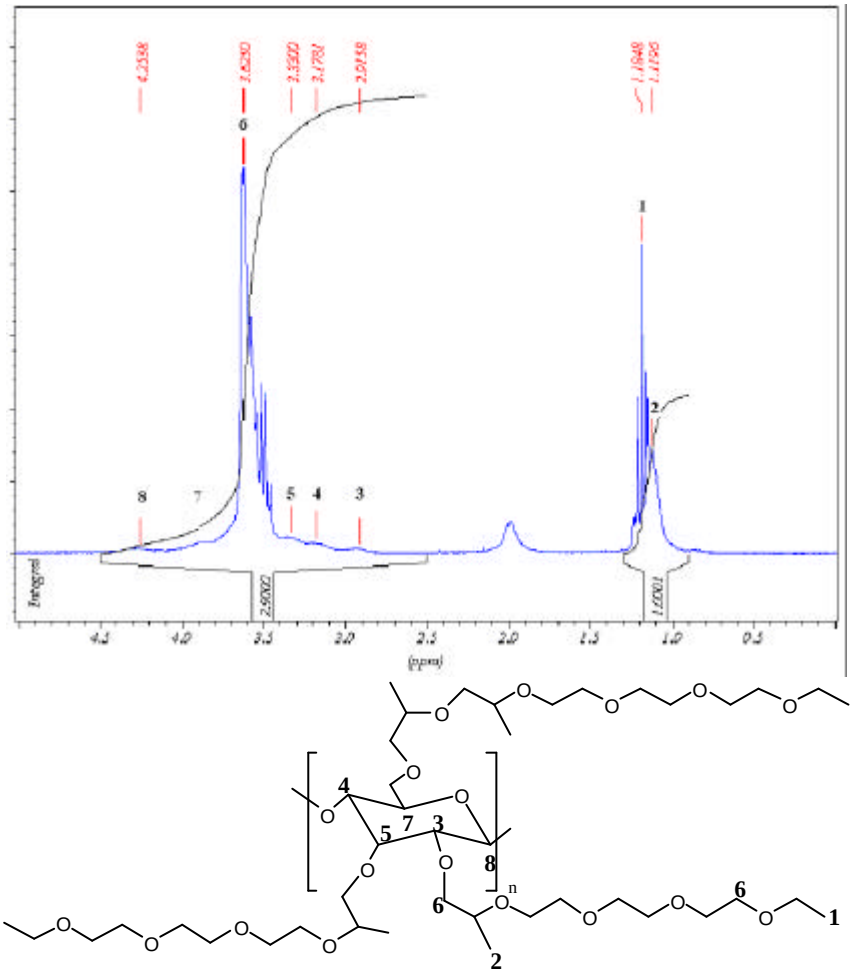

Figure 18. ^{1}H–NMR spectrum in $CDCl_3$ and molecular structure of the PEO-HPC.

Because of broad resonance signals and their very narrow separation the number of hydrogen resonances coming from -CH_2 groups and the cellulose molecule were assigned based on their integrated peak intensity in particular from 2,5 – 4,5 ppm. The -CH_3 signals coming from 2-hydroxypropyl substituents and ω-ethoxy-tris(oxyethylen) chains are easy to distinguish, but not separable. Firstly, the difference in the mobility of the groups has consequences for the shape of the signal, and secondly the position and environment of the protons in a PEO-HPC causes differences in the chemical shifts. The calculation of the DS was based on the integrated peak intensity of the resonance signals in the shift range from 0,9 – 1,3 ppm. The established method for DS calculation is based on the ratio of the integrated peak intensity of the –CH_2 and –CH_3 signals in the ^{1}H-NMR spectra. Based on the calculated theoretical values (Table 4) a function for the dependence of the signal intensity ratio and DS

has been found (Figure 19). The theoretical values were calculated based on molecular structures of HPC, PEO-HPC DS=1, PEO-HPC DS=2 and PEO-HPC DS=3. Additionally the general recipe for unrestricted DS=n was formulated (Table 4).

	DS=0	DS=1	DS=2	DS=3	DS=n
	HPC	HPC+1 side chain	HPC+2 side chains	HPC+3 side chains	HPC+n side chains
Amount H from CH_2	19	19+14	19+2*14	19+3*14	19+n*14
Amount H from CH_3	12	12+3	12+2*3	12+3*3	12+n*3

	Peak ratio
HPC deriv. DS=0	1,583
HPC deriv. DS=1	2,200
HPC deriv. DS=2	2,611
HPC deriv. DS=3	2,905

Table 4 Theoretical values of the integrated peak intensity ratio based on the number of protons provided.

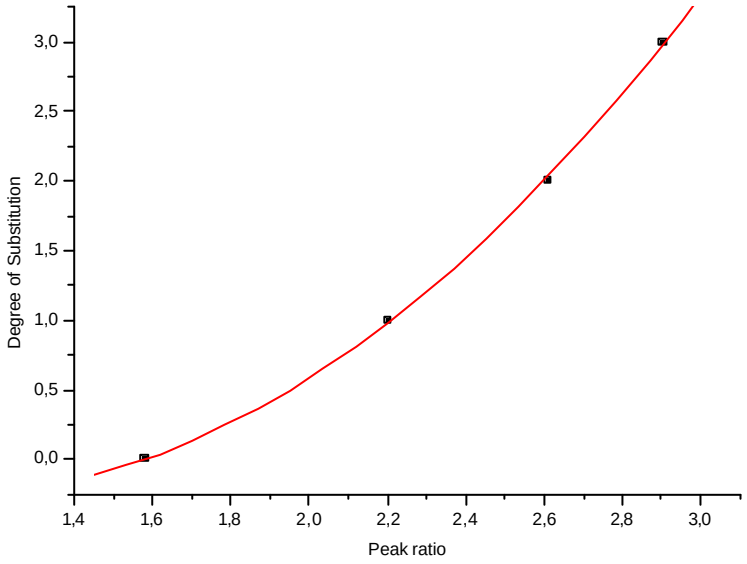

Figure 19. Degree of substitution as related to the integrated peak intensity ratio.

The function for the dependence of the signal intensity ratio and DS (Figure 19) has been found with a polynominal fit. The polynominal fit is the method that compute the coefficients of the polynomial that best fits the input data in a least squares sense. The relation has been found to be:

$$Y = 1,58 + 0,68*X - 0,08*X^2$$

where X is the peak ratio and Y is the DS.

In order to prove the precision of the analytical method five samples of the same product were prepared and measured. The ratios of the integrated peak intensities in the shift range 2,5-4,5 and 0,9-1,3 were calculated. An average value of 2,76 was obtained. The error value found with the least squares method is on an acceptable level of ± 0,03, corresponding to 1,4 % (Figure 20. upper points, Table 5). Method was used for the DS determination of all samples.

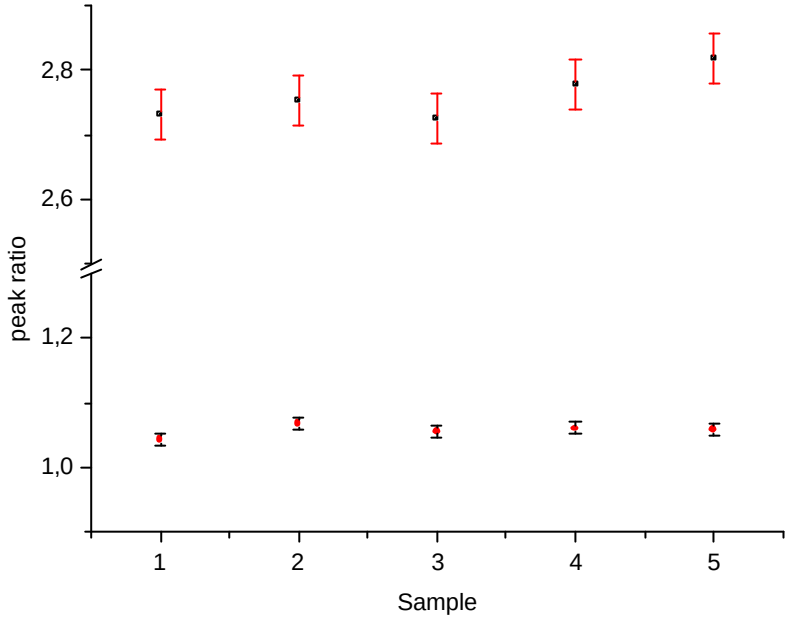

Figure 20. Peak integration relatio n and its variance:

? 2,5-4,5 / 0,9-1,3 Mean(Y)=2,76 sd(YEr±)=0,03

• 1,15-1,3 / 0,9-1,15 Mean(Y)=1,05 sd(YEr±)=0,01

	Ratios of the integrated peak intensities in the shift range:	
Sample	2,5-4,5 / 0,9-1,3	1,15-1,3 / 0,9-1,15
1	2,73	1,04
2	2,75	1,07
3	2,72	1,06
4	2,78	1,06
5	2,82	1,06
Average	2,76	1,06
Error	0,03	0,01

Table 5. Values of the peak integration relation and its variance.

Using the same measurements the precision of an alternative method based on the $-CH_3$ group signals was checked. The ratios of the integrated peak intensity in the shift range 1,15-1,3 and 0,9-1,15 were calculated. An average value of 1,05 was found which is bigger than the theoretically maximal value of 1,0. This is the consequence of broad resonance signals from the propyl $-CH_3$ group and the very narrow appearance of both peaks. This method was recognized as not confident enough (Figure 20, Table 5).

The analysis of the PEO-HPC ^{13}C–NMR spectrum presented in Figure 21 is more complicated. The signals of the cellulose ring carbon responses are weak or not visible at all. Only a small, broad peak around 74,9 ppm appears. To simplify the peak assignment a spectrum of the tri(ethylene glycol) monoethyl ether in the same solvent was recorded (Figure 22). The numbers of resonance signals corresponds to the carbon numbers as marked on the molecular structure. In the PEO-HPC the resonance signals coming from carbon in the side chain are shifted in comparison to the tri(ethylene glycol) monoethyl ether (Number 5 and 6, Figure 22). The high viscosity of HPC solutions is a serious limitation for the use of ^{13}C–NMR technique and precludes the recording of HPC spectra.

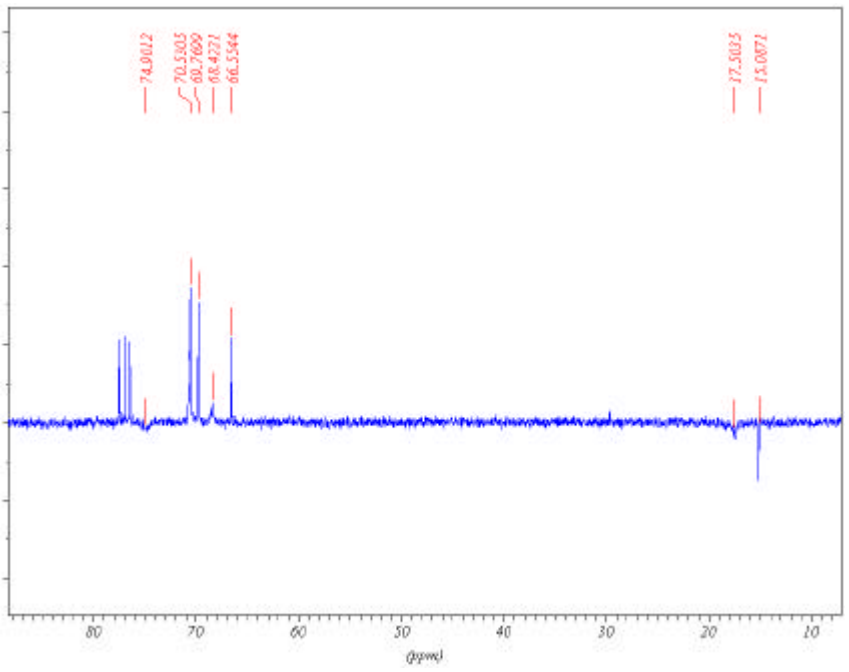

Figure 21. ^{13}C–NMR spectra of the ω-ethoxy-tris(oxyethylen) grafted 2-hydroxypropylcellulose in $CDCl_3$.

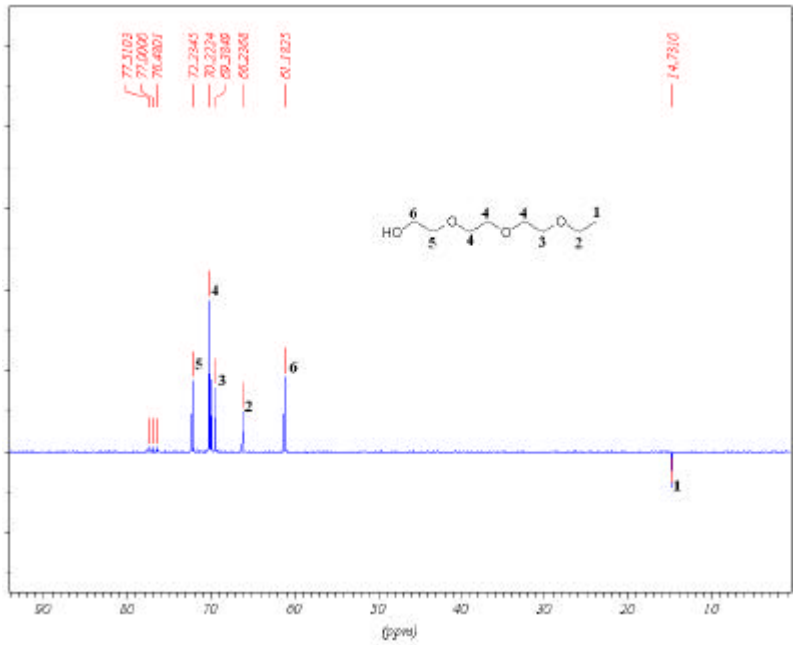

Figure 22. ^{13}C–NMR spectra of the tri(ethylene glycol) monoethyl ether in $CDCl_3$.

3.1.3 IR

In order to confirm a degree of substitution in PEO-HPC with a maximum DS=3, infrared spectroscopy measurements were performed additionally. The starting hydroxypropyl cellulose has secondary hydroxyl groups. These groups easily undergo exchange reaction in deuterated water according to the reaction scheme:

R-OH ? R-OD Equation 28

Such change in structure has consequences for the shape of the IR spectra. The hydroxyl groups absorb around 3000 – 2600 cm^{-1}. Deuteration shifts the hydroxyl absorption. The purified PEO-HPC was first analysed by IR, than dissolved in D_2O and stirred over night at room temperature. After solvent evaporation, the dried polymer was checked with IR again. The resultant spectra are presented in Figure 23.

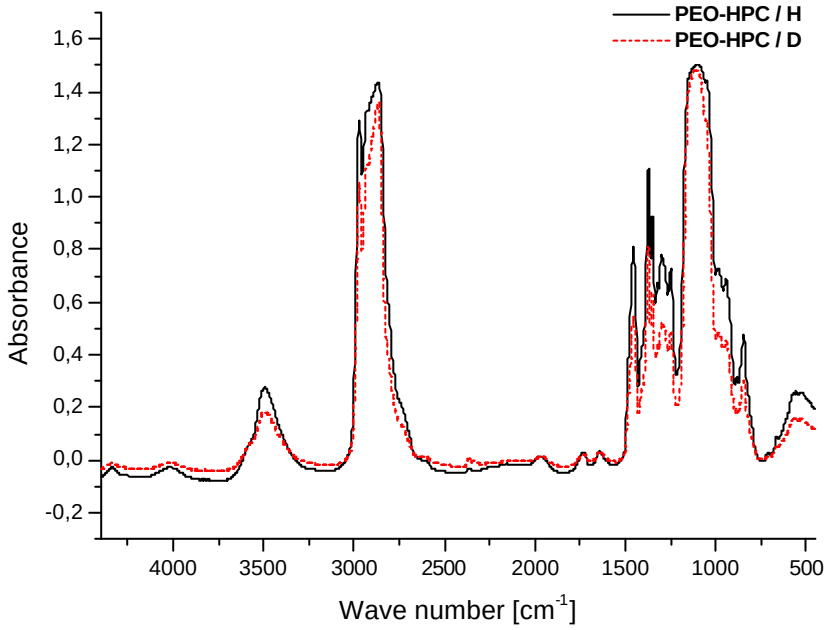

Figure 23. FT-IR spectra of PEO-HPC in the wave number range 4400 - 450 cm^{-1}

PEO-HPC / H : with potonated hydroxyl groups

PEO-HPC / D : with deuterated hydroxyl groups

Both spectra have the same peaks. The spectra are quantitatively identical. No exchange of oxygen/deuterium in the PEO-HPC was observed, what is a proof of the absence of free hydroxyl groups in final product.

3.2 Molecular Mass Determination

3.2.1 Gel Permeation Chromatography

The molecular weight of a particular macromolecule is a product of its degree of polymerization and the molecular weight of the repeating unit. The polymer molecular weight the average molecular weight of all macromolecules in question and is important because it determines its physical properties. Some examples include the temperatures for transitions from liquids to solids and mechanical properties such as stiffness, strength, viscoelasticity and viscosity. If molecular weight is too low, the transition temperatures and the mechanical properties will generally be too low for the polymer material to have any useful applications. For a polymer to be useful it must have mechanical properties sufficient to bear the design loads.

Two methods were employed in order to determine the average molecular weight of PEO-HPC. The first was gel permeation chromatography (GPC). The measurements were done in three different solvents: N,N-dimethylformamide (DMF), tetrahydrofuran (THF) and water. In all experiments the infrared (IR) detector was used and additionally, where possible, the ultraviolet (UV) detector. Measurements were done for the starting material (commercial HPC, Aldrich M_w=80.000) and for the fully substituted end product (PEO-HPC DS=3.0). Results are presented in Table 6.

	Solvent	Calibration	M_w IR detector	Polydispersity	M_w UV detector	Polydispersity
HPC	DMF	PEO	$1,5?10^5$	5,5		
PEO-HPC	DMF	PEO	$2,5?10^4$	3,3		
HPC	THF	PS	$9,3?10^4$	3,8		
PEO-HPC	THF	PS	$5,7?10^4$	3,9		
HPC	0,7mol NaCL in H_2O	PEO	$7,5?10^4$	2,8	$1,0?10^5$	4,7
PEO-HPC	0,7mol NaCL in H_2O	PEO	$9,0?10^4$	3,6	$6,1?10^4$	4,1

Table 6. Results of gel permeation chromatography of HPC and PEO-HPC.

The theoretical molecular weight of PEO-HPC with a degree of substitution DS=3 was calculated with the assumption that the starting HPC with M_w=80.000 does not undergo any degradation process in the substitution reaction. Its molecular weight is approximately 177.000 g/mol. The GPC measurement results listed above do not confirm this calculation. The molecular weight of PEO-HPC seems to vary from 25.000 up to over 90.000 for the same sample, depending on the solvent, calibration method and detector used. Similar irregularities are observed for the HPC with M_w=80.000 as well. Such problems can be caused by the specificity of the cellulose based polymers. The PEO-HPC may be considered as a so called polymer brush based on cellulose. The chemical structure and topology of the polymers used as GPC standards differ strongly from the investigated material. This is a general problem of the relative molecular weight measurement methods. Moreover, one can not exclude interaction or adsorption of the cellulose derivatives on the column packing material. The polydispersity of HPC and in consequence also of PEO-HPC seems to be higher than 3, what is in agreement with our expectations. However, the GPC elution behaviour depends on the molecular structure as well and in the case of PEO-HPC can be strongly influenced by it.

3.2.2 Other methods

An other method of the molecular weight determination is dynamic light scattering (DLS). It is an absolute method for molecular weight determination. No calibration and standards are necessary. The only requirement is good solubility in solvents typically used for light scattering. The PEO-HPC with DS=3 was measured in THF, DMF and MeOH.
In all samples agglomerates were observed which made a proper molecular weight determination difficult or impossible.

The characterization of crosslinked materials by dynamic mechanical analysis and ultraviolet spectroscopy is described in the chapter 4.1 “Dynamic Mechanical Thermal Analysis”. The thermogravimetric and differential scanning calorimetry measurement results are discussed in chapter 4.2 “Thermal analysis”.

4. Experimental Results

The PEO-HPC itself is an insulating material like the great majority of polymers. The electrical conductivity in such kind of materials is caused by the mobility of charged species like ions in response to an electrical field. In common solid state conductors like metals, the charge carriers are electrons or holes and used to be described as electronic conductivity. Our target material belongs to the group of ionic conductors in which the electrical conductivity is due to the motion of ions which were brought into the material by blending the PEO-HPC with Li-salts. The conductivity s is defined as the product of the carrier charge (e±), its concentration (n) and mobility (m) and is expressed in [S/cm]. The type of cation, anion and salt concentration influences the ion-ion and ion-polymer interactions. Polyethylene oxide – alkali salt blends and their potential as solid electrolytes were first reported by Wright [132][26] and Armand [133][134]. Recently Wieczorek et al. [136][136] demonstrated the influence of the alkali metal type as well as salt concentration on the conductivity of the polymer blends. It has been demonstrated that either at low or high salt concentration the conductivities of lithium ion based electrolytes are considerably higher than those based on other alkali metal ions. This is important since lithium was recognized as the best alkali metal for rechargeable batteries. Conductivities of solutions of lithium thiocyanates in low molecular weight liquid copolymers of ethylene oxide and propylene oxide have been measured by Cameron et al. [137]. The conductivity curves as function of the salt concentration show well defined maxima at salt concentrations situated in the range 0,8 – 0,12 [Li]/[O]. Moreover, the conductivity is independent of polymer molecular weight but is enhanced by raising the ethylene oxide content in the copolymer [137][59].

One of the most commonly used lithium salt in polymer-salt blends are lithium trifluoromethane sulfonate ($LiCF_3SO_3$) and lithium bis(trifluorosulfone) imide ($LiN(SO_2CF3)_2$). In this work additionally lithium tetrafluoroborate ($LiBF_4$) was investigated. The salts were mixed with the polymer in various concentrations. In the following the salt concentrations are given as the molar ratio [Li]:[O] of lithium to the total number of oxygen atoms present in the polymer repeat unit and vary from 0.02 up to 0.2. In order to obtain a homogeneous distribution of salts in polymer matrix, the components were carefully dried and dissolved in freshly distilled, anhydrous THF. After few hours of stirring the solvent was quickly evaporated and the samples dried once again in a high vacuum at elevated temperature (70°C). The dry materials were used for the measurements.

4.1 Dynamic Mechanical Analysis

Having in mind the assignment of materials under investigation for all-solid-state batteries, the mechanical and viscoelastic properties are of crucial importance. The mechanical properties are a consequence of the chemical composition of the polymer and also of its structure at the molecular and supermolecular level.
The most useful technique for characterizing the viscoelastic properties of polymers is the dynamic mechanical analysis (DMA).

Dynamic mechanical properties refer to the response of a material as it is subjected to a periodic force. These properties may be expressed in terms of a dynamic modulus, a dynamic loss modulus, and a mechanical damping term. Typical values of dynamic moduli for polymers range from 100 kPa to 100 GPa (10^6-10^{12} dyne/cm^2) depending on the type of polymer, temperature, and frequency.
For an applied stress varied sinusoidally with time, a viscoelastic material will respond with a sinusoidal strain for low amplitudes of stress. The sinusoidal variation in time is usually described as a rate specified by the frequency (f = Hz; w =rad/sec). The strain of a viscoelastic body is out of phase with the stress applied, by the phase angle, d . This phase lag is due to the excess time necessary for molecular motions and relaxations to occur. Dynamic stress, s , and strain, e , given as:

$$s = s_0 \sin(wt + d) \qquad \text{Equation 29}$$

$$e = e_0 \sin(wt) \qquad \text{Equation 30}$$

where w is the angular frequency. Using this notation, stress can be divided into an “in-phase” component ($s_0 \cos d$) and an “out-of-phase” component ($s_0 \sin d$) and rewritten as,

$$s = s_0 \sin(wt)\cos d + s_0 \cos(wt)\sin d \qquad \text{Equation 31}$$

Dividing stress by strain to yield a modulus and using the symbols E´ and E´´ for the in-phase (real) and out-of-phase (imaginary) moduli yields:

$$s = e_0 E' \sin(wt) + e_0 E'' \cos(wt) \qquad \text{Equation 32}$$

$$E' = \frac{s_0}{e_0}\cos d \qquad E'' = \frac{s_0}{e_0}\sin d \qquad \text{Equation 33}$$

$$e = e_0 \exp(iwt) \qquad s = s_0 \exp(wt + d)i \qquad \text{Equation 34}$$

$$E^* = \frac{s}{e} = \frac{s_0}{e_0}e^{id} = \frac{s_0}{e_0}(\cos d + i\sin d) = E' + iE'' \qquad \text{Equation 35}$$

Equation 35 shows that the complex modulus obtained from a dynamic mechanical test consists of "real" and "imaginary" parts. The real (storage) part describes the ability of the material to store potential energy and release it upon deformation. The imaginary (loss) portion is associated with energy dissipation in the form of heat upon deformation. The above equation is rewritten for shear modulus as,

$$G^* = G' + iG'' \qquad \text{Equation 36}$$

where G' is the storage modulus and G'' is the loss modulus. The phase angle d is given by:

$$\tan d = \frac{G'}{G''} \qquad \text{Equation 37}$$

The storage modulus is often associated with "stiffness" of a material and is related to the Young's modulus, E. The dynamic loss modulus is often associated with "internal friction" and is sensitive to different kinds of molecular motions, relaxation processes, transitions, morphology and other structural heterogeneities. Thus, the dynamic properties provide information at the molecular level to understanding the polymer mechanical behaviour.

An alternative representation of Equation 35 is often used in the study of polymer melts and solutions. Such materials are more fluid than solid and it is convenient to divide the stress by strain rate $\dot{e}$ and not strain e. The complex dynamic viscosity h^* is defined as [140]:

$$h^* = h' - ih'' = \frac{s}{\dot{e}} \qquad \text{Equation 38}$$

where $\dot{e} = e_0 w \sin(wt)$. Equation 39

Due to the viscoelastic nature of polymeric materials, the analysis of their long-term behaviour is essential. For a viscoelastic polymer, the modulus is known to be a function of

time at a constant temperature. The modulus is also a function of temperature at a constant time. According to this time-temperature correspondence, long-term behaviour of a polymer may be measured by two different means. First, experiments for extended periods of time can be carried out at a given temperature, and the response measured directly. This technique becomes increasingly time consuming due to the long response times of many polymers. The second method takes advantage of the principles of time-temperature correspondence wherein experiments are performed over a short time frame at a given temperature, and then repeated over the same time frame at another temperature. The two methods are equivalent according to the principles of time-temperature superpositioning.

These principles for studying long-term behaviour of polymers have been well established by Williams, Landel, and Ferry. The methods of time-temperature superpositioning (i.e. reduced variables) are used to accelerate the mechanism of a relaxation or molecular event by either increasing the temperature or increasing the stress, in the experiment.

By scanning the temperature during a DMA experiment phase transitions can be observed and in addition the T_g can be determined. The detection of other processes such as g and b relaxations in the glassy region is also possible.

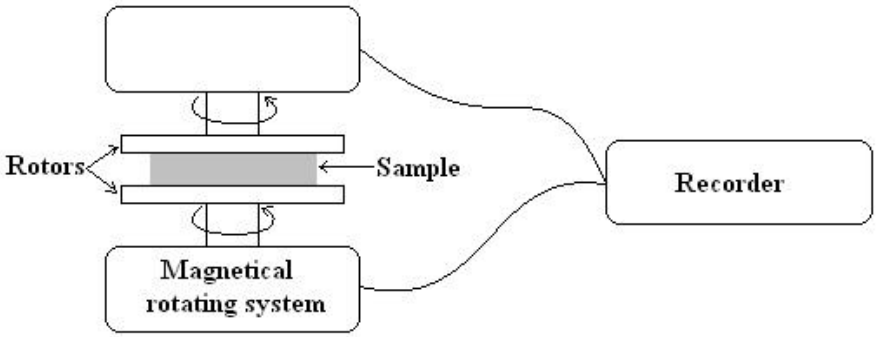

Figure 24. Parallel plate rheometer.

The samples were prepared in form of cylindrical tablets with a diameter of 6 and a height of 2 mm. The sample is sandwiched between two parallel circular surfaces and the sample chamber is filled with nitrogen gas. A magnetically suspended rotating system applied the torque with the demand angular frequency on one side of the sample, hence the rotor touching the sample on the other side moves with a phase shift (Figure 24). The resulting deformation and parameters are recorded and evaluated.

Firstly two samples were investigated in order to find out the viscoelastic characteristics of PEO-HPC and its blend with $LiN(SO_2CF_3)_2$.

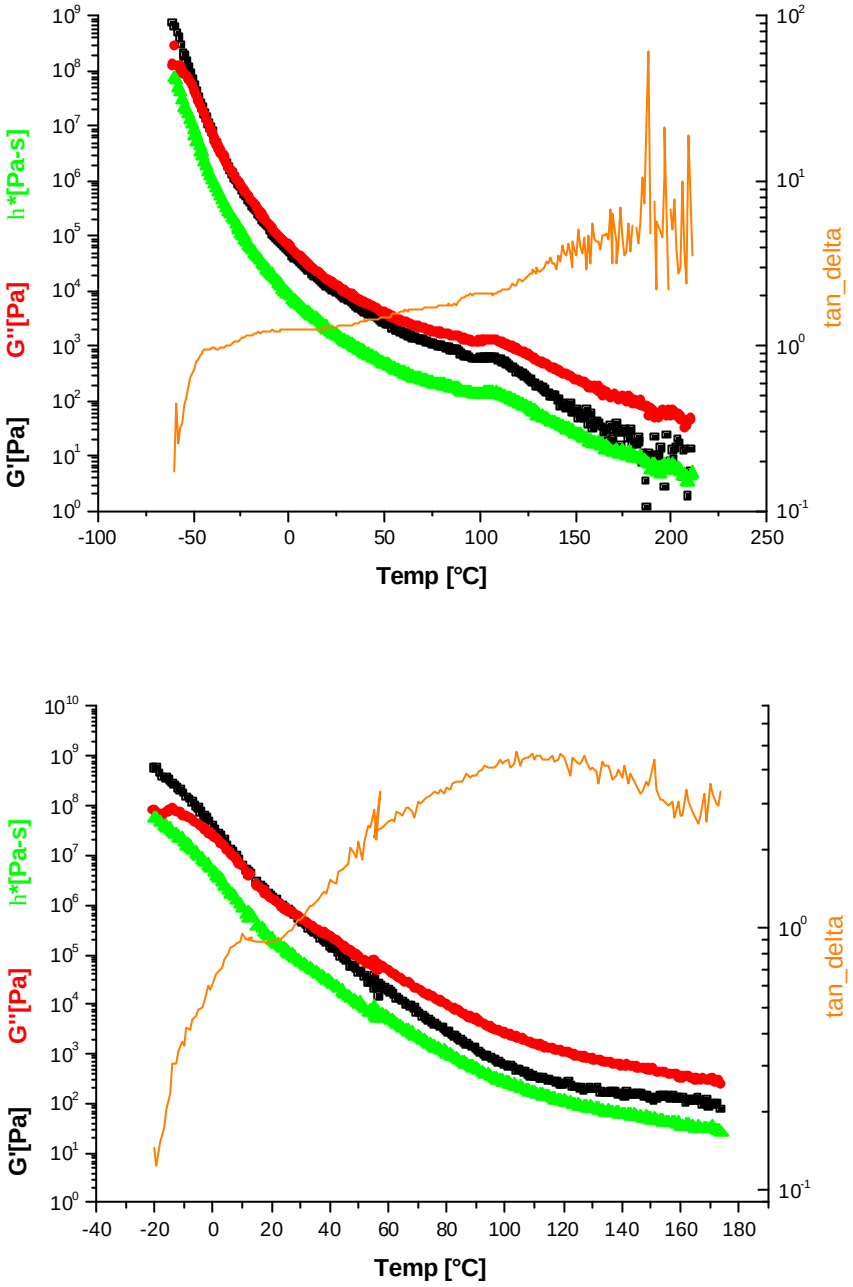

Figure 25. DMA of PEO-HPC DS=2,8

a) pure

b) with $LiN(SO_2CF_3)_2$ [Li]/[O]=0,09

In Figure 25 the storage modulus G', the loss modulus G'', the complex viscosity h^* and the loss tangent (tan_delta) are presented. The measurements were done in a temperature ranges starting shortly above T_g, that results in the negative slope of modulus, loss modulus and the complex viscosity. The subsequent gradual decrease of the parameters with increasing temperature give evidence of the liquid like nature of the materials under investigation.

Aiming at the improvement of the mechanical properties two crosslinking methods were tried. The chemical background of the processes is described in the chapter 2.3 “Crosslinking methods”.

The modified diisocyanate based crosslink agent was tested in four concentrations of 2:1, 1:1, 2:3 (1:1,5) and 1:2 calculated as the ratio of free hydroxyl groups in PEO-HPC to the isocyanate groups in diisocyanate crosslink agent. Figure 26 gives the results of the DMA investigation of PEO-HPC DS=2,8 / $LiN(SO_2CF_3)_2$ / diisocyanate crosslinker ; [Li]/[O]= 0,098 ; [OH]/[NCO]=2:3 blend.

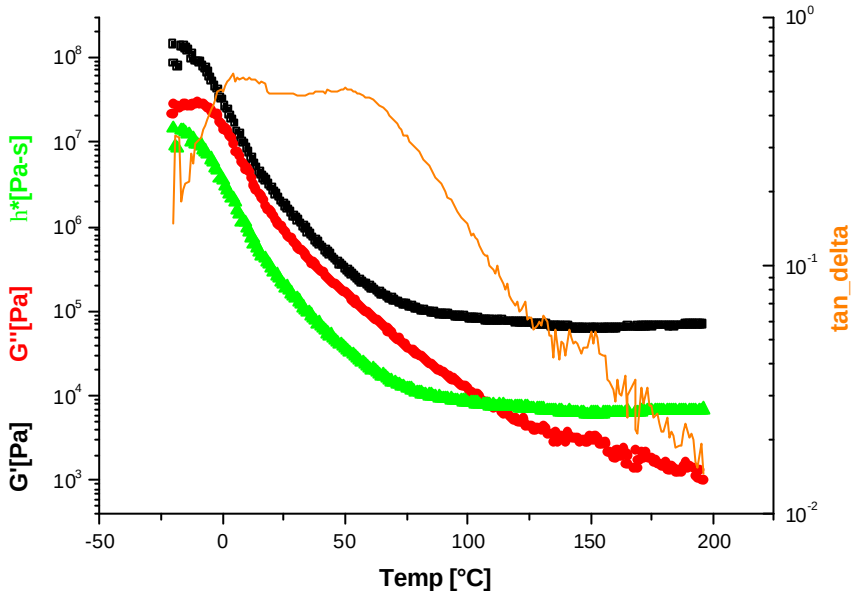

Figure 26. DMA of PEO-HPC DS=2,8 / $LiN(SO_2CF_3)_2$ / Diisocyanate crosslinker ; [Li]/[O]= 0,098 ; [OH]/[NCO]=2:3 blend.

The measurement was started at –20 °C and carried out up to 200 °C. In the lower temperature range (up to ~25 [°C]) G’, G’’ and h^* show similar characteristics as compared to the uncrosslinked samples. At elevated temperatures the initially negative slope of the modulus and of h^*, runs out into a plateau. This demonstrates that the materials are crosslinked. The storage modulus of polymer, polymer with salt and after croslinking is presented in Figure 27.

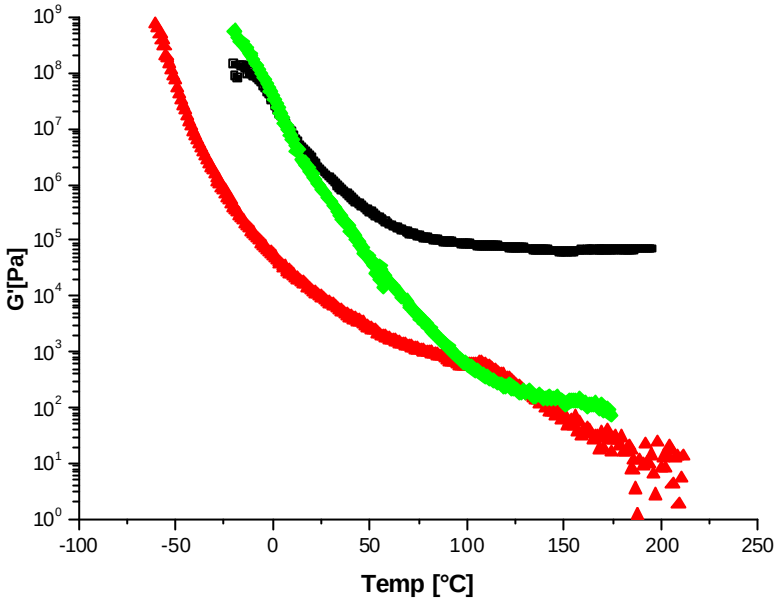

Figure 27. The G' of polymer, polymer with salt (blend) and crosslinked polymer blended with salt:

? G'[Pa] PEO-HPC DS=2,8

? G'[Pa] PEO-HPC DS=2,8 [Li]/[O]=0,098

¦ G'[Pa] PEO-HPC DS=2,8 / $LiN(SO_2CF_3)_2$ / Diisocyanate crosslinker ; [Li]/[O]= 0,098 ; [OH]/[NCO]=2:3 blend.

It is clearly visible that the presence of salt enhances the modulus of the blend at low temperatures but does not change its liquid character generally (the curves appear near each other at higher temperatures and presents typical flow behaviour). On the other side the crosslinked material has a T_g on the same level like the uncrosslinked material with the same lithium salt concentration, which results in the almost identical conducting characteristics (see chapter 4.3.2 "Conductivity from Impedance Spectroscopy"). The only but crucial difference is the change from liquid, to rubbery character in the crosslinked material giving rise to a G' plateau around 10^5 GPa over the entire temperature range from 50 to almost 200°C. This is very important for the application of this material as separator membrane.

4.2 Thermal Analysis

The PEO-HPC with DS=3 and its blends with lithium salts was investigated with thermogravimetric (TGA) and differential thermal analysis (DSC). The ability of the material to cope with temperature and glass transition temperature T_g were checked and discussed. Because of the hygroscopic character of the oligoethylen oxide chains and Li-salts, samples were carefully dried before the measurements. The presence of water in a measured materials could give rise to misstatement in samples weighting that has consequences in wrong specific heat capacity determination and changes the shape of thermal analysis curves. It typically has a strong influence on T_g as well.

The glass transition temperature is the main characteristic temperature of the amorphous state. A liquid becomes a solid at cooling over the glass transition temperature. The microscopic process involved is the freezing of large-scale molecular motion without change in structure. Since the heat capacity of the glass is always lower than that of the corresponding liquid at the same temperature, and since there is no latent heat in stopping molecular motion, the glass transition is a thermodynamic second-order transition. The freezing of molecular motion is time dependent, so that the glass transition occurs at a recognizable transition temperature because of a rather large temperature dependence of the relaxation time for large-scale molecular motion in the glass transition region [138].

The thermogravimetric analysis (TGA) is defined as a testing procedure in which changes in weight of a specimen are recorded as the specimen is exposed to a temperature program in a controlled atmosphere. During the experiment a sample is heated and weighed continuously. Thermograms provide information regarding polycondensation reactions, degradation, oxidation, evaporation or sublimation processes, the efficiencies of stabilizers and activators and the thermal stability of materials. This method allows to determine the water content in samples [139][140][141]. In a broad sense, a carefully controlled pyrolysis can also be considered as a qualitative or quantitative analytical method. The capability of the method for materials characterization can be greatly increased if techniques other than thermal are connected to the thermal analyzer to identify further either the residue or the effluent during a certain thermal event. Such technique would include various methods. In this work coupled thermogravimetry – mass spectrometry [142] was used. Thermal analysis with simultaneous evolved gas analysis describes the thermal event more precisely and completely.

DSC is an analytical method in which the specimen and an inert reference material are heated concurrently at a linear temperature rate, each having its own temperature sensing. The heat exchange of samples during heating/cooling cycles is monitored. The heat flow changes, either endothermic or exothermic, which occur in the course of heating, are plotted against temperature. The origin of the recorded heat exchange can either be physical or chemical in nature. As long as almost all chemical and structural changes are accompanied by energetic effects they are visible in DSC thermograms [143]. The thermograms provide data on the chemical and physical transformations that have occurred, such as melting, sublimation, glass transition, crystal transitions, and crystallization [139][144]. The differential thermal analysis gives information about specific heat. The specific heat c_p is the amount of heat which must be added per weight unit of a substance to raise the temperature by one degree. The molar heat C_p is the specific heat multiplied by the molar mass or molar mass of a structural unit in the case of polymers. Specific and molar heat may be defined at constant volume or constant pressure. The heat added causes a change in the internal energy U and in the enthalpy H of the substance. The following notations can be formulated [145]:

- specific heat at constant volume:

$$c_v = \left(\frac{\partial U}{\partial T} \right)_v \qquad [\text{J/kg·K}] \qquad \text{Equation 40}$$

- specific heat at constant pressure:

$$c_p = \left(\frac{\partial (U + pV)}{\partial T} \right)_p = \left(\frac{\partial H}{\partial T} \right)_p \qquad [\text{J/kg·K}] \qquad \text{Equation 41}$$

- molar heat at constant volume

$$C_v = Mc_v \qquad [\text{J/mol·K}] \qquad \text{Equation 42}$$

- molar heat at constant pressure:

$$C_p = Mc_p \qquad [\text{J/mol·K}] \qquad \text{Equation 43}$$

The first step in the thermal investigation of a new material is usually the preliminary thermogravimetric analysis. Such measurement done on PEO-HPC with DS=3 without any additives and with lithium salt, describes the thermal stability of the material. Figure 28 presents the TGA thermograms of pure polymer and polymer-salt blend with a salt concentration [Li]/[O]=0,12. TGA data were obtained under inert N_2 atmosphere at a scan rate of 10 degree/minute.

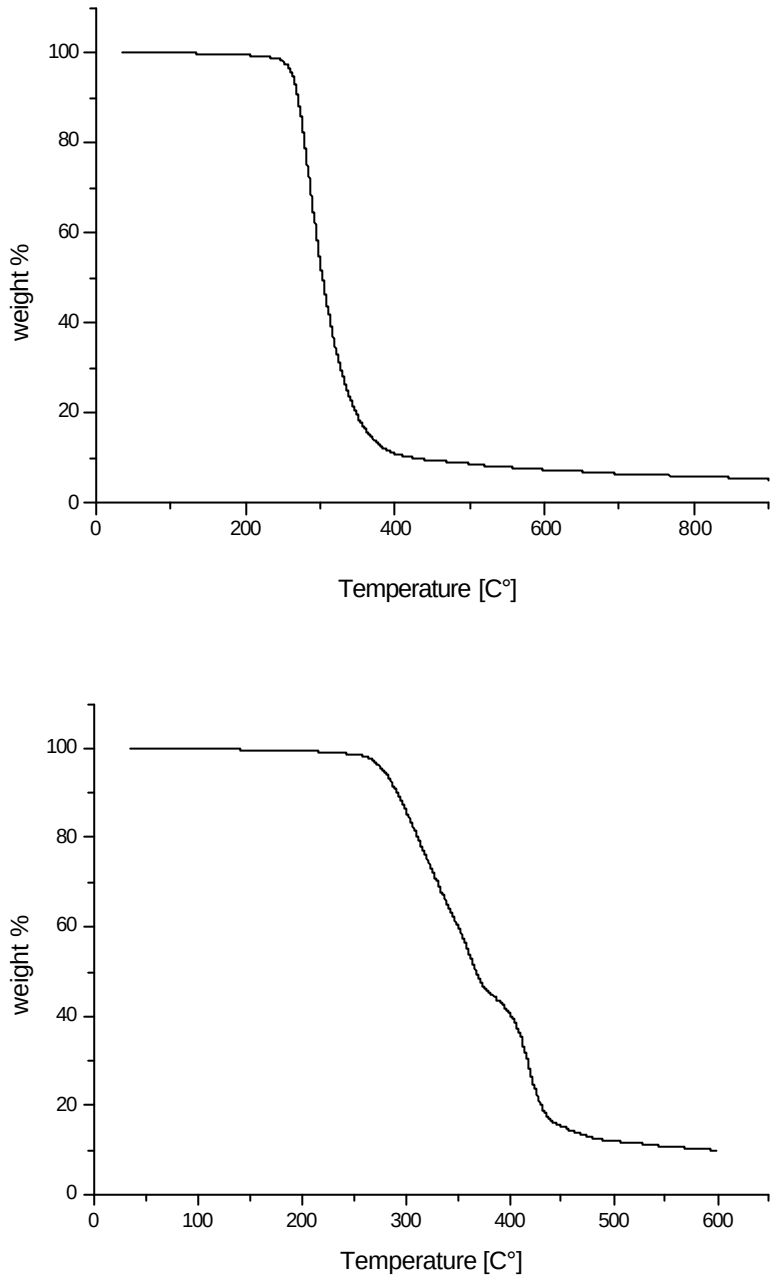

Figure 28. TGA scan under N_2 of
a) PEO-HPC DS=3 b) PEO-HPC DS=3 – $LiCF_3SO_3$ blend [Li]/[O]=0,12

It is clearly seen that the polymer is stable up to approximately 230 °C (513 K). But a small (0,015%) weight loss is observed already between 200 and 230 °C. The total decomposition reactions take place between 250 – 300 °C. Knowing this values the DSC of the same samples was done in the temperature range from –100 °C to 200 °C. As T_g of the pure polymer –65 °C (208K) was found. The DCS measurements of the blends with lithium salts of PEO-HPC were initially done in the same way but then some changes were observed (Figure 29).

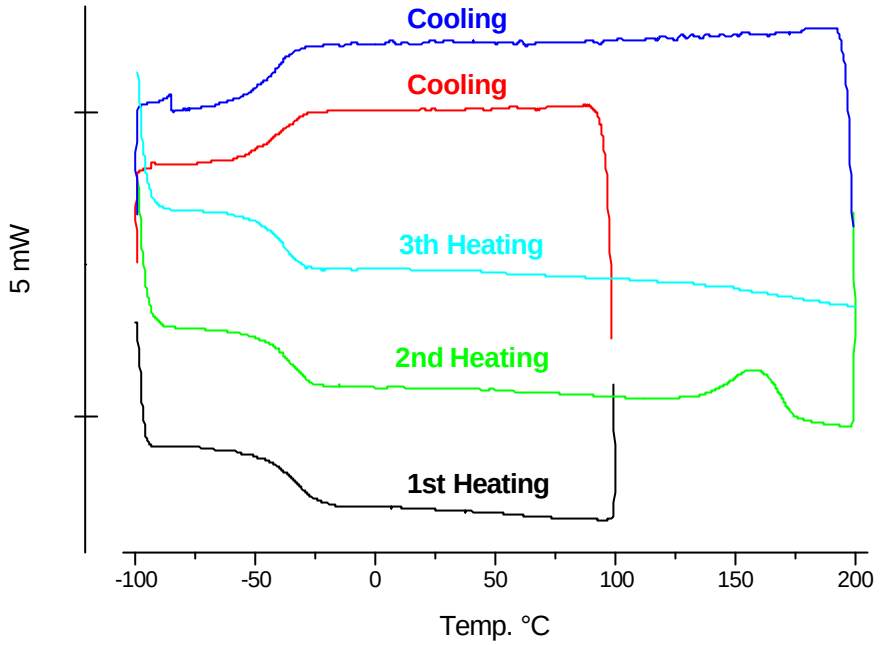

Figure 29. DSC curves of $LiN(SO_2CF_3)_2$ blend with PEO-HPC [Li]/[O]=0,063.

In the temperature range 150–170 °C some exothermic process takes place. The strength of this process changes with content of salt and influences the glass transitions temperature. The influence of repeated heating up to 200 °C on T_g was tested on PEO-HPC blends with $LiCF_3SO_3$ (Figure 30).

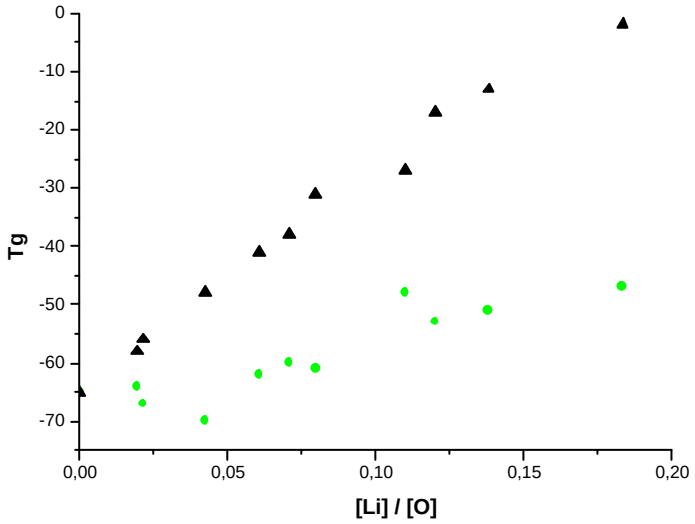

Figure 30. Influence of repeated heating on the glass transition temperature

? 1st Heating ? 2nd Heating

It is clearly visible that T_g increases systematically with salt content as long as the sample is not heated above ~160 °C. Overheated samples (second heating) show no systematic dependence of T_g on concentration (2nd heating).

The nature of the reaction of the polymer in presence of salt is not known, but it seems to be some chemical change because it appears only during the first run over the critical temperature range. The reaction takes place in the presence of lithium salts and can be related to the $N(SO_2CF_3)_2^-$, $CF_3SO_3^-$ and BF_4^- groups. The TGA-MS investigation proves that there are no low molecular weight species in the effluent gases (Figure 31).

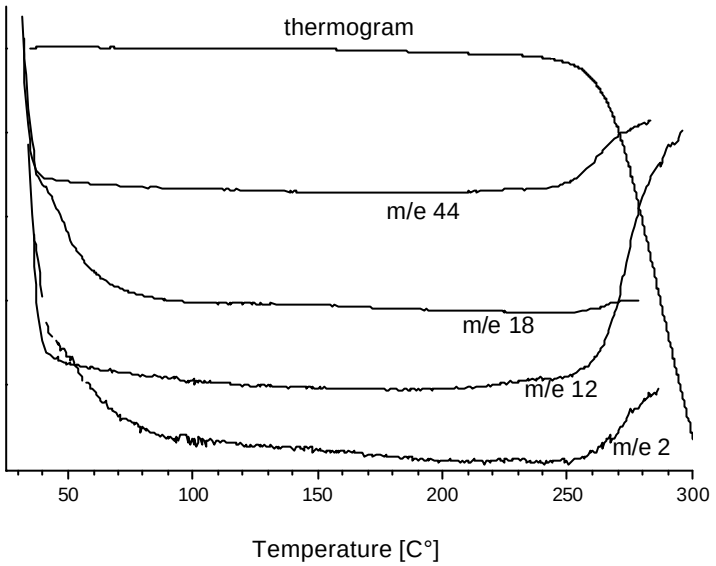

Figure 31. TGA-MS scan of PEO-HPC DS=3

The plot in Figure 31 presents mass abundance scans and thermograms simultaneously. Measurements were done for masses 2 (e.g. H_2), 12 (e.g. C), 18 (e.g. H_2O) and 44 (e.g. CO_2). Since one does not observe any peaks or changes in the mass flux in the temperature range up to 230 °C one must conclude that the sample does not suffer from degradation.

Subsequently all DSC experiments were performed only in a narrow temperature range starting from –100 up to 100 °C. Five heating cycles were registered and the T_g values were estimated based on the average of the last four. The T_g changes with increasing salt concentration and its dependence from the salt concentration for three kinds of salts are presented in Figure 32. The concentration is a molar ratio of Li and O and, therefore, all data are normalized for molar concentration of the salt in the blends.

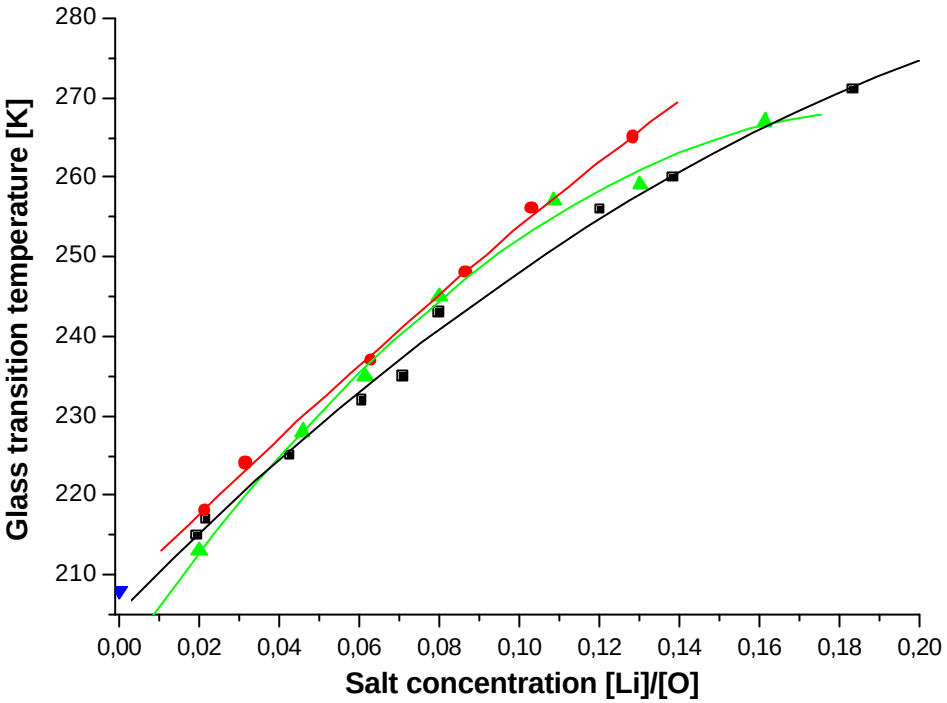

Figure 32. Influence of salt concentration on T_g.

? pure PEO-HPC

¦ $LiCF_3SO_3$ $T_g = 207 + 465 * c_{[Li]/[O]} - 611 * c_{[Li]/[O]}^2$

? $LiN(SO_2CF_3)_2$ $T_g = 208 + 502 * c_{[Li]/[O]} - 426 * c_{[Li]/[O]}^2$

? $LiBF_4$ $T_g = 199 + 711 * c_{[Li]/[O]} - 1827 * c_{[Li]/[O]}^2$

With all three kinds of salts T_g increases with salt content but the rate of increase depends on the type of salt. For polymer blends with inorganic salts there is no universal relationship for T_g versus composition. Instead the Fox rule is applied [80][146]. Since the polymer has a low T_g the influence of salt can be described as that of an antiplasticizer. The antiplasticizer raises the T_g of polymers in accordance with the Fox equation:

$$\frac{1}{T_g} = \frac{1}{T_{g0}} - \frac{n y_0}{1 - y_0} * \left(\frac{1}{T_{g0}} - \frac{1}{T_{gb}} \right) \qquad \text{Equation 44}$$

where: T_{g0} - glass transition temperature of salt-free polymer

T_{gb} - glass transition temperature of fully salt-complexed polymer

y_0 - mole fraction of salt

n - coordination number of the coordinating ion (hire: Li^+).

The last procedure in the polymer electrolyte preparation is crosslinking. The influence of such reactions on T_g is of great importance for their application. The T_g is directly connected with the free volume level in the polymer and the latter governs the ion mobility of the system. The influence of crosslinking to T_g was tested with polymers without salt as well as in blends with $LiN(SO_2CF_3)_2$. The investigations were realized with diisocyanate crosslinker (compound 7, Figure 10).

	[OH] : [NCO]								PEO-HPC without crosslinking agent
	2 : 1		1 : 1		1 : 1,5		1 : 2		
[Li]/[O]	before	after	before	after	before	after	before	after	
0			-53	-53	-52	-52	-54	-53	-65
0,05	-31	-31							-36
0,08	-16	-15	-12	-11					-25
0,10					-7	-7	-4	-3	-17
0,13							-9	-8	-8

Table 7. Glass transition temperature of samples in °C at different concentrations of $LiN(SO_2CF_3)_2$ and diisocyanate crosslinking agent before and after crosslinking reaction

The data presented in Table 7 suggest that the changes of T_g upon crosslinking are really small. Based on the comparison with the T_g values of the samples without diisocyanate crosslinking agent (last column), the addition of the latter caused an overall increase of T_g. However, it is possible that the crosslinking reaction already takes place in the course of mixing so that terms before and after crosslinking are not relevant. Crosslinking reactions do not influence significantly the conducting characteristic of the material, as proved later in this work.

Based on the TGA analysis of the PEO-HPC crosslinked with diisocyanate the thermal stability of the final product was found to be similar to the thermal stability of the uncrosslinked samples (Figure 33).

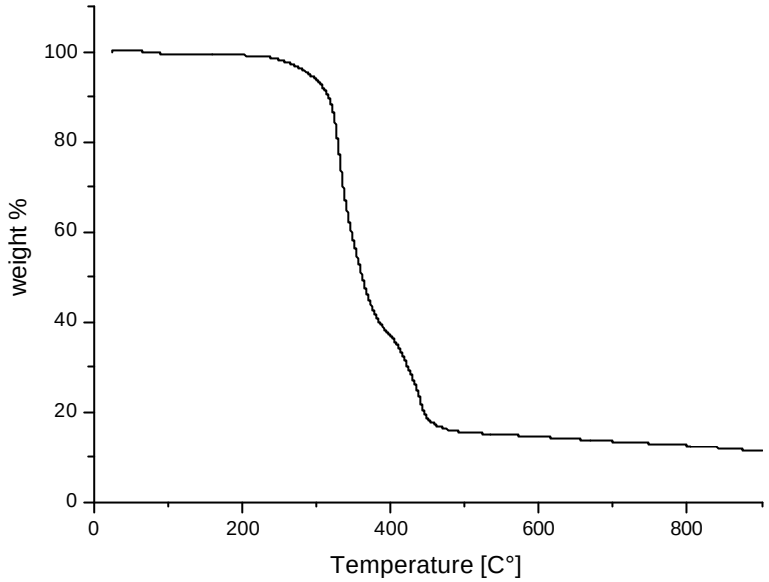

Figure 33. TGA scan of PEO-HPC / $LiN(SO_2CF_3)_2$ crosslinked with diisocyanate [OH]/[NCO]=1:1

4.3 Impedance Spectroscopy

The interaction of electromagnetic radiation with matter is of fundamental importance for research on polymer-based electrolytes. The response of material to electromagnetic waves is the subject of several research techniques. The frequency regime between 10^{-6} and 10^{12} Hz is the domain of broadband dielectric spectroscopy. In this dynamic range molecular and collective dipolar fluctuations, charge transport and polarizations effects at inner and outer boundaries take place. Such phenomena determine the dielectric properties of the material and provide information on the dynamics of dipoles and mobile charge carriers depending on the materials structure. The magnitude of the effects and the frequency location of the energy absorption features associated with these processes will depend markedly upon the chemical and physical nature of a material and the temperature and pressure at which it is studied. Studies of electric polarization and conduction processes are summarized under the terms: "Dielectric Relaxation Spectroscopy" (DRS), "Impedance Spectroscopy" (IS), "Electrical Impedance Spectroscopy" (EIS) and "Electrical Relaxation Spectroscopy" (ERS). The variation of the complex dielectric permittivity with frequency gives information on the natural diffusion motions of dipolar molecules in a material in the absence of an applied electric field. Dielectric experiments are used to study hopping conduction of charged species in polar solids and semi conductors. From the variation of electrical conductivity with frequency information on the translational diffusion of ions in a material in the absence of an applied field may be derived [147-150].

Electrical conductivity is a measure of how well a material accommodates the transport of electric charge. Castellan [7] defined conductivity as following:
The quantity of electrical charge that passes any point in a conductor in unit time is the current. The current passing through unit area perpendicular to the direction of flow is the current density j. By the general law of transport, the current density in the x direction is proportional to the potential gradient:

$$j = -k\frac{\partial f}{\partial x} \qquad \text{Equation 45}$$

The constant of proportionality k is the conductivity of the substance expressed in [S/m] where:

$$S = \frac{1}{\Omega}. \qquad \text{Equation 46}$$

The conductance *G*, as defined by Atkins [8], is the inverse of the resistance R:

$$G = \frac{1}{R}$$ Equation 47

and is expressed in Ω^{-1}. The conductance of a sample decreases with its length *l* and increases with its cross-sectional area *A*:

$$G = \frac{kA}{l}$$ Equation 48

The techniques used to characterize the ionic conductivity of polymers are both, direct current (DC) measurements and alternating current (AC) measurements [63][61][155]. Direct current techniques represent the most straightforward methods but their use is less common in ionic conductivity studies. This is because of the problems arising from the electrode contacts on the measured electrolyte conductivity. The effect of blocking electrodes is caused by the simple effect that ions can not be discharged at the surface of a metal electrode, which is currently used. Thus, an electrical potential is constructed caused by the formation of an ion gradient. Sinusoidal voltage applied in alternating current techniques eliminates such problems. Additionally, the AC-data provide knowledge about polarization phenomena occurring within the cell. The measurements of ionic conductivity with impedance spectroscopy has become a standard method in polymer electrolyte research.

Kremer and Schönhals [149] presented the scheme of an impedance bridge shown in Figure 34 which consists of the sample capacitance $Z_S^*(w)$ and the adjustable compensation impedance $Z_C^*(w)$. On the left hand side of the bridge, the generator drives the sample with the fixed and known a.c. voltage $U_S^*(w)$ which causes the current $I_S^*(w)$ to flow into P_I. On the right hand side of the bridge, the variable amplitude-phase generator feeds the current $I_C^*(w)$ through the compensation impedance $Z_C^*(w)$ into P_I. The bridge is balanced , if $I_S^*(w)$ equals $-I_C^*(w)$ which corresponds to $I_0 = 0$. Any deviation is detected by the zero voltage detector which changes the amplitude and phase of the variable amplitude phase generator as long as $I_0 \neq 0$ [149].

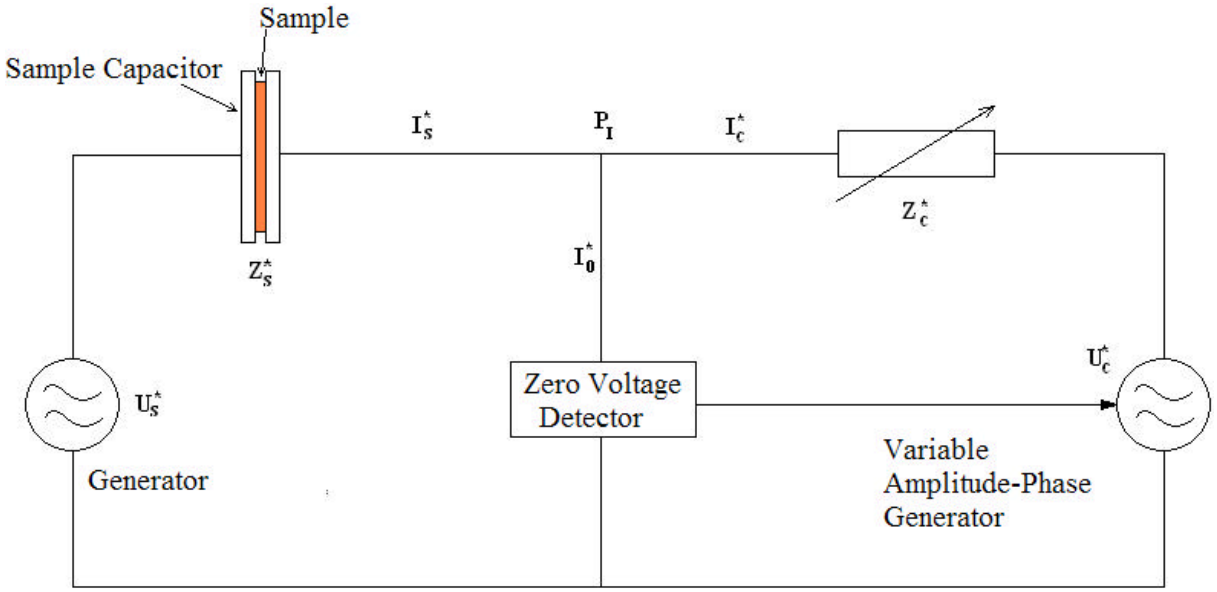

Figure 34. Schematic representation of an impedance bridge displaying the measuring cell and principal design of the external electrical circuit.

Electrical conductivity of polymer electrolytes was measured using a cell with the configuration of metal (Pt) electrode / electrolyte / metal (Pt) electrode. The sample was placed between two parallel platinum electrodes so that the mobile species in the electrolyte do not participate in any electrode reactions. In such a cell blocking with electrodes, the electrode / electrolyte interfacial impedance, caused from the double layer capacitance and charge-transfer resistance, influences the overall response in addition to the bulk electrolyte impedance. The impedance is a unit of measure, expressed in Ohms, of the total response (resistance, capacitance and inductance) of the material on to the alternating electrical field. The cell impedance is dependent on frequency. The resistance is the opposition that a material offers to the flow of electricity in a circuit. The capacitance is a property of a system of conductors and dielectrics that permits the storage of electrically separated charges when potential differences exist between the conductors. The inductance is a property of an electric circuit that causes it to store energy in the form of a magnetic field and because of which a varying current in a circuit induces an electromotive force (voltage) in that circuit or a neighbouring circuit. The bulk electrolyte resistance, the property that determines the current, produced by a given potential difference, is estimated from the corresponding component of an equivalent circuit required to account for the impedance diagrams. The equivalent circuit is an electronic circuit used to provide the same performance as another electronic circuit based on the movement of free electrons (and or holes). An equivalent circuit differs from an analogous circuit which emulates systems that do not utilize free electrons in their operation.

Since all investigated lithium salt blends of PEO-HPC have a homogenous, amorphous structure, the equivalent circuit adequately describing the impedance behaviour of electrolyte cell systems over a frequency range of 10^{-1} – 10^{6} Hz is shown in Figure 35.

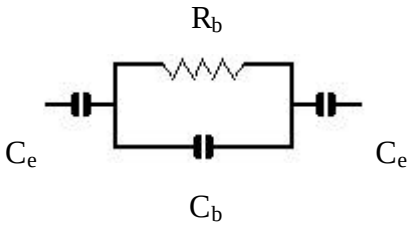

Figure 35. Schematic representation of an equivalent circuit

The equivalent circuit components of the electrolyte cell system are:

- electrode capacitance C_e representing the polarisation at the electrodes
- electrolyte capacitance C_b representing the bulk polarisation
- electrolyte resistance R_b representing the ion mobility.

The most important component in the case of Li^+ conductors is the resistance R_b representing the mobility of the lithium ions in the polymer matrix. The capacitance C_b represents the dielectric polarisation of immobile polymer chains in the alternating field. This response type appears in the polymer material when it is free from mobile charges as well.

$$C_b = \frac{e e_0 A}{l} \qquad \text{Equation 49}$$

where: e - dielectric permitivity of the polymer; e_0 = $8.854 \cdot 10^{-12}$ $C^2/N \cdot m^2$ - vacuum permittivity, A - area, l - length

When an alternating current is applied the mobile ions accumulate and deplete within the electrolyte near each blocking electrode. These charges are balanced by electronic charges on the electrodes andboth sides together form a parallel-plate capacitor of capacitance C_e.

The principle of dielectric spectroscopy is the application of a sinusoidal alternating voltage

$$V(t) = V_0 \cdot \sin(wt) \qquad \text{Equation 50}$$

to a cell containing a polymer electrolyte and measuring the amplitude I_0 and phase difference ? between the applied potential and current I in the sample:

$$I(t) = I_0 \cdot \sin(wt + q) \; . \qquad \text{Equation 51}$$

As representation the ratio V_0/I_0 (event. only I_0) and phase difference ? are used. Typical experiment rely on the determination of the complex impedance of a measured system. For a sample with linear characteristics of its response the complex impedance Z is:

$$Z(w) = \frac{V_0}{I_0} e^{iq}. \qquad \text{Equation 52}$$

The impedance is a time independent function of the frequency:

$$Z(w) = Z' - iZ''. \qquad \text{Equation 53}$$

The complex impedance of elements in the circuit when put into series is additive:

$$Z_{total}(w) = Z_1(w) + Z_2(w) + \ldots. \qquad \text{Equation 54}$$

When components are connected in parallel the sum of the reciprocal complex impedance gives the total reciprocal complex impedance:

$$\frac{1}{Z_{total}(w)} = \frac{1}{Z_1(w)} + \frac{1}{Z_2(w)} + \ldots \qquad \text{Equation 55}$$

If the impedance of the resistance R is $Z(w) = R$ and the impedance of the capacitor C is $Z(w) = -i\frac{1}{wC}$, then the electrode capacitance C_e is in series with the parallel combination of electrolyte resistance R_b and the electrolyte capacitance C_b, with the total impedance Z_{total} being the sum of the impedances of the capacitor C_e and the product R_bC_b:

$$Z_{Total} = R_b\left[\frac{1}{1+(wR_bC_b)^2}\right] - i\left(R_b\left[\frac{wR_bC_b}{1+(wR_bC_b)^2}\right] + \frac{1}{wC_e}\right). \qquad \text{Equation 56}$$

The complex impedance plot for the equivalent circuit predicted by Equation 56 is shown in Figure 36.

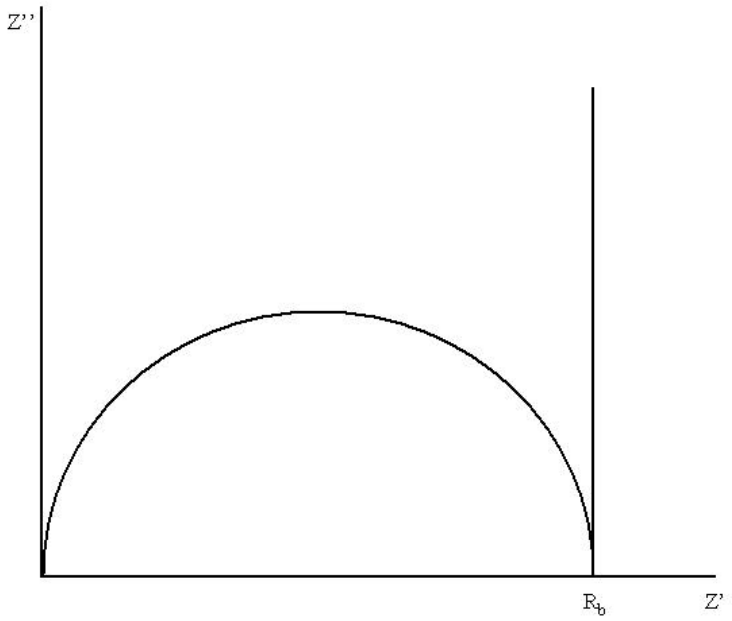

Figure 36. Complex impedance plot for the equivalent circuit.

The complex impedance plot for the equivalent circuit representing a sample is valid only over a limited frequency range. For $w \to 0$ the function origin evolves at the coordinate system (0,0). When $w \to \infty$ the function touches its second zero-point at (R_b,0). For higher angular frequencies $\frac{1}{wC_b} >> R_b$ the equivalent circuit reduces to a series combination of R_b and C_e which corresponds to a vertical spike displaced at $Z' = R_b$. The semicircle appearing between both zero-points is the response of the measured material. In this frequency range the impedance of the bulk resistance and capacitance are of the same magnitude, $\frac{1}{wC_b} \approx R_b$ both contribute to the overall impedance. The impedance of the electrode capacitance ($C_e \approx 10^{-6} C_b$) makes only a negligible contribution to the total impedance. Thus at $w \to 0$ from (R_b,0) the equivalent circuit reduces to a parallel R_bC_b combination and appears as a semicircle in the complex impedance plane.

Knowing the complex impedance of the measured sample it is possible to calculate:

a) the specific direct current conductivity s_{DC} from the electrolyte resistance R_b with Equation 57:

$$s_{DC} = \frac{d}{A}\frac{1}{R_b} \qquad \text{Equation 57}$$

with

d - sample thickness (electrode separation) [m]

A - electrode area [m]

R_b – Z' in the second zero-point [Ω]

b) the capacitance of the sample from the maximum of the semicircle in the complex impedance plane based on the Equation 58:

$$R_b w_{\max} C_b = 1 \quad \Rightarrow \quad C_b = \frac{1}{R_b w_{\max}} \qquad \text{Equation 58}$$

c) the dielectric constant at $w_{\max}$ of the sample:

$$C_b = \frac{e e_0 A}{d} \quad \Rightarrow \quad e = \frac{C_b d}{e_0 A} \qquad \text{Equation 59}$$

provided that the sample response function in the complex impedance plot is close to the perfect (theoretical) ones. The complex impedance plot of real cells is often deformed in such a way that the semicircles exhibit spikes which are distinctly non-vertical. This can be the result of several factors like rough electrode/electrolyte interface, ion-ion interactions and formation of ion-ion associations, inhomogeneities in the electrolyte, electrolyte surface roughness and impurities. Deformation of the semicircle itself from theoretical Z''/Z' plots have formal reasons, e.g. more than one relaxation time or multiple relaxation processes.

The complex impedance $Z(w)$ and its reciprocal admittance $Y(w) = \frac{1}{Z(w)}$ are dependent on the geometry of a sample. The experimental results can be presented in the form of a complex formalisms:

- Impedance Z(?) = Z'- *i*Z''

$$Z(w) = \frac{1}{Y(w)} = \frac{1}{iwC_o e(w)} \qquad \text{Equation 60}$$

- Admittance Y(?) = Y'- *i*Y''

$$Y(w) = \frac{1}{Z(w)} = iwC_o e(w) \qquad \text{Equation 61}$$

- Permittivity e(?) = e'- *i*e''

$$e(w) = \frac{1}{M(w)} = \frac{1}{iwC_o Z(w)} = \frac{Y(w)}{iwC_o} \qquad \text{Equation 62}$$

- Electric modulus M(?) = M'- *i*M''

$$M(w) = \frac{1}{e(w)} = iwC_o Z(w) = \frac{iwC_o}{Y(w)}$$ Equation 63

- Conductivity s(?) = s'- *i*s''

$$s(w) = íwe_v e(w)$$ Equation 64

where $w = 2pf$.

Those quantities are interrelated and can be used alternatively. Interrelationships between $e(w), M(w), s(w), Z(w)$ and $Y(w)$ are expressed as:

$$e(w) = \frac{1}{M(w)} = \frac{s(w)}{iwe_0} = \frac{1}{iwC_0 Z(w)} = \frac{Y(w)}{iwC_0}$$ Equation 65

where C_0 is the capacitance of the empty measurement cell given as:

$$C_0 = A\frac{e_0}{d}$$ Equation 66

The results of the measurements are presented as the frequency dependence of the real $e'(w)$ and imaginary part of the permittivity $e''(w)$ in a logarithmic scale:

$$e'' = -\mathrm{Im}\left(\frac{d}{iwAe_0 Z(w)}\right) = \frac{d}{we_0 A} i\frac{Z'}{Z'^2 + Z''^2}$$ Equation 67

$$e' = \mathrm{Re}\left(\frac{d}{iwAe_0 Z(w)}\right) = \frac{d}{we_0 A} i\frac{Z''}{Z'^2 + Z''^2}$$ Equation 68

or as the frequency dependence of the real $s'(w)$ and imaginary part of the permittivity $s''(w)$ in a logarithmic scale:

$$s' = \mathrm{Re}(íwe_v e(w)) = we_v e''$$ Equation 69

$$s'' = -\mathrm{Im}(íwe_v e(w)) = we_v e'$$ Equation 70

This enables in most cases to identify the type of dielectric phenomenon taking place in the material under investigation. There are two basic types of response, one connected with the natural diffusion of motions of molecules in a material (relaxations) and the other describing the hopping motion of charged carriers in solids (conductivity).

In the case of materials which exhibit only polar relaxations the real part of the permittivity $e'(w)$ decreases with increasing frequency and the imaginary part of permittivity $e''(w)$ shows a peak as shown in Figure 37a. For pure conducting materials the real permittivity

$e'(w)$ is independent of frequency and the imaginary part $e''(w)$ decreases monotonically with increasing frequency as shown in Figure 37b.

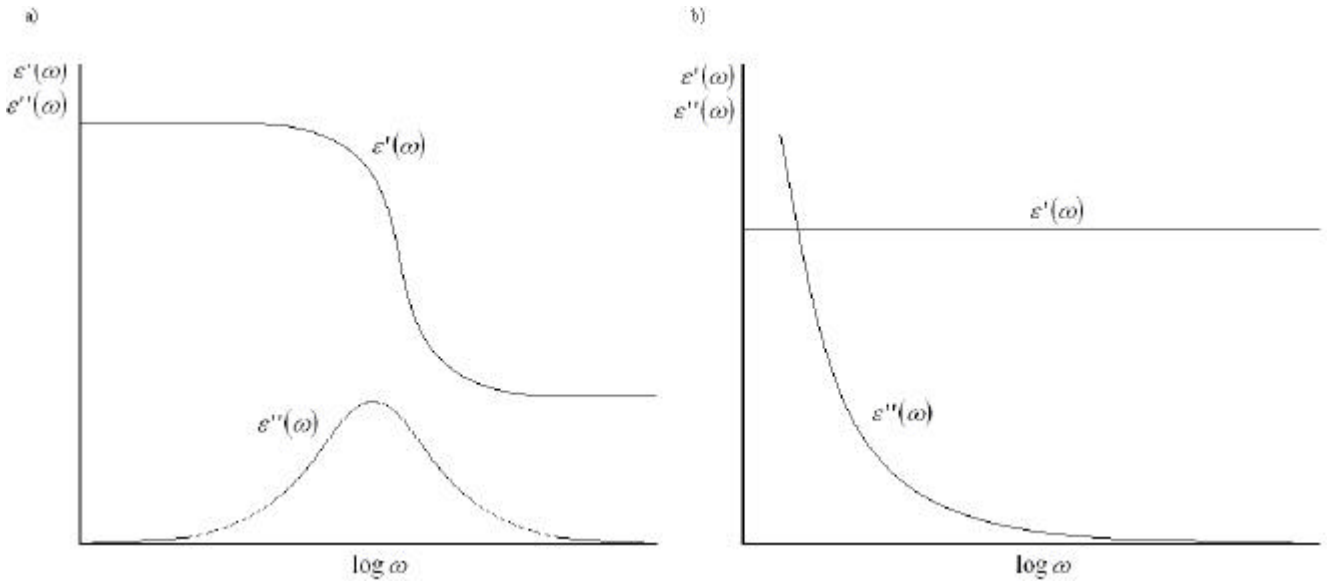

Figure 37. Schematic plots of the dispersion of $e'(w)$ and $e''(w)$ in the frequency domain for:

a) samples that exhibit dielectric relaxation
b) samples that exhibit conduction.

Several distinct conformational relaxations usually exist in polymeric materials. The rates of such processes may cover a wide frequency range. The glass transition is assigned as a relaxation and describes the motion of the segments of macromolecules. It occurs in the low frequency range and/or at higher temperatures (Time-Temperature Superposition TTS). The b and g relaxations describe localized motions of dipoles associated with subunits of the molecules and occur in the higher frequency range similar to those in ordinary liquids [156].

4.3.1 Dielectric Data Evaluation

All impedance spectroscopy measurements were carried out in the temperature range – 50 to 100 °C and frequency range 0,1 to 10^6 Hz. Based on these data the dielectric behaviour of the investigated materials can be discussed. On the basis of the Cole-Cole plots and its frequency dependence one can find the second zero points (R_b,0) and corresponding frequencies at each measured temperature (Figure 38).

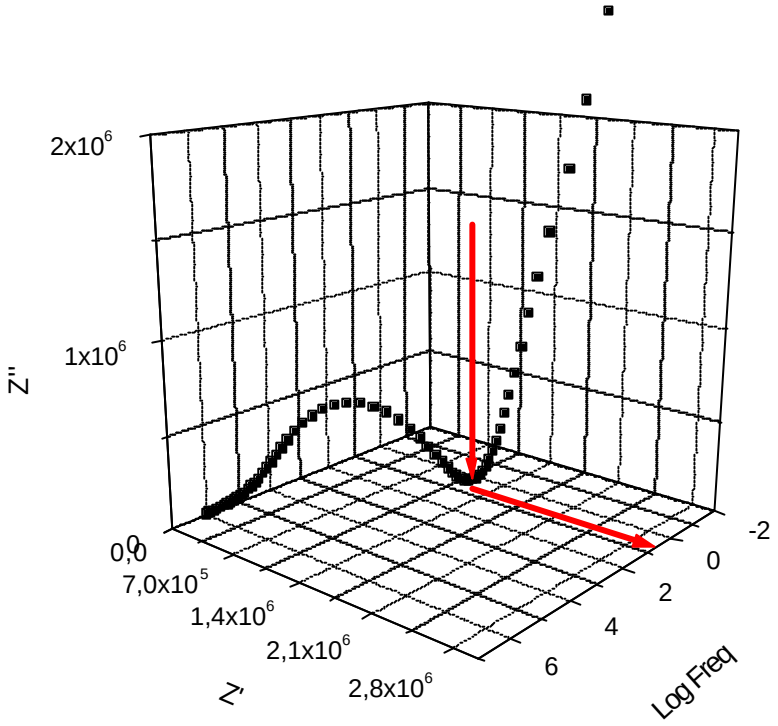

Figure 38. The frequency dependence of the Cole-Cole plot at 0°C for a PEO-HPC blend with $LiCF_3SO_3$ [Li/O]=0,07

Knowing that only the semicircle represents the bulk materials response and the spike is part of the effect of electrode polarization, the frequency range above the second zero point (R_b,0) should not be considered any more. With the same procedure the minimum points for all measured temperatures were found and transfered into the log e' vs log frequency, log e'' vs log frequency, log s' vs log frequency and log s'' vs log frequency plots (black lines in Figures 39 and 40).

a)

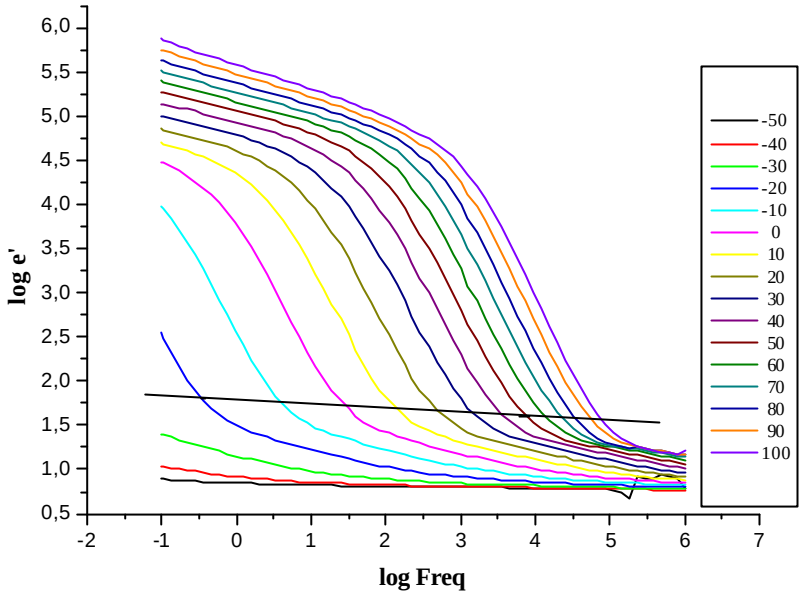

b)

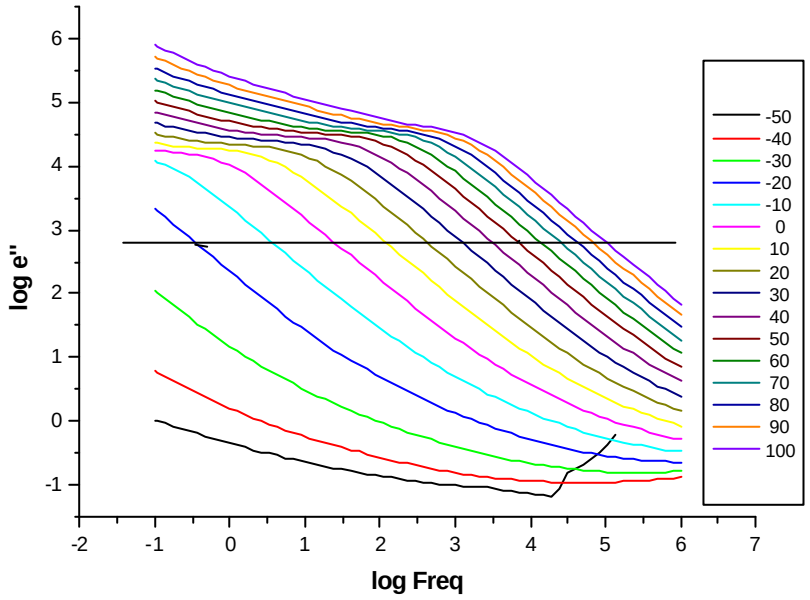

Figure 39. Dielectric spectroscopy data of $LiCF_3SO_3$ blend of PEO-HPC DS=3, [Li]/[O]=0,0707

a) real part of dielectric permittivity b) dielectric loss

a)

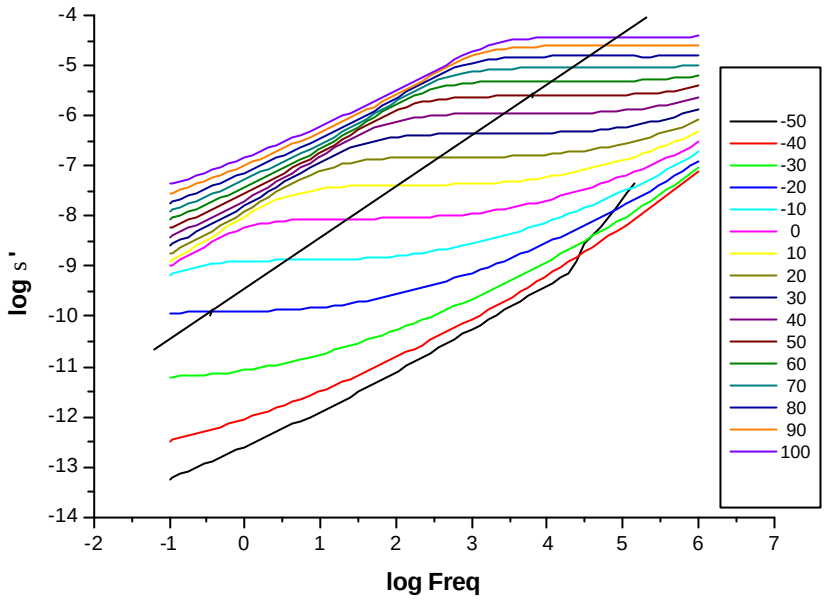

b)

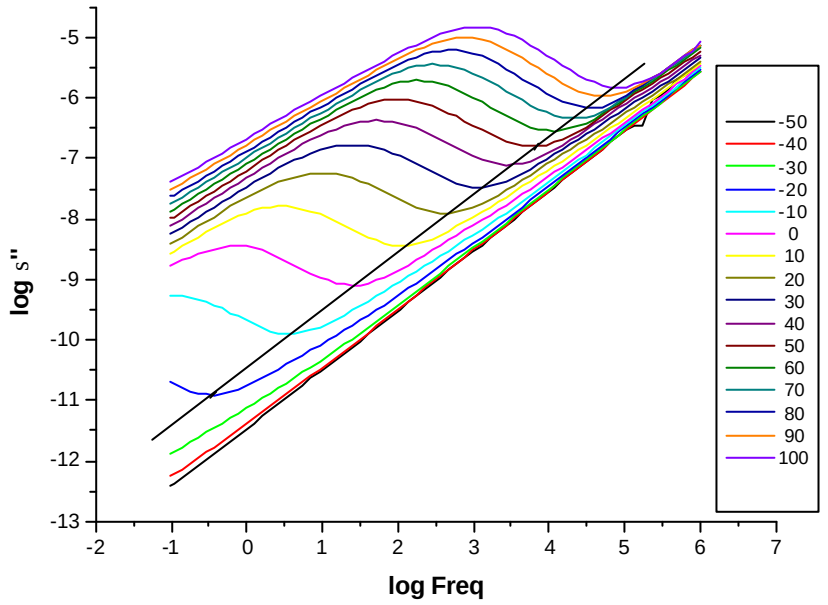

Figure 40. Dielectric spectroscopy data of $LiCF_3SO_3$ blend of PEO-HPC DS=3, [Li]/[O]=0,0707

a) real part of conductivity b) conductivity loss

The lines based on the points divide the planes in two parts. The upper (left hand side) one is concerning the lower frequency range and exhibits the electrode polarization response. In this

part the data evaluation and interpretation is not accurate any more. The lower part (right hand side) describes the conduction due to charged species. The real part of the permittivity as well as the real part of the conductivity is frequency independent whilst the loss permittivity decreases and the loss conductivity increases monotonically with increasing frequency. In consequence, in the measured frequency range there are no further relaxation processes visible. If there are some extremely weak relaxation phenomena hidden, they are screened by the conductivity effect.

All other samples show similar behaviour what is in agreement with expectations because all are based on the same polymer material. The only differences are the conductivities of samples which change with the type and concentration of salt.

4.3.2 Conductivity from Impedance Spectroscopy [147-150]

Among all the intensive experimental quantities the most useful in the present context is the alternating current conductivity (AC) s . The conductivity is a complex quantity :

$$s(w) = s' - is''. \qquad \text{Equation 71}$$

Its measurement provides a fast and comfortable method for the estimation of the direct current conductivity (DC). Figure 41 shows the frequency dependence of the real part of the AC conductivity $s'(w)$ in a logarithmic scale for the temperature range from –50°C to 100°C.

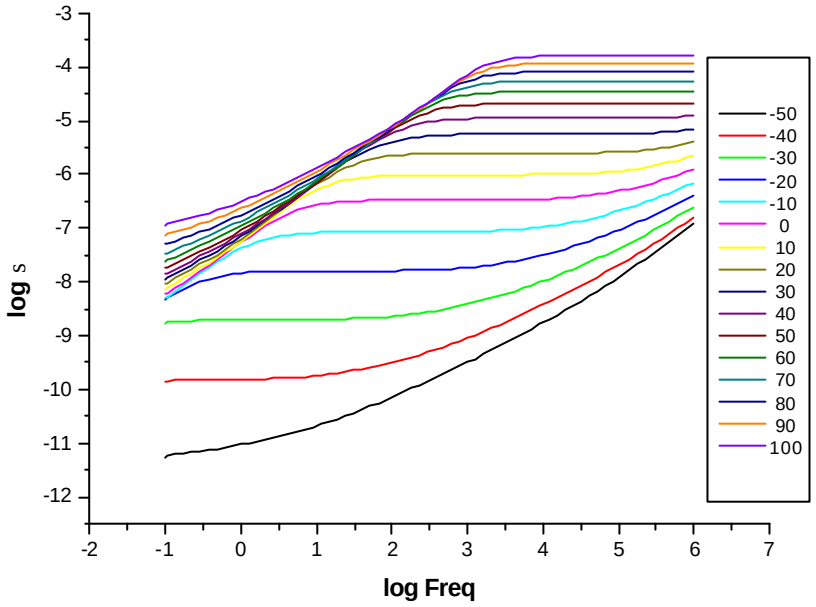

Figure 41. log s –vs- log Freq; PEO-HPC blend with $LiN(SO_2CF_3)_2$ [Li/O]=0,031

Each curve represents the changes in the real part of the AC conductivity with frequency at particular temperatures. All curves have a specific frequency region in which s' is independent from frequency. The extrapolation of the plateau to $w = 0$ defines the value of DC conductivity. Strong changes in AC conductivity at lower frequencies and increase at higher frequencies is the result of electrode polarization and motions of charge carriers in potential wells, respectively. The precision of this extrapolation method was checked by comparison of the results with values obtained based on the complex impedance plot evaluation (Figure 42). The data obtained by both ways are in good agreement.

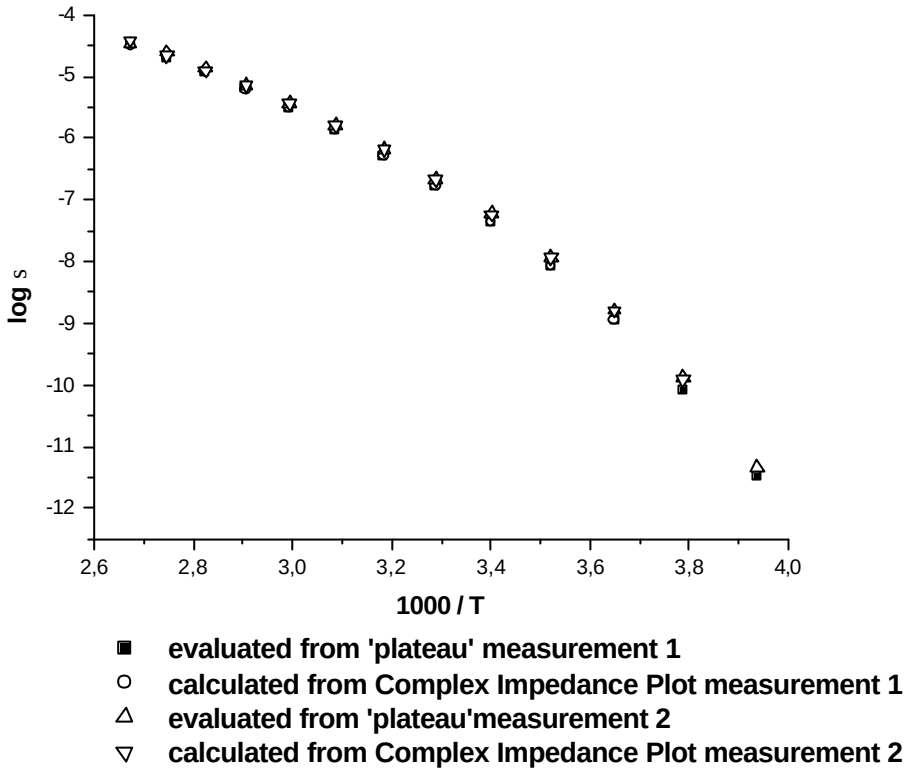

Figure 42. Comparsion of the DC-data evaluation;
PEO-HPC blend with $LiSO_3CF_3$ [Li]/[O]=0,11

The extrapolation method was used for data evaluation in all other cases. Figure 43 presents the temperature dependence of the conductivity for the PEO-HPC blend with $LiCF_3SO_3$. The concentration range was from [Li]/[O]=0,02 to [Li]/[O]=0,18 (Figure 43).

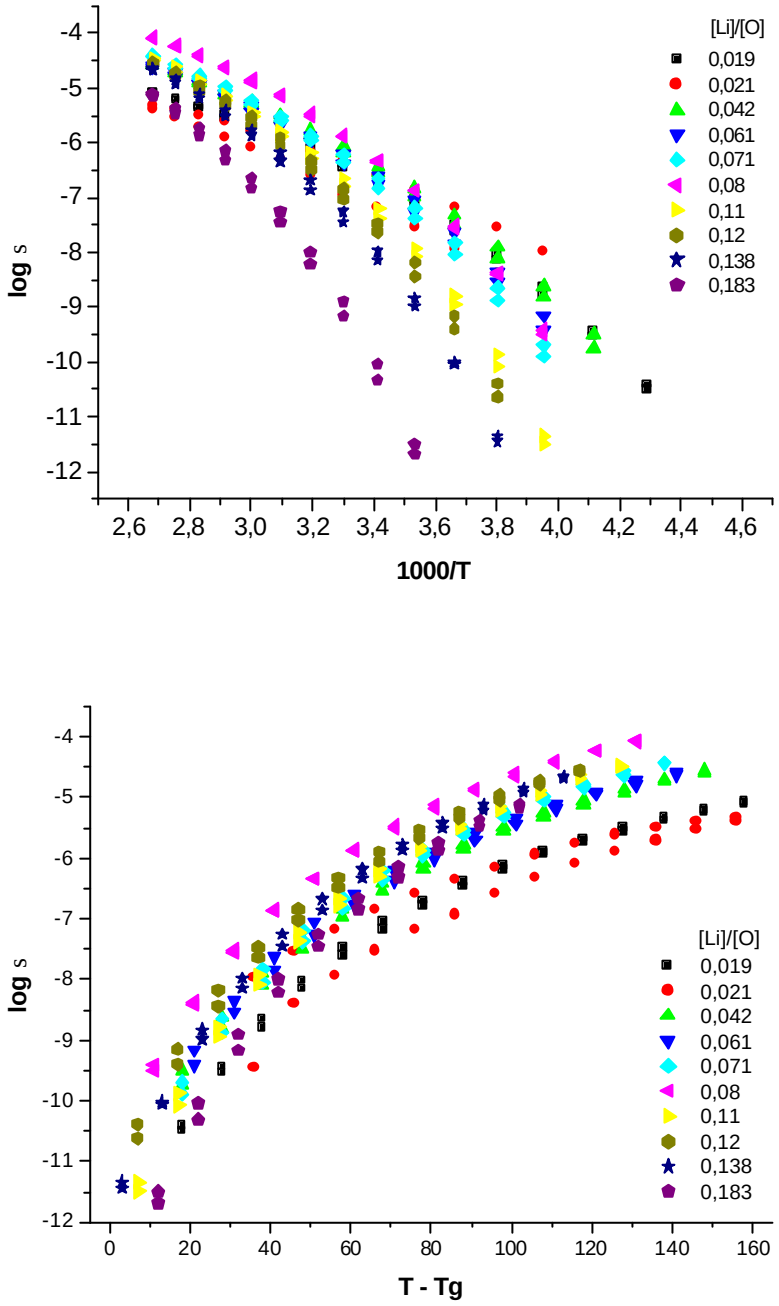

Figure 43.Temperature dependence of the DC conductivity for the PEO-HPC blend with $LiCF_3SO_3$.

Based on the shape of the curves the ion transport mechanism was recognized as a phenomenon governed by the local mobility of the chain segments. The nonlinear dependence in whole temperature range excludes ion hopping transport mechanism.

The data were fitted by the WLF and VTF equations. In the first step the glass transition temperature T_g was determined for each polymer-salt blend by DSC. These temperatures were used as parameters (s at T_g, C_1, C_2 and T_g) in the WLF equation. The VTF fitting was

initially done with the assumption that $T_0 = T_g - C_2$ and finally with three free parameters: T_g, A and B. The results of the fitting procedure for the $LiCF_3SO_3$ / PEO-HPC are presented in the Table 8.

[Li]/[O]	T_g [K]	s at T_g [S/cm]	C_1	C_2 [K]	T_0 [K]	A [S/cm]	B [K]
0,019	215	2.4E-14 ±5.7-14	25.9 ±1.9	50.6 ±9.1	164.4 ±9.2	4.3E-3 ±1.5E-3	1310 ±131
0,021	217	9.2E-12 ±5.8E-11	17.4 ±5.0	50.5 ±37.3	165.6 ±38.7	3.7E-4 ±4.1E-4	900 ±399
0,042	225	2.3E-13 ±3.6E-13	25.5 ±1.2	55.4 ±7.3	169.6 ±7.5	2.7E-2 ±8.5E-3	1412 ±117
0,061	232	1.7E-12 ±9.4E-12	23.6 ±3.8	61.4 ±33.8	171.6 ±34.5	3.0E-2 ±4.5E-2	1439 ±550
0,071	235	3.5E-13 ±1.2E-12	26.7 ±2.5	61.5 ±19.7	173.3 ±20.4	1.4E-1 ±1.3E-1	1645 ±371
0,08	243	1.1E-11 ±2.1E-11	22.1 ±1.5	50.6 ±10.0	192.4 ±10.5	4.2E-2 ±1.9E-2	1119 ±146
0,11	246	3.5E-13 ±7.2E-13	26.9 ±1.4	59.6 ±11.2	187.1 ±11.6	1.6E-1 ±1.0E-1	1590 ±216
0,12	256	1.2E-13 ±2.7E-13	27.3 ±1.7	48.9 ±9.6	209.2 ±10.1	7.7E-2 ±4.3E-2	1300 ±173
0,138	260	2.9E-13 ±3.6E-13	27.1 ±0.8	56.9 ±6.6	203.7 ±7.3	1.7E-2 ±7.7E-3	1525 ±141
0,183	271	2.6E-13 ±1.2E-12	29.5 ±1.6	73.7 ±39.6	257.7 ±9.3	1.4E-2 ±1.0E-2	878 ±149

Table 8. WLF and VTF fitting parameters for the DC conductivity data of $LiCF_3SO_3$/ PEO-HPC blens

As presented in Table 8, increasing of the [Li]/[O] ratio causes an increase of the glass transition temperature. The conductivity at T_g is similar for all samples and at a very low level which is in agreement with the expectations. The value of C_1 averages around 25 and seems to be the characteristic for the investigated material. The C2 value varies from 48 [K] to 61 [K] with an average around 55 [K] which is almost the literature value [63]. The C_2 value for

the sample with [Li]/[O]= 0,1834 strongly differs from the others values (34% over average) and is loaded with a big error (53%). This may caused by a too high salt concentration or sample contamination.

Figure 44 and Figure 45 present the temperature dependences of the conductivity for the PEO-HPC blends with $LiN(SO_2CF_3)_2$ and $LiBF_4$, respectively. The ratio [Li]/[O] was varied from 0,02 to 0,12 for the $LiN(SO_2CF_3)_2$ blends and 0,02 to 0,13 in the case of $LiBF_4$.
Table 9 and Table 10 include WLF and VTF fitting data obtained by the same way like above.

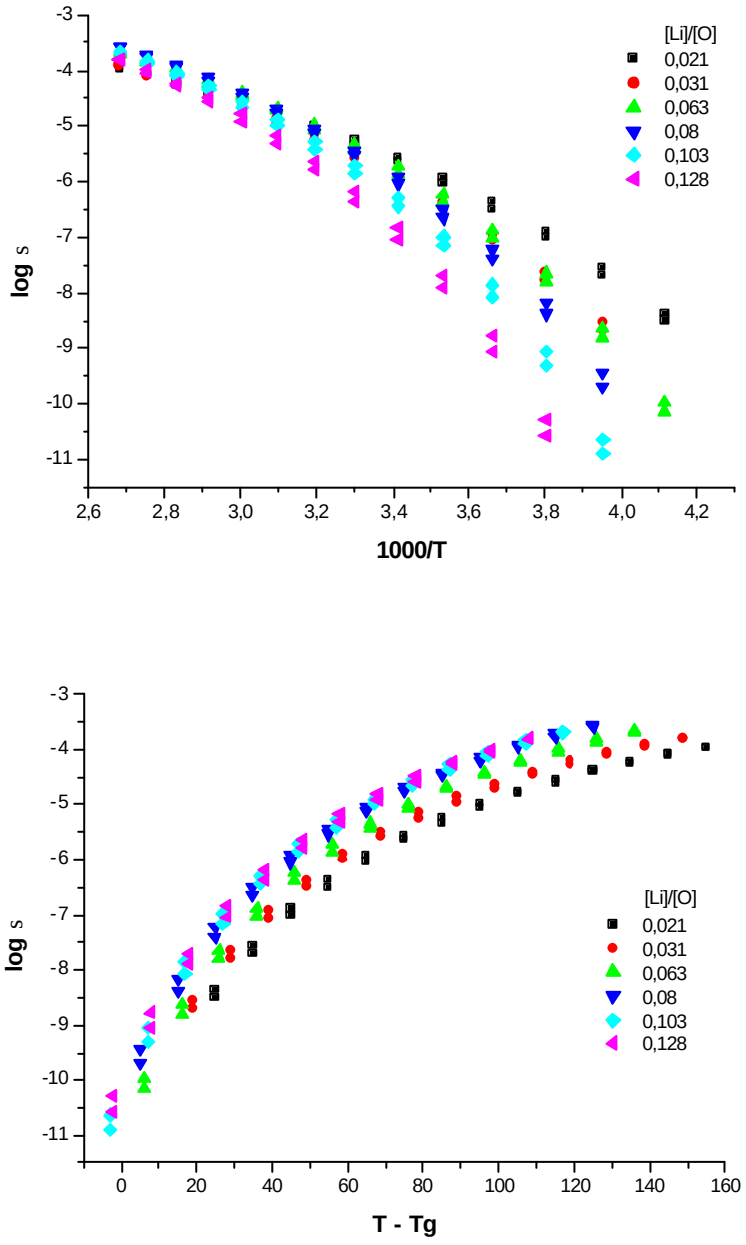

Figure 44. Temperature dependence of the DC conductivity for the PEO-HPC blend with $LiN(SO_2CF_3)_2$.

[Li]/[O]	T_g [K]	σ at T_g [S/cm]	C_1	C_2 [K]	T_0 [K]	A [S/cm]	B [K]
0,021	218	9.6E-13 ±3.9E-12	24.6 ±3.2	50.5 ±16.8	177.3 ±15.3	3.2E-2 ±1.8E-2	1112 ±199
0,031	224	1.0E-11 ±1.9E-11	23.3 ±1.4	59.9 ±11.4	154.5 ±12.0	1.9E-1 ±9.0E-2	1540 ±191
0,06	237	1.3E-11 ±2.5E-11	23.4 ±1.4	56.0 ±10.7	180.8 ±11.2	1.9E-1 ±9.0E-2	1313 ±171
0,864	248	1.3E-11 ±2.1E-11	23.5 ±1.2	49.5 ±7.5	212.5 ±5.2	1.1E-1 ±2.5E-2	964 ±70
0,103	256	1.3E-11 ±2.4E-11	23.5 ±1.3	48.9 ±9.0	213.5 ±8.8	1.5E-1 ±6.7E-2	1055 ±129
0,128	265	9.1E-10 ±1.4E-9	22.1 ±0.3	89.5 ±25.3	175.0 ±27.3	3.6 ±5.6	1985 ±595

Table 9. WLF and VTF fitting parameters for the DC conductivity data of $LiN(SO_2CF_3)_2$ / PEO-HPC blens

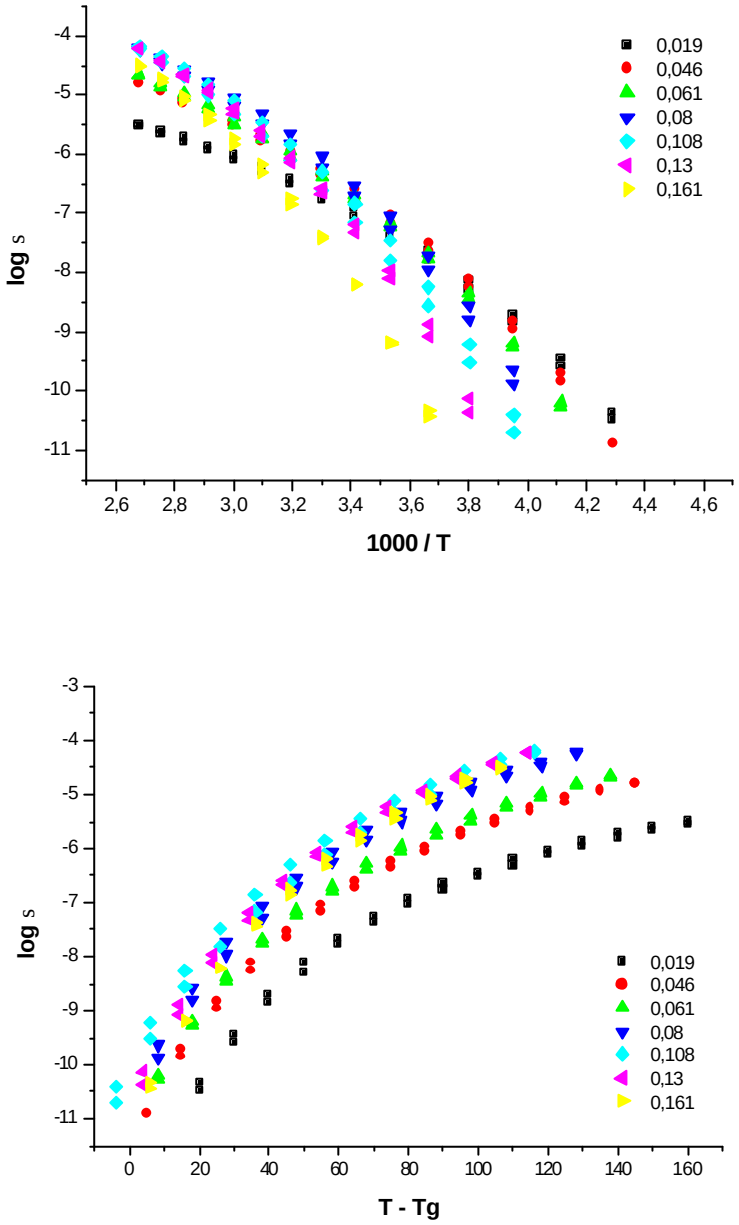

Figure 45. Temperature dependence of the DC conductivity for the PEO-HPC blend with $LiBF_4$.

[Li]/[O]	T_g [K]	σ at T_g [S/cm]	C_1	C_2 [K]	T_0 [K]	A [S/cm]	B [K]
0,0198	213	2.5E-13 ±2.8E-13	22.3 ±0.9	58.9 ±6.8	158.2 ±6.5	1.0E-3 ±2.4E-4	1261 ±88
0,0457	228	8.6E-13 ±1.4E-12	23.8 ±1.2	61.6 ±10.0	158.5 ±9.5	2.6E-2 ±1.1E-2	1592 ±157
0,0613	235	6.9E-12 ±7.0E-12	23.1 ±0.6	75.6 ±9.1	158.8 ±9.3	7.7E-2 ±3.3E-2	1757 ±169
0,0798	245	1.2E-11 ±3.3E-11	24.1 ±1.5	73.3 ±23.8	169.2 ±24.8	4.1E-1 ±5.2E-1	1814 ±485
0,1085	257	5.0E-13 ±6.1E-13	26.5 ±0.9	49.6 ±5.3	207.4 ±5.8	1.7E-1 ±5.4E-2	1317 ±100
0,1300	259	5.2E-12 ±4.4E-12	24.5 ±0.5	57.7 ±5.12	201.3 ±5.7	2.2E-1 ±6.9E-2	1411 ±101
0,1612	267	6.2E-12 ±2.2E-11	25.3 ±1.6	68.2 ±29.7	199.2 ±32.9	5.9E-1 ±1.2	1720 ±697

Table 10. WLF and VTF fitting parameters for the DC conductivity data of $LiBF_4$/ PEO-HPC blens

The influence of the salt concentration is dependent on the salt type, its melting point and molecular weight. The shape of the curves do not agree with an Arrhenius type hopping mechanism of ion transport but with VTF behaviour. The value of C_1 amounts to an average of 23,4 for $LiN(SO_2CF_3)_2$ and 24,2 for $LiBF_4$ respectively with a maximum error of ±3,2.

C_2 has an overall average of 59,5. For all tree kinds of Lithium salts the C_2 value is higher than the average when the salt concentration is high. It goes up to 89,4 in the case of $LiN(SO_2CF_3)_2$ / PEO - HPC [Li]/[O]=0,1285. Excluding those extraordinary numbers the overall average C_2 is 55,5 [K] , a value in agreement with literature [63].

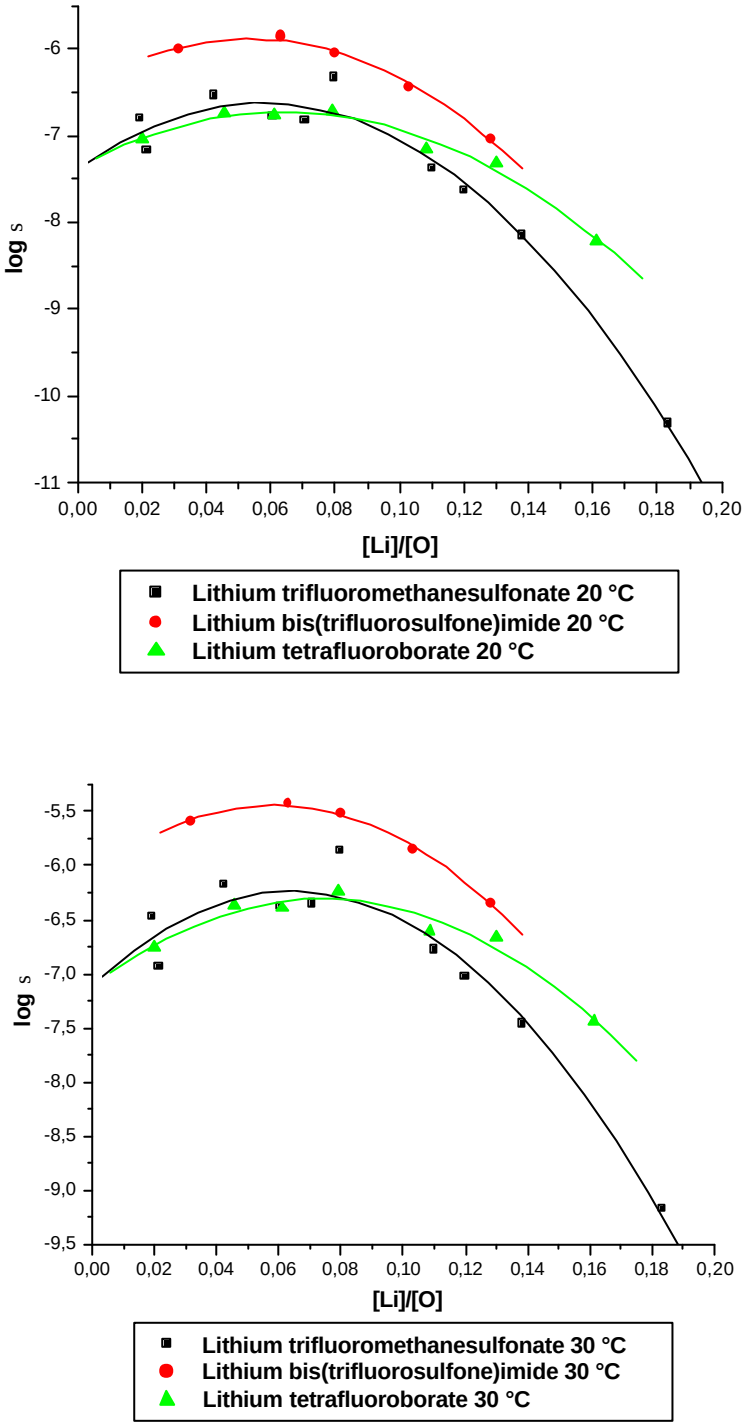

Figure 46. Comparison of the conductivity of the salts at 20 and 30 °C.

The temperature dependence of the conductivity plots in Figures 43, 44 and 45) reveal as well that the best conducting materials are not the ones with the highest Lithium salt concentrations. Drawing the conductivity as a function of the salt concentration one finds a curve with a maximum (Figure 46). The maximum of conductivity varies with the type of salt and appears for concentrations around 0,06 – 0,08 [Li]/[O]. Further enhancing the salt

concentration does not lead to an increasing conductivity. The best results were obtained for samples with the $LiN(SO_2CF_3)_2$ which can be the consequence of the electronegativity of the bis(trifluorosulfone) imide group.

Influence of Crosslinking on the Conductivity of the Materials

The influence of crosslinking of the polymer blends on their conductivity was tested with PEO-HPC / $LiN(SO_2CF_3)_2$ blends, as it is the one exhibiting the highest conductivity. The effect should be the same as for all others salts. The crosslinking reaction was carried out with a diisocyanate crosslink agent (see chapter 2.3). First the impedance spectroscopy of samples with all components mixed in was measured as usual and then, the samples were cured for 12 hours at 120 °C in order to facilitate and accelerate the crosslinking reaction. Afterwards the impedance spectroscopy measurements were repeated.

Figure 47 presents the temperature dependence of conductivity for the PEO-HPC blends with $LiN(SO_2CF_3)_2$. The concentration range was varied from 0,08 to 0,13 in terms of [Li]/[O]. The concentration of the crosslinking agent was calculated as the ratio of free hydroxyl (–OH) to isocyanate (-NCO) groups was 2:1, 1:1, 2:3 and 1:2. The measured temperatures range is above the glass transition temperature for all samples. Based on the presented results one can assume, that there are no significant changes in conductivity caused by crosslinking.

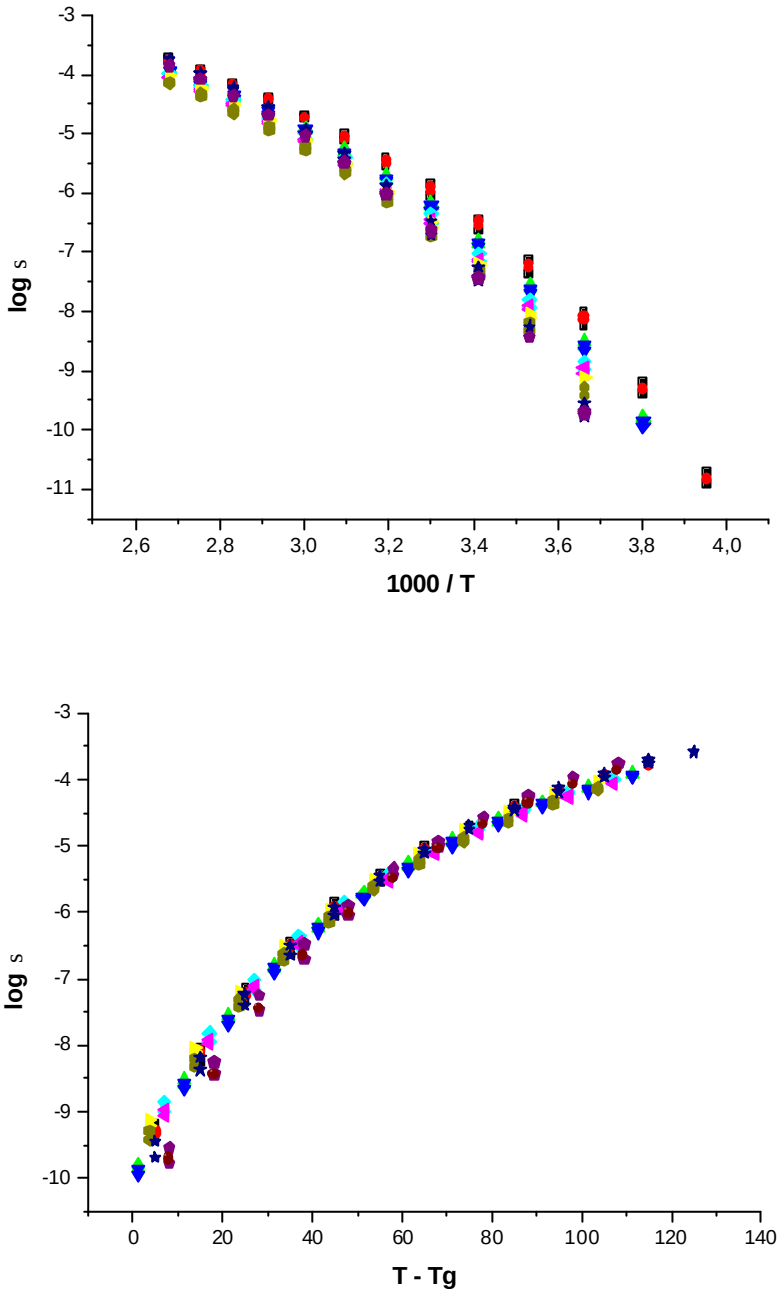

Figure 47. Comparison of the conductivity of the samples before and after curing for 12 hours at 120 °C.

The curves representing individual samples before and after curing almost perfectly cover each other. Slight differences appear only at lower temperatures in the sample with high salt and crosslink agent concentration (Figure 48). The magnitude of those changes is relatively small and can be ignored.

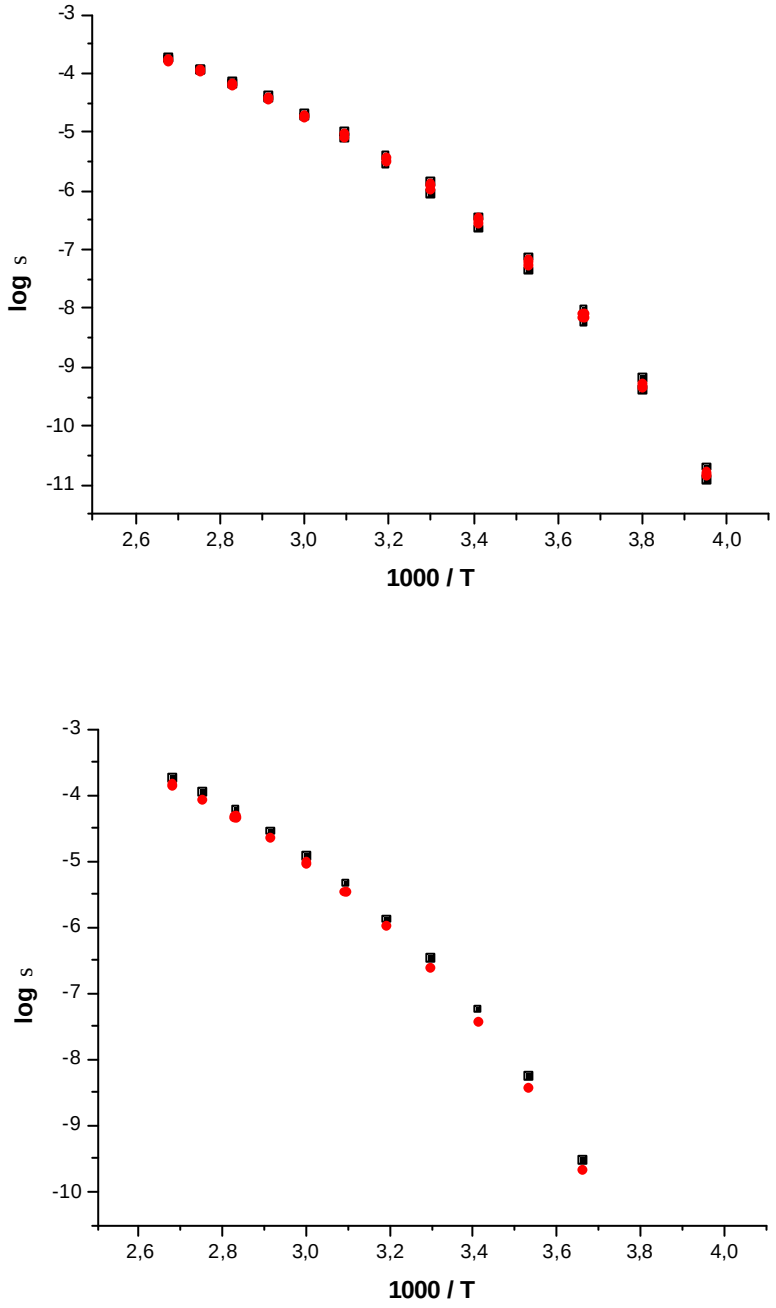

Figure 48. Temperature dependence of the conductivity before and after curing for 12 hours at 120 °C for PEO-HPC blends with $LiN(SO_2CF_3)_2$ and diisocyanate:

a) [Li]/[O]= 0,0869 ; [OH]/[NCO]=2:1 b)[Li]/[O]= 0,1259 ; [OH]/[NCO]=1:2

However, the simple addition of diisocyanate crosslinking agent to the blend influences the materials conductivity. Figure 49 presents the temperature dependence of the conductivity for the blends with similar content of lithium salt, but different diisocyanate crosslinker content.

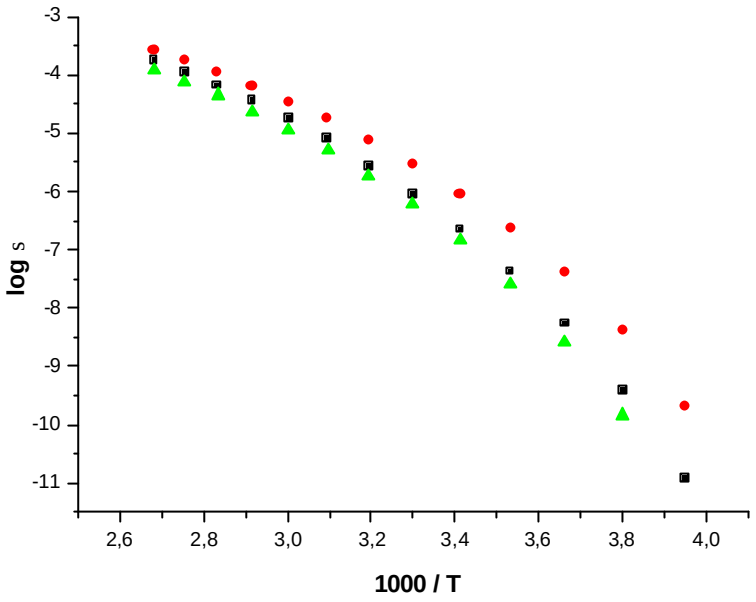

Figure 49. Temperature dependence of the conductivity for:

? PEO-HPC / $LiN(SO_2CF_3)_2$; [Li]/[O]=0,0865

¦ PEO-HPC / $LiN(SO_2CF_3)_2$ / Diisocyanate [Li]/[O]=0,0869 ; [OH]/[NCO]=2:1 ;

? PEO-HPC / $LiN(SO_2CF_3)_2$ / Diisocyanate [Li]/[O]=0,0858 ; [OH]/[NCO]=1:1 ;

The changes in conductivity caused by the simple addition of diisocyanate crosslinker are temperature dependent. The conductivity decrease is lower at 100°C temperature and becomes bigger with decreasing temperature. At room temperature (20°C) the difference in conductivity reaches 0,8 and at 0°C about 1,2 orders of magnitude.

Small magnitudes of conductivity changes before and after sample curing (Figure 47 and 48) and relatively big influence of diisocyanate crosslinker addition (Figure 49) suggest that the presence of the later causes considerable changes in polymer properties and decreases the conductivity of lithium salt blends. Moreover, the reaction with hydroxyl groups probably occurs directly after mixing of PEO-HPC and diisocyanate crosslinker solutions. The curing procedure (12 hours at 120 °C) only enhances the yield of reaction.

Influence of Overheating to Conductivity of Materials

The influence overheating the sample on the materials conductivity was tested with PEO-HPC blends of the $LiCF_3SO_3$. The experiment involves heating of each sample to 210 °C end subsequently investigating the conductivity in a wide temperature range from –50 to 210 °C. As presented in Figure 50 the change in polymer structure strongly influence the conducting character of the blends.

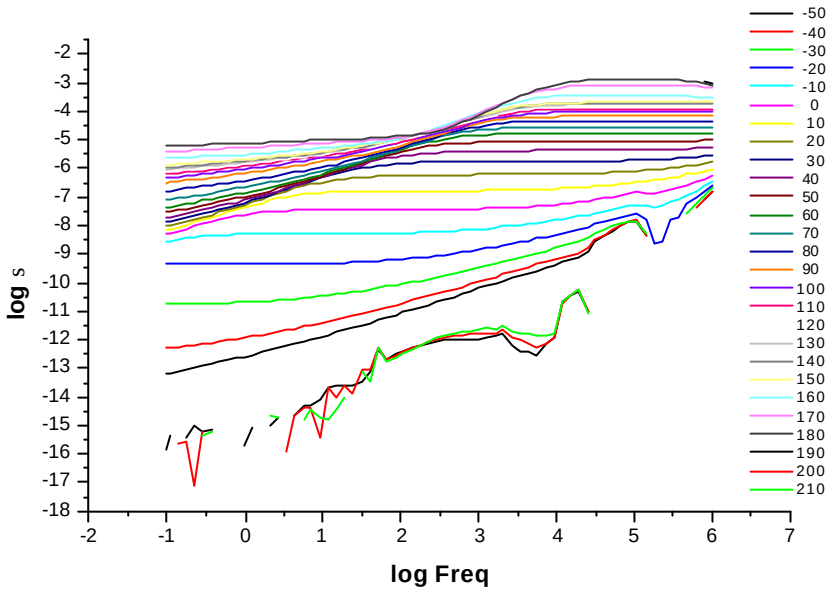

Figure 50. Influence of repeated heating of he samples to 210 °C on the conductivity of PEO-HPC blends of the $LiCF_3SO_3$ [Li]/[O]=0,021

The kinetics of the irreversible change are relatively fast. The conductivity in the heating cycle is stepwise increased up to 180 °C however above 180 °C it is than fading away to a level which can be defined as non-conducting. Since the heating/cooling of the sample to the next programmed temperature and its stabilization takes less than 12 minutes, the decomposition reaction must take place almost during the same period of time. Although the loss of the conducting character when overheated undoubtedly is a disadvantage of our material, in every day battery applications it is not important as long as it happens at temperatures higher than 180 °C.

4.3.3 Impedance Spectroscopy with non-Blocking Electrodes

Impedance spectroscopy with non-blocking electrodes enables the investigation of the ionic nature of the conductivity and the relative contributions of the different charge carrier (cation vs anion). The transport number of ions is a most significant property when considering the new material as a candidate for an application as electrolyte in batteries. The IUPAC Compendium of Chemical Terminology [10] defined the transport number *t* of ions B, as the current density due to ions B divided by the sum of current densities of all the ions in the electrolyte. ISO recommends the name current fraction of ions B.

The higher the ionic conductivity for an electrolyte, the lower the resistive polarization during discharge of a lithium cell utilizing the electrolyte. On the other hand, a transport number less than 1 for Li^+ implies the migration of the anions to the lithium electrode during cell discharge until a steady-state discharge current is reached. This results in the accumulation of lithium salt at the lithium electrolyte interface and possible interfacial polarization of the Li-electrode [53]. Thus, knowledge of the electrolyte conductivity itself does not give a sufficient picture for the resistance of the electrolyte when used in a battery. The higher both, the ionic conductivity and the transport number of an electrolyte, the lower the resistive polarization during discharge of the cell [157].

The use of active electrodes implies the presence of finite and reversible electrode reactions for participating ions [63]. In consequence, the double layer capacitance is decreased by the reversible lithium ion transfer at the electrode / electrolyte interface.

A general theory of the impedance of a cell consisting of parallel non-blocking electrodes and an electrolyte with two mobile ions has been given by MacDonald [158][159]. According to those and the following interpretations [63][54][160][161][157][162] the equivalent circuit for binary electrolytes with cation non-blocking electrodes has been constructed as series of:

- bulk resistance R_b and bulk capacitance C_b as parallel combination
- electrode resistance R_e and electrode capacitance C_e as parallel combination
- diffusional impedance Z_d (Figure 51).

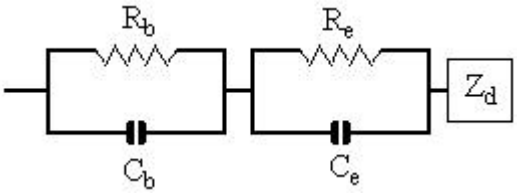

Figure 51. Schematic representation of an equivalent circuit for an electrolyte cell with non-blocking electrodes.

The diffusional impedance Z_d is attributed to the diffusion arising from the presence of concentration gradients within the electrolyte. Based on the equivalent circuit the predicted complex impedance plane is a composition of three semicircles (Figure 52).

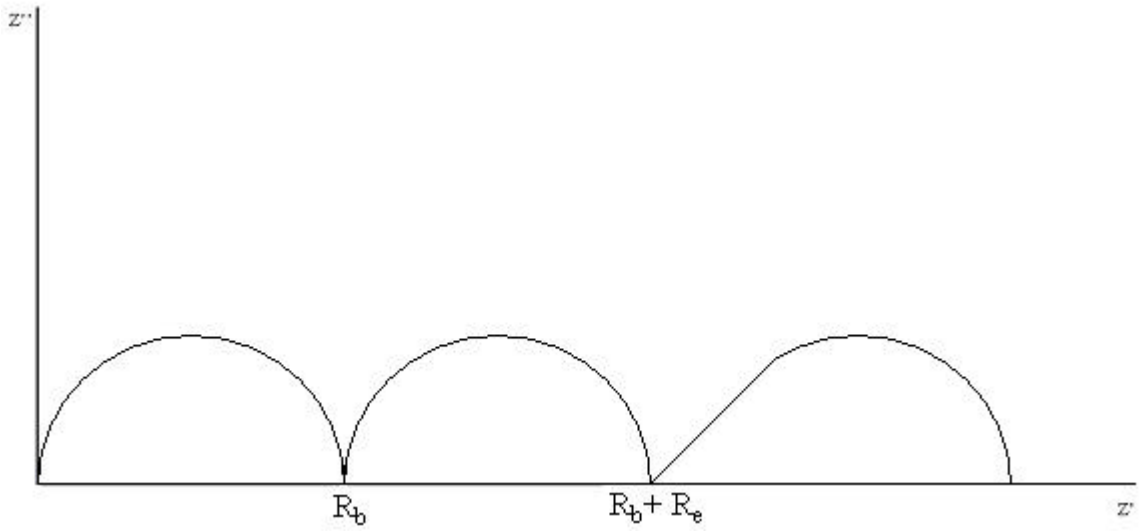

Figure 52. Complex impedance plot for the equivalent circuit of a cell with non-blocking electrodes.

In order to investigate our blend system the alternating current and direct current response of the polymer/salt blends sandwiched between metallic lithium electrodes which are non-blocking towards lithium ions, has been recorded. The impedance spectroscopy measurements were performed with one of the best investigated salts, namely $LiN(SO_2CF_3)_2$ blended with PEO-HPC at salt concentration [Li]/[O]=0,1009. The material was crosslinked with diisocyanate crosslinker in the ratio [OH]/[NCO]=2:3. The polymer electrolyte layer thickness was 0,068mm. The measurements were recorded in the extended frequency range from 10^{-2} to 10^{6} Hz for selected temperatures as presented in Figure 53, 54 and 55 in form of the complex impedance plot.

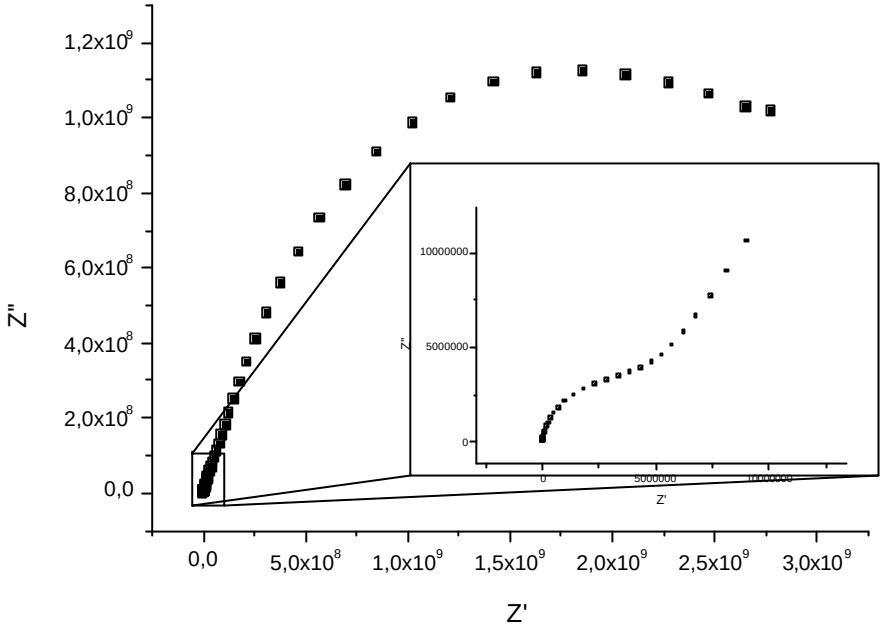

Figure 53. Complex impedance plot for PEO-HPC / $LiN(SO_2CF_3)_2$ / diisocyanate crosslinker [Li]/[O]= 0,1009 ; [OH]/[NCO]=2:3 at 30°C with Li-electrods.

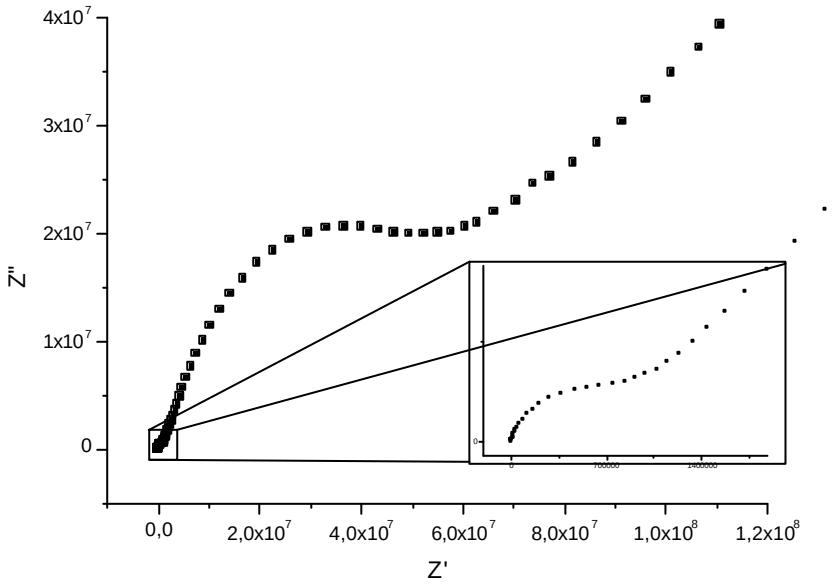

Figure 54. Complex impedance plot for PEO-HPC / $LiN(SO_2CF_3)_2$ / diisocyanate crosslinker [Li]/[O]= 0,1009 ; [OH]/[NCO]=2:3 at 60°C with Li-electrods.

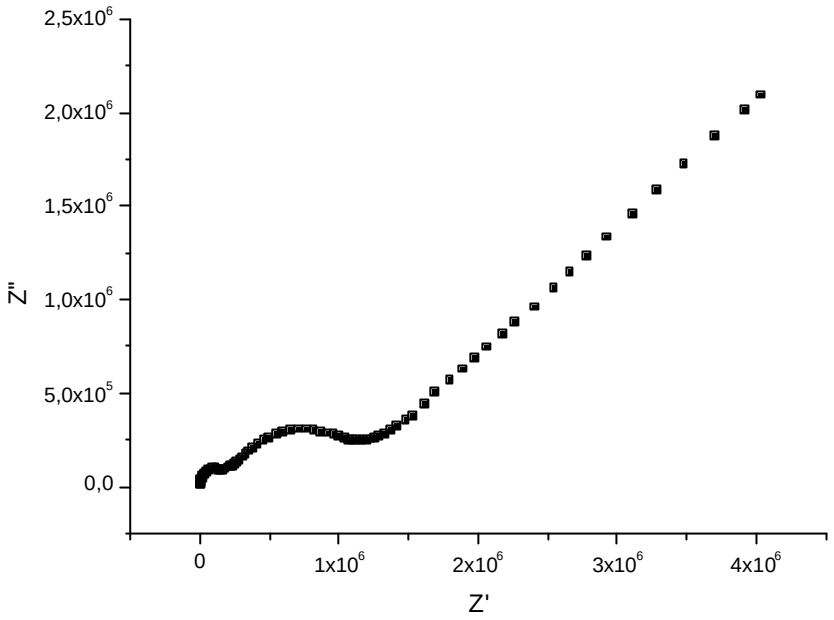

Figure 55. Complex impedance plot for PEO-HPC / $LiN(SO_2CF_3)_2$ / diisocyanate crosslinker ; [Li]/[O]= 0,1009 ; [OH]/[NCO]=2:3 ; at 100°C with Li-electrods.

The first, smallest arc which is present at all temperatures is the electrolyte material response. Similar arcs but followed by a spike were observed when blocking platinum electrodes were employed. When the Li/Li^+ reversible electrodes are used, the spike is missing and a second arc appears, which can be described as a parallel pair of resistance and double layer capacitance at the reversible electrode / electrolyte interface. The arc width represents the resistance of the ion reaction at the electrodes.

The third part of the material AC response appears only above 50 °C at low frequencies. It is attributed to the diffusion arising from the presence of a concentration gradient within the electrolyte. At very low frequencies and sufficiently enough high temperatures, the amount of charge transferred in the electrode reactions during a half cycle is sufficient to produce concentration gradients in the electrolyte. In the impedance plots this is reflected as the line having a slope of 1. Theoretically, at still lower frequencies, concentration waves and quasi steady state profiles may develop causing the cell impedance to return to the real axis. This process depends on the electrolyte thickness.

A slope of 1 in the Z'' / Z' plot determined for PEO-HPC / $LiN(SO_2CF_3)_2$ / diisocyanate crosslinker with non-blocking electrodes is the prove that the polymer electrolyte under investigation is a binary SPE, it means both cations and anions participate in charge transfer.

Secondly, the transport number of the Li ion is less than 1.This implies migration of the anion to the Li electrode or the migration of ion clusters. This may lead to the accumulation of lithium salt at the lithium electrolyte interface and possibly to an interfacial polarization of the Li-electrode. The ion transport number determinations was not possible in the whole temperature and frequency range. The determination of the ion transport numbers was realized with the potentiostatic polarization technique.

4.4 The Potentiostatic Polarization Method

In the potentiostatic polarization experiment, a constant potential of 500 mV is applied to a cell with the electrolyte sandwiched between cation-reversible electrodes and the resulting current was monitored as a function of time until a steady state current is obtained. Complete cell polarization occurs when the anion diffusion exactly opposes the migration of this ion under the influence of the applied potential. The ratio of final current, due to the cation only, to the initial current, due to the cation and anion, yields the cation transport number. In Figure 56 the current vs. time polarization curve is presented exhibiting a smooth, gradual decay until the cell is polarized, after which a constant current is observed.

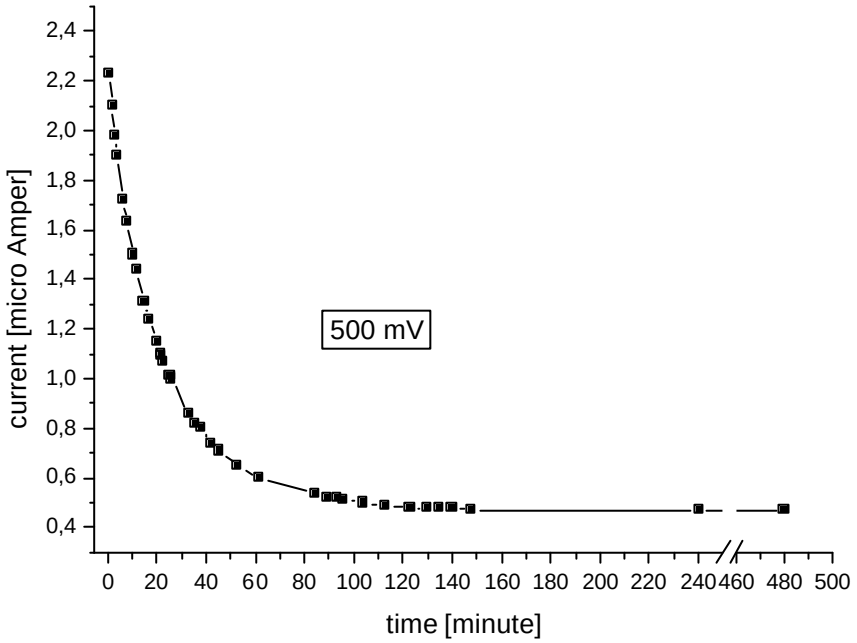

Figure 56. The potentiostatic polarization current vs. time curve for PEO-HPC / $LiN(SO_2CF_3)_2$ / diisocyanate crosslinker ; [Li]/[O]= 0,1009 ; [OH]/[NCO]=2:3

The cation transport number is affected by the cation and anion employed but appears to be concentration independent [53][54]. The lithium ion transport number for blend of PEO-HPC with $LiN(SO_2CF_3)_2$ with a salt concentration of [Li]/[O] = 0,1009 and crosslinked with diisocyanate crosslinker was found to be t_+=0,22. This value is somewhat lower than the transport numbers of others solid polymer electrolyte systems reported in the literature [53][54][160][161][157], which range from 0,23 (polyethylene oxide / lithium perchlorate [160]) to 0,44 (poly(bis((methoxyethoxy)ethoxy)phosphazene / lithium perchlorate [53]). The

reason for the low transport number of our system is not yet clear. However, the transport numbers depend to a considerable extent on the method of determination and thus are not likely to be comparable in all cases. Moreover, the transport number reported here does not strictly represent the transport number for the lithium ion. Since the mobile cations in polymer electrolytes may be triple and/or quadruple ions, it is more accurately described as the DC conductivity which transports lithium ions from the negative to the positive electrode [53].

5. Battery Experiment

Based on the battery construction recipe described in the chapter 1.2 “Batteries”, a simple lithium ion cell was prepared. Since the polymer electrolyte is the key material in the research of this work, for the construction of the cell two easily available electrodes were used, which do not necessarily provide the best overall performance. The experiments simply aims at a proof of applicability of the developed lithium ion solid polymer electrolyte. The battery involves exclusively all-solid, solvent-free parts. Metallic lithium is used as reversible anode – the source of lithium ions during discharge. The corresponding Li - ion sink (cathode) was prepared separately as a mixture of 60% $LiCoO_2$, 20% carbon black and 20% PEO-HPC / $LiN(SO_2CF_3)_2$ [Li]/[O]= 0,1009 with DS=2,8. The cathode material was cast on to aluminum foil as current collector as uniformly as possible and was carefully dried.

The anode and cathode were separated by a thin-film of PEO-HPC with DS=2,8 with $LiN(SO_2CF_3)_2$ with a ratio of [Li]/[O] = 0,1009 and diisocyanate crosslinker [OH]/[NCO]=2:3. All components were dissolved in THF and cast onto a Teflon plate and dried to form a film. The film was cured in vacuum at 120 °C over 12h. Finally the film was carefully dried in a high vacuum system and separated from the Teflon.

The battery cell was constructed with a pre-prepared cathode on the aluminum foil, PEO-HPC / $LiN(SO_2CF_3)_2$ / diisocyanate crosslinker [Li]/[O]= 0,1009 ; [OH]/[NCO]=2:3 polymer electrolyte and metallic lithium as anode. A Copper foil was used as current collector at the cathode side.

The parameters of the constructed cell were:

- copper foil thickness: 0,025mm
- lithium metal thickness: 0,75mm, squared piece with dimensions 45mm × 45mm
- PEO-HPC / $LiN(SO_2CF_3)_2$ / diisocyanate crosslinker [Li]/[O]= 0,1009 ; [OH]/[NCO]=2:3 polymer electrolyte thickness:
  0,07mm, piece covering the anode with redundancy
- $LiCoO_2$, carbon black and PEO-HPC cathode thickness:
  0,044mm, squared piece with dimensions 45mm × 45mm
- aluminum foil thickness: 0,015mm
- copper foil thickness: 0,025mm

The constructed cell reveals the voltage of about 3,2 V. After charging at a constant DC voltage the cell shows an open circuit voltage of 3,65 V. After discharge to 1,75 V the cell could be recharged up to 3,65 V, again, when a voltage was applied.
The charging and discharging was carried out in a controlled way with a voltage/time recorder. The discharge of the cell was realized with a resistance load of R=300 kΩ. The electric scheme for the discharging is presented in Figure 57.

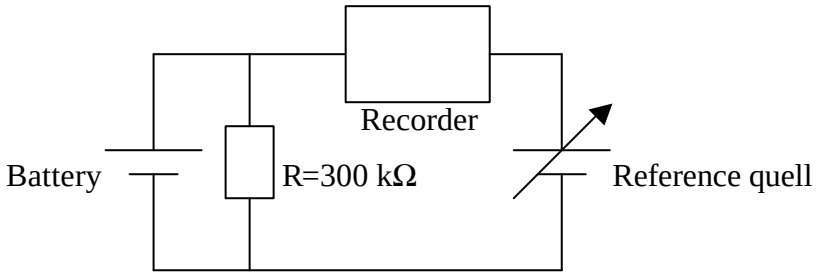

Figure 57. The electric scheme for discharging the Li - ion cell.

The charging process was done at a constant DC voltage. The external charging voltage was initially set to 4,5 V and after 4 hours increased to 5,6 V. The electric scheme contained the protective resistance R= 470 kΩ (Figure 58).

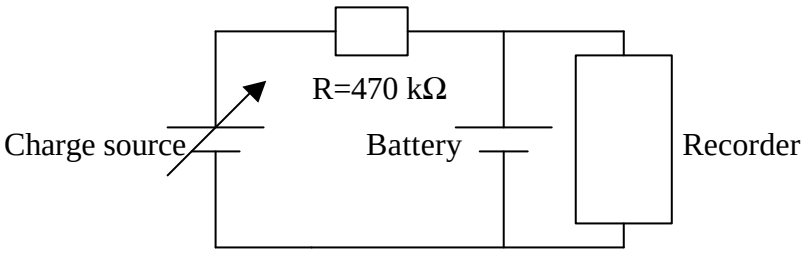

Figure 58. The electric scheme for charging the Li - ion cell..

The voltage - time curves of charging and discharging are presented in Figure 59.

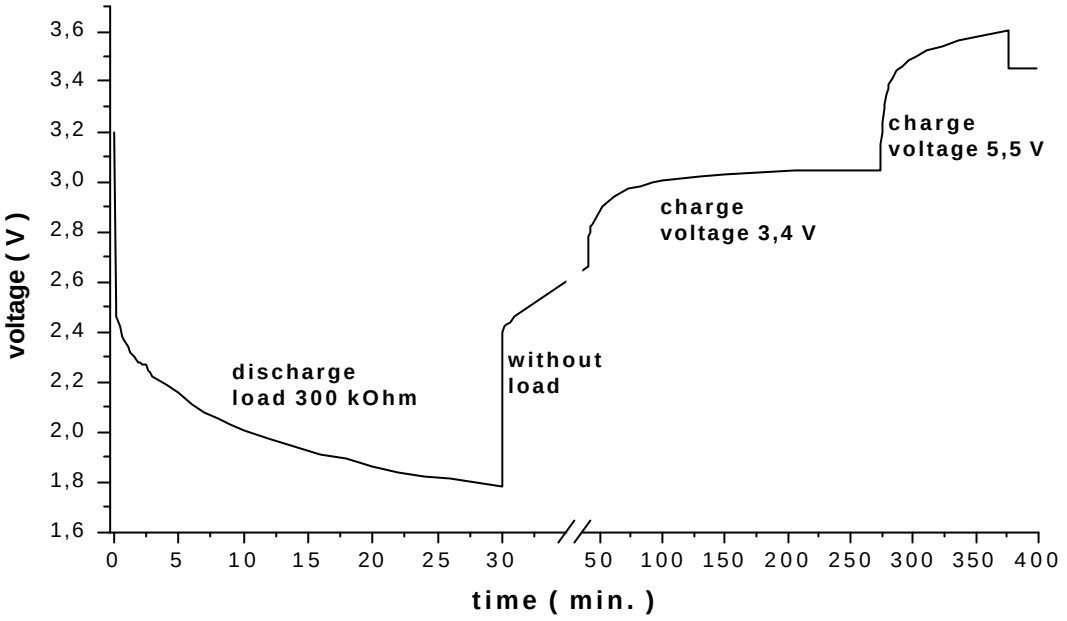

Figure 59. The charge and discharge curves of the Li – ion cell described in chapter 5 "Battery Experiment"

The investigated cell shows the typically properties of a secondary battery i.e. the cell is reversibly rechargeable. The maximum cell voltage of 3,65 V is similar to the commercial lithium ion battery voltage. The very low discharge current of 10 µA is probably caused by a large internal battery resistance. The internal resistance influences the energy density and overall capacity of the cell. Its characteristic can be improved by decreasing the polymer electrolyte thickness, by improvement of the cathode performance and lowering the surface roughness (mostly at the cathode) which would increase the inter layer contacts. The anode material performance could be ameliorated as well.

6. Conclusions

In the frame of this work a new generation of solid polymer electrolytes with a cellulose backbone and a soft side chain structure was investigated. The novel material is based on cheap substrates and its synthesis is not complicated aiming at low overall production costs.

The new materials are based on hydroxypropylcellulose and oligoethyleneoxide derivatives as starting materials. A new synthetic pathway for the derivatization of HPC with PEO side chains has been found and its parameters have been optimized. The PEO-HPC exhibit a well-defined chemical structure and a high side chain grafting density up to the maximum degree of substitution level of 3. The DS was evaluated by comparing the integrated intensity of the ^1H – NMR signal arising from the terminal methyl group of the side chains with that of the backbone hydrogens of the cellulose molecule. The absence of unsubtitued hydroxyl groups in fully substituted cellulose was confirmed with infrared spectroscopy.

The gel permeation chromatography (GPC) and dynamic light scattering (DLS) techniques were applied to specify the molecular mass distribution of the reaction products. Unfortunately, the non – availability of a correct calibration standard for the GPC and the presence of agglomerates in the polymer solutions preclude a proper molecular weight determination. The high polydispersity of the modified cellulose foreclose the use of matrix-assisted laser desorption/ionization-time of flight mass spectrometry (MALDI-TOF MS).

PEO - HPC was blended with $LiCF_3SO_3$, $LiN(SO_2CF_3)_2$ and $LiBF_4$. The molar ratios of salt to polymer were in the [Li]/[O] range from 0,02 to 0,2. The polymer – salt blends have been characterized with thermal gravimetric analysis (TGA), differential scanning calorimetry (DSC) and impedance spectroscopy. The effect of salt concentration on the thermal behaviour has been characterized. The PEO - HPC derivatives are highly viscous liquids at room temperature with glass transition temperatures above 208 K. The T_g of the polymer – salt blends increase linearly with the salt content. The presence of Li - salts decrease the thermal stability of the blends to about 70 – 100 K lower in comparison to pure PEO - HPC.

Dynamic mechanical analysis (DMA) experiments evidenced the liquid like nature of the material before crossliking. In order to improve the mechanical properties the materials were crosslinked. Two different conceptions have been engaged based on either urethane chemistry or photosensitive dimethylmaleinimide derivatives. The mechanical measurements demonstrate the positive changes in materials characteristics and contemporary DSC measurements demonstrate only a slight increase of the glass transition temperatures of the PEO side chains after crosslinking reaction.

The dielectric response of the investigated polymer - salt blends proves that the material exhibits only a conduction due to charged species but no other relaxations.
The best conductivity reaches 10^{-3} Scm^{-1} at 100°C for a $LiN(SO_2CF_3)_2$ salt blend with a [Li]/[O] ratio of 0,8. The conductivity of the polymer – salt complexes change with the content and type of the salt. The conductivity maximum is depending on the type of salt and ranges from 0,06 to 0,08 [Li]/[O]. Further salt concentration increase gives no conductivity improvement. The conductivity of the individual blends have been found to be almost identical before and after crosslinking.

The transport number for Li^+ has been investigated with the potentiostatic polarization technique and was found to be 0,22.
The applicability of our PEO - HPC material for lithium ion batteries was proved with the construction of a single cell battery which was rechargeable. A freshly constructed cell reveals a voltage of about 3,2 V and can be recharged with a constant DC voltage up to the open circuit voltage of 3,65 V.

7. Experimental

7.1 Instrumentation and Procedures

NMR Nuclear Magnetic Resonance experiments have been performed on a Bruker 250 MHz spectrometer or Bruker AC 300 FT- spectrometer at ambient temperature. For measurements at elevated temperatures the Bruker AMX 500 has been used. Solvent peaks have been used as internal standards.

FTIR Fourier Transform Infrared Spectroscopy measurements have been recorded with a Perkin Elmer Paragon 1000 spectrophotometer. The spectra have been recorded by depositing the sample as a thin film on KBr tablets.

UV Spectra have been taken from thin films using Perkin Elmer Lambda spectrophotometer. Blanc substrates have been used as reference (background).

TGA Thermo Gravimetric Analysis; Thermal stabilities of polymers and its blends have been investigated using a TGA Mettler Toledo TG 50 thermobalance. All measurements have been carried out with standardized conditions with a heating rate of 10 °C/min. from 30 °C up to 600 °C under N_2.

DSC Differential Scanning Calorimetry results have been obtained from a Mettler Toledo DSC-3000. DSC experiments have always been prefaced by a TGA analysis. The samples in amount of about 10 mg closed in aluminum pans were loaded to the measurement cell together; the same kind of empty aluminum pans were used as reference. The samples were firstly cooled in the apparatus from room temperature to the starting temperature, which for all samples, was –100 °C, next scanned 3 to 5 times with a scan rate of 10 °C/min. For the evaluation the second or subsequent heating curves were taken.

Impedance Spectroscopy measurements of all lithium salt blends of PEO-HPC have been carried on a Novocontrol dielectric spectrometer equipped with a cryostat system in the temperature range from –50 °C to 100 °C with a precision of ±0.01 °C. The sample was placed between two parallel platinum electrodes with a sample thickness of 0,1 mm and 5mm

diameter. The thickness was determined by Teflon stripes and the diameter was fitted by the size of the smaller platinum electrode. Thickness control was executed with a micrometer screw. To facilitate film formation from the polymeric blends the metallic substrates have been preheated up to ca. 80 °C. Measurements were carried out beginning from the minimum temperatures with steps of 10 K in the frequency range 10^{-1} – 10^{5} Hz.

The impedance measurements of the crosslinked material were done in the same way. The samples were placed between two parallel platinum electrodes and first measured, than heated for 12 hours in 100 °C (in order to activate the crosslink reaction), cooled to –50 °C and finally tested again. The procedure allows to get the fully comparable data and enables to estimate the influence of the crosslinking reaction on the materials conductivity characteristic.

Dynamic Mechanical Thermal Analysis has been performed by the parallel plate rheometer RMS-800 with a cooling rate of 10 K/minute and a constant frequency $w = 10\frac{rad}{s}$. The samples were prepared in the form of cylindrical tablets with a diameter of 6 and height of 2 mm. The samples were hot pressed at the temperatures above their T_g in a special form prepared from Teflon. The probes of the crosslinked material were first preformed by the same procedure and subsequently crosslinked.

7.2 Chemicals

All chemicals and solvents were obtained from Fluka, Aldrich, Merck or Riedel de Haen. Materials in pro analysis quality were used without further purification or drying if not mentioned otherwise. THF was heated and distilled with Na and benzophenone in an Ar atmosphere aiming for trapping of peroxides and water. Highly hygroscopic lithium salts were stored in a dry box. Before use, the needed amount of salt was dried 48 hours in a high vacuum system at 100 °C in an oil bath. All procedures using lithium salts were carried out in a dry box.

Chemical used:

2-Hydroxypropylcellulose (HPC), Aldrich MW=80.000; 100.000; 360.000; 1.000.000

M $_{C_{18}H_{34}O_9}$ = 394; MS=4.0; DS=3.0

Tri(ethylene glycol) monoethyl ether, Aldrich 95%, M $C_8H_{18}O_4$ = 178,23 g/mol; CAS: 112-50-5

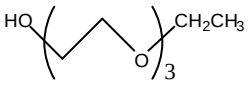

Tri(ethylene glycol), Fluka 99%, $C_6H_{14}O_4$ = 150,17 g/mol ;CAS: 112-27-6

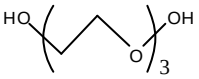

p-Toluenesulfonyl chloride, Aldrich 98%, $C_7H_7SO_2Cl$ = 190.65 g/mol; CAS: 98-59-9

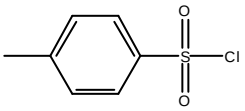

Potassium tert-butoxide, Fluka ≥97%, C_4H_9KO = 112,22 g/mol; CAS: 865-47-4

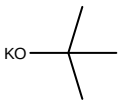

2,4-Toluene-di-isocyanate, Riedel de Haen 95%, $C_9H_6N_2O_2$ = 174,16 g/mol; CAS: 584-84-9

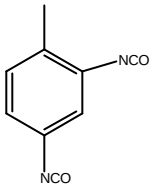

2,3-Dimethylmaleic anhydride, Aldrich 98%, $C_6H_6O_3$ = 126.11 g/mol; CAS: 766-39-23

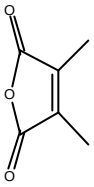

3-Aminopropyl bromide hydrobromide, Fluka ≥98%, $C_3H_8BrN.HBr$ = 218,92 g/mol; CAS: 5003-71-4

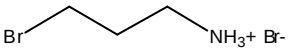

2-(2-Aminoethoxy)-ethanol, Aldrich 98%, $C_4H_{11}NO_2$ = 105.14 g/mol; CAS: 929-06-6

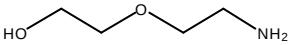

1,4-Diazabicyclo [2.2.2] octan (DABCO), Fluka 97%, $C_6H_{12}N_2$ = 112,18 g/mol

Phosphorus tribromide, Aldrich 99%, PBr3 = 270,70 g/mol; CAS: 7789-60-8

Lithium trifluoromethanesulfonate, $LiCF_3SO_3$

Lithium bis(trifluorosulfone) imide, $LiN(SO_2CF_3)_2$

Lithium tetrafluoroborate, $LiBF_4$

7.3 Synthesis and Purifications

α-(p-Toluolsulfonyl)-ω-ethoxy-tris(oxyethylen)

100 g (0,561 mol) tri(ethyleneglycol)monoethyl ether was added to 200 ml THF in a three necked, one litre flask equipped with a thermometer, mechanical stirrer and dropper. A solution of 33,6 g (0,840 mol) NaOH in 100 ml distilled water was prepared separately and added to the bulb. The reaction mixture was cooled down with a salted ice bath to 0 °C and stirred for about 30 minutes. 108 g (0,566 mol) toluene-4-sulfonyl chloride was shared in to approximately three portions. One was dissolved in 100 ml THF and two left in other 100 ml THF. The solutions were added dropwise to the reaction bulb such that the temperature did not increase higher than 7° C. The reaction mixture was stirred overnight. To work up, diethyl ether was added to the mixture and phases were separated in to an organic phase and water. The same procedure was done with the water phase at least two more times. The organic phases were combined and extracted with a saturated NaCl solution three times. The organic phase was dried with Na_2SO_4. Solvents were evaporated and the product isolated and checked by NMR spectroscopy.

α-Bromo-ω-ethoxy-tris(oxyethylen)

38 g (0,14 mol) of phosphorus tribromide and 50 ml of distilled dichloromethane were placed in a three-necked flask, equipped with a dropper, stirrer, and thermometer. The reaction mixture was cooled to –5 °C. To the cold, rapidly stirred solution 25 g (0,14 mol) of tri(ethyleneglycol)monoethyl ether was dropped over a period of 2 hours. The reaction mixture was stirred and cooled for additional 3 h. To quench the PBr_3, water and methanol was added. Afterwards the stirrer was switched off and the mixture was left for phase separation. The ether solution was decanted and the solvent evaporated. The product was separated with column chromatography.

(ω-Ethoxy-tris(oxyethylen))-2-oxypropylcellulose from α-(p-Toluolsulfonyl)-ω-ethoxy-tris(oxyethylen)

2,01 g (0,006 mol) 2-hydroxypropylcellulose (HPC) was dissolved in 200 ml of dried THF. 2,25 g (0,02 mol – 110% excess to each -OH group in the HPC) of potassium tert-butoxide was inserted to the HPC solution and all together were stirred over night at ambient temperature. The reaction mixture was cooled with a ice bath to 0 °C, and 5,45g (0,02 mol) of α-(p-toluolsulfonyl)-ω-ethoxy-tris(oxyethylen) was added dropwise. The mixture was cooled 8-10 h and stirring for another 3 days. To work up, the reaction mixture was centrifuged (15min.; 3800 rpm) and the precipitate separated. The solvent was evaporated (THF; 40 °C; 300) and the remnant dissolved in distilled water. If needed, the water phase must be separated from unreacted side chain reagent (organic phase). A water solution was prepared from the product and purified with dialysis. To do so, a dialysis membrane Spectra Por with diameter 29 mm and a molecular weight cut off (MWCO) 1.000 was used. In order to obtain a highly pure end product and to minimize process time, a concentration gradient was kept on the maximum possible level. Demineralized water was used and changed twice a day. Because of difficulties with evaporation under vacuum the product was first freeze-dried and next dried in a high vacuum system at 80 °C in an oil bath.

(ω-Ethoxy-tris(oxyethylen))-2-oxypropylcellulose from α-bromo-ω-ethoxy-tris(oxyethylen)

2 g (0,006 mol) of 2-hydroxypropylcellulose (HPC) was dissolved in 200 ml of dried THF. 8,1 g (0,072 mol – 400% excess to each -OH group in the HPC) of potassium tert-butoxide was inserted to the HPC solution and all together were stirred for 30 minutes. The reaction mixture was cooled with a salted ice bath to 0 °C, and 18,6 g (0,072 mol) of α-bromo-ω-ethoxy-tris(oxyethylen) was added dropwise. The mixture was stirred for 3 days. The solvent was evaporated (THF; 40 °C; 300) from the solution. A water solution was prepared and purified with the dialysis process. To do so, the same procedure as above was used.

N-(3-propylbromide)- dimethylmaleimide

3-Aminopropyl bromide hydrobromide was dissolved in dichloromethane and extracted with an aqueous solution of NaOH. The organic phase was washed 2 times with water. The organic phase was dried with Na_2SO_4, filtrated and the solvent was evaporated. 2 g (0,014 mol) of 3-aminopropylbromide and an equimolar amount of 2,3-dimethylmaleic anhydride (1,83 g) were dissolved in 100 ml freshly distilled o-xylene. The stirred mixture was heated to 180 °C in a Dean-Stark apparatus under reflux for a minimum of 8 hours. The conversion was followed with thin layer chromatography. The product and dimethylmaleic anhydride are visible in UV light. After reaction (no more dimethylmaleic anhydride peak visible) o-xylene was distilled off.

N-(2-Ethoxyethanol)- dimethylmaleimide

2 g (0,019 mol) of 2-(2-aminoethoxy)-ethanol and an equimolar amount of 2,3-dimethylmaleic anhydride (2,4 g) were dissolved in 100 ml freshly distilled o-xylene. The stirred mixture was heated to 180 °C in a Dean-Stark apparatus under reflux for a minimum of 8 hours. The conversion can be followed with thin layer chromatography. Product and dimethylmaleic anhydride are visible in UV light. After reaction (no more dimethylmaleic anhydride peak visible) o-xylene was distilled off.

N-(2-Ethoxy-ω-bromoethan)- dimethylmaleimide

3,8 g (0,014 mol) of phosphorus tribromide and 10 ml of dry diethyl-ether were placed in a three-necked flask, equipped with an dropping funnel, stirrer, reflux condenser and cooled to –5 °C. To the cold, rapidly stirred solution 3 g (0,014 mol) of N-(2-ethoxyethanol)-dimethylmaleimide in 5 ml of dry diethyl-ether were added slowly over a period of 30 minutes. The reaction mixture was stirred additionally for two hours in the cold. To quench the PBr_3 a few minutes before the end, a water/methanol mixture was added. Afterwards the stirrer was switched off and the mixture was left for sedimentation in a salted ice bath. The ether solution was decanted and the solvent evaporated. The product was separated with column chromatography.

Diisocyanate crosslinking agent

All chemicals needed in this synthesis were dried before use and handled under constant argon flow. To the round bottom flask equipped with a stopcock and stirrer 1,5 g (1,3 ml; 0,0088 mol) of 2,4-toluene isocyanate and 5 ml of THF with DABCO catalyst were added. To the rapidly stirred solution 0,667 g (0,593 ml; 0,0044 mol) of tri(ethyleneglycol) were dropped. The mixture was stirred additionally for 30 minutes and used directly.

PEO-HPC N-(di(oxyethylen)-dimethylmaleimidol) Derivatives preparation

For this synthesis (ω-ethoxy-tris(oxyethylen))-2-oxypropylcellulose had been prepared separatly. A decreased concentration of potassium-tert-butoxide and (α-(p-toluolsulfonyl)-ω-ethoxy-tris(oxyethylen)) was effective to achieve PEO - HPC with a degree of substitution of about 2,8 (PEO - HPC-2,8).
1g of PEO - HPC-2,8 were dissolved in a flask equipped with a stirrer. To the solution 0,09 g of KOH and 0,19 g of KJ was added and stirred ~15 minutes. 0,34 g of N-(2-ethoxy-ω-bromoethan)- dimethylmaleimide was added and the reaction mixture was stirred over night. The solvent was evaporated and the residue dissolved in water. After work up and phase separation, the water phase was transferred into the dialysis membrane (Spectra Por with diameter 29 mm and molecular weight cut off (MWCO) 1.000). After purification, the water solution was freeze-dried and later dried with high vacuum system in an oil bath at 80 °C.

PEO-graft-oxypropylcellulose N-(propyl)- dimethylmaleimide derivatives preparation

The preparation was identical to the synthesis with N-(2-ethoxy-ω-bromoethan)-dimethylmaleimide. As reagent N-(3-propylbromide)- dimethylmaleimide was used.

Blends of Lithium Salts and PEO-HPC Preparation.

The dried polymer material and the appropriate salts were weighted carefully in a dry box and brought together to the round bottom flask equipped with a stopcock. Under constant argon flow freshly dried THF was added. Polymer and salt was dissolved and stirred for a few hours. Finally the solvent was carefully evaporated in vacuum and the remainder dried in high vacuum at 80 °C in an oil bath for about 48 hours.

Crosslinking

Crosslinking with diisocyanate crosslink agent

Carefully dried and weighted portions of the blends of lithium salt and PEO-HPC DS=2,8 were dissolved in freshly dried THF under argon atmosphere. The calculated amounts of freshly prepared diisocyanate crosslink agent were added with an Eppendorf pipette and the mixture stirred for a while. The films were cast from solution or the solvent was evaporated. Ductile materials were used to form tablets. The tablets with diameter of 6 mm and thickness 2 mm were prepared for dynamic mechanical analysis. Samples were cured in vacuum for 12 hours at 120 °C in order to facilitate and accelerate the crosslinking reaction.

Crosslinking with dimethylmaleimide groups

Blends of lithium salts and the appropriate PEO-HPC derivatives were placed under a low pressure mercury lamp and irradiated with strong UV light. After 20 minutes no left over dimethylmaleimide groups were detected.

8. References

1. Buchmann I.; *Batteries in a Portable World*
2. Sequeira C.A.C., Hooper A.; *Solid State Batteries*; Martinus Nijhoff Publishers; Dordrecht 1985
3. Wakihara M., Yamamoto O.; *Lithium Ion Batteries – Fundamentals and Performance*; Wiley-VCH; Berlin 1998
4. Lauter U., Meyer W.H., Wegner G.; *Macromol.*1997, **30**, 2092
5. Scrosati B.; *Nature* 1995, **373**, 557
6. Tarascon J.M., Armand M.; *Nature* 2001, **414**, 359
7. Castellan G.W.; *Physical Chemistry* Addison-Wesley Publishing Company London 1983
8. Atkins, P. W.; *Physical Chemistry*; Freeman; New York 1998
9. Linden D.; *Handbook of Batteries and Fuel Cells*; Mc Graw Hill; New York 1984
10. *IUPAC Compendium of Chemical Terminology* 2nd Edition (1997)
11. Hammami A., Raymond N., Armand M.; *Nature*; 2003, **424**, 635
12. Frankfurter Allgemeine Zeitung; Frankfurt; 19/8/2003
13. Megahed S., Scrosati B.; *J. Power Sources* 1994, **51**, 79
14. Koksbang R., Barker J., Shi H., Saidi M.Y.; *Solid State Ionics* 1996, **84**, 1
15. Nishi Y., Azuma H., Omaru A.; U.S. Patent 4959281, 1990
16. Ingram M.; *Nature*; 1993, **362**, 112
17. Song J.Y., Wang Y.Y., Wan C.C.; *J. Power Sources*; 1999, **77**, 183
18. Armand M.; *Solid State Ionic*; 1994, **69**, 309
19. Hashmi S.A., Latham R.J., Linford R.G., Schlindwein W.S.; *J. Chem. Soc.Faraday Transactions*; 1997, **93**, 4177
20. Bruce P.G.; *Solid State Electrochemistry*; Cambridge University Press; Cambridge 1995
21. Hayashi A., Ishikawa Y., Hama S., Minami T., Tatsumisago M.; *Electrochem. Solid-State Lett.*; 2003, **6**, 3, A47
22. Hayashi A., Yoshizawa M., Angell C.A., Mizuno F., Minami T., Tatsumisago M.; *Electrochem. Solid-State Lett.*; 2003, **6,** 8, E19
23. Angell C.A., Liu C., Sanchez E.; *Nature*; 1993, **362**, 137
24. Bruce P.G., Vincent C.A.; *J. Chem. Soc.Faraday Transactions*; 1993, **89**, 3187
25. Fenton, D. E., Parker, J. M., Wright, P. V.; *Polymer*; 1973, **14**, 589
26. Wright, P. V.; *Br. Polym. J.*; 1975, **7**, 319
27. Armand, M., Chabagno, J. M., Duclot, M. J.; *Second International Conference on Solid Electrolytes*; St Andrews, UK, 20-22 Sept. 1978, Paper 6.5.
28. Cowie J.M.G.; *Polym. Int.*; 1998, **47**, 20
29. Wright P.V.; *Electrochim. Acta*; 1998, **43**, 1137
30. Murata K., Izuchi S., Yoshihisa Y.; *Electrochim. Acta*; 2000, **45**, 1501
31. Vanysek P.; *Handbook of Chemistry and Physics*; CRC Press, 74th edition, London 1994
32. Wegner G.; *Mol. Cryst. Liq. Cryst.*; 1993, **235**, 1
33. Wegner G.; *Thin Solid Films*; 1992, **216**, 105
34. Helmer-Metzmann F., Ballauff M., Schulz R.C., Wegner G.; *Macromol. Chem.*; 1989, **190**, 985

35. Kuo P.L., Liang W.J., Lin C.L.; *Macromol. Chem. Phys.*; 2002, **203**, 230
36. Ballard D.G.H., Cheshire P., Mann T.S., Przeworski J.E.; *Macromol.*; 1990, **23**, 1256
37. Gray F.M ., MacCallum J.R., Vincent C.A.; *Macromol.*; 1988, **21**, 392
38. Khan I.M., Yuan Y., Fish D., Wu E., Smid J.; *Macromol.*; 1988, **21**, 2684
39. Neugebauer D., Zhang Y., Pakula T., Sheiko S., Matyjaszewski K.; *Macromol.*; 2003, **36**, 6746
40. Neugebauer D., Zhang Y., Pakula T., Matyjaszewski K.; *Polymer*; 2003, **44**, 6863
41. Berthier C., Gorecki W., Minier M., Armand M.B., Chabagno J.M., Rigaud P.; *Solid State Ionic*; 1983, **11**, 91
42. Killis A., LeNest J.F., Chradame H.; *Makromol. Chem. Rapid Commun.*; 1980, **1,** 595
43. Watanabe M., Susuki S., Sanui K., Ogata N., Kaishi N.K.; *Macromol.*; 1984, 17, 2908
44. Armstrong R.D., Clarke M.D.; *Electrochim. Acta*; 1984, **29,** 442
45. Dupon R., Papke B.L., Rather M.A., Shriver D.F.; *J. Electrochem. Soc.*; 1884, **131,** 586
46. Roux Ch., Sanchez J-Y.; *Electrochim. Acta*; 1995, 40**,** 953
47. Watanabe M., Rikukawa M., Sanui K., Ogata N.; *Macromol.*; 1986, **19**, 188
48. Chiang C.K., Davis G.T., Harding C.A., Takahashi T.; *Macromol.*; 1985, **18**, 825
49. Blonsky P.M., Schriver D.F., Austin P., Allcock H.R.; *J. Am. Chem. Soc.*; 1984, **106**, 6854
50. Fish D., Kahn I.M., Smid J.; *Makromol. Chem. Rapid Commun.*; 1986, **7**, 115
51. Xia D.W., Soltz D., Staid J.; *Solid State Ionics*; 1984, **14**, 221
52. Lauter U., Meyer W.H., Enkelmann V., Wegner G.; *Macromol. Chem. Phys.*; 1998, **199**, 2129
53. Abraham K. M., Alamgir M.; *Chem. Mater.*; 1991**,3,** 339
54. Blonsky P.M., Shriver D.F; *Solid State Ionics*; 1986, **18&19**, 258
55. Allcock H.R., Prange R., Hartle T.J.; *Macromol*; 2001, **34**, 5463
56. Zoppi R.A., Fonseca C.M.N.P., DePaoli M.A., Nunes S.P.; *Solid State Ionics*; 1996, **91**, 123
57. Regiani A.M., Machado G.O., LeNest J-F., Gandini A., Pawlicka A.; *Macromol. Symp.*; 2001, **175**, 45
58. Yue Z., McEwen I.J., Cowie J.M.G.; *Solid State Ionic*; 2003,**156**, 155
59. Nishaburi A.; *Dissertation*; Mainz; 2000
60. Cowie J.M.G., Yue Z; *Polymer* 2002, **43**, 4453
61. Owen J.; *Ionic Conductivity*; in A. Geoffrey [Ed.] *Comprehensive polymer science*; Pergamon Press, Oxford 1989
62. McCrum N.G., Read B.E., Williams G.; *Anelastic and Dielectric Effects in Polymeric Solids*; Wiley&Sons Ltd., London 1967
63. MacCallum J.R., Vincent C.A.; *Polymer Electrolyte Reviews*; Elsevier Science Publishers LTD; Essex 1989
64. Vogel; *Phy.Z.*, 1921, **22**, 645, Tamman G., Hesse G., *Z. Anorg. Allgem. Chem.*; 1926, 245
65. Doolittle; *J. Appl. Phys.*; 1951, **22**, 1471
66. Cohen, D. Turnbull; *J. Chem. Phys.*; 1959, **31**, 1164
67. Ratner M.A., Nitzan A.; *Faraday Disscuss. Chem. Soc.*; 1992, **88**, 693
68. Angell; *Annu. Rev. Phys. Chem.*; 1992, 43, 693
69. M.Schuster; *Dissertation*; Mainz 2002
70. Bozkurt A. ; *Dissertation*; Mainz 1998
71. Williams M.L, Landel S.F., Ferry J.D.; *J. Am. Chem. Soc.*; 1955, **77**, 3701

72. Kennedy J.F., Philips G.O., Williams P.A.; *Cellulose – Structural and Functional Aspects*; Ellis Horwood Limited, Southampton 1989
73. Krässig H.A.; *Cellulose – Structure, Accessibility and Reactivity*; Gordon & Breach Science Publishers S.A.; Yverdon 1993
74. Rencurosi A., Röhrling J., Pauli J., Potthast A., Jäger C., Pérez S., Kosma P., Imberty A.; *Angew. Chem. Inter. Ed. Engl.*; 41, **22**, 4277
75. Kamide K., Saito M.; *Adv. Polym. Sci. - Biopolymers*; 1987, **83**; Springer-Verlag Berlin Heidelberg
76. Choon-Kong W.; *Dissertation*; Mainz; 2000
77. Meier F.; *Dissertation*; Mainz; 1999
78. Schnabelrauch M., Heinze T., Klemm D.; *Acta Polymerica*; 1990, **41**, 112
79. Klempner D., Frisch K.C.; *Polymer Alloys – Blends, Blocks, Grafts and Interpenetrating Networks*; Plenum Press; London 1977
80. Olabisi O., Robeson L.M., Shaw M.T.; *Polymer-Polymer Miscibility*; Academic Press INC.; London 1979
81. Croon I., Whistler R.L.; *Methode in Carbohydrate Chemistry*; Vol.III; Academic Press INC.; New York 1963
82. Isogai A., Ishizu A., Nakano J.; *J. Appl. Polym. Sci.*; 1984, **29**, 2097
83. Isogai A., Ishizu A., Nakano J.; *J. Appl. Polym. Sci.*; 1984, **29**, 3873
84. Stöhr T., Petzold K., Wolf B.A., Klemm D.O.; *Macromol. Chem. Phys.*; 1998, **199**, 1895
85. Klemm D., Heinze T., Philipp B.; *Acta Polymerica*; 1997, **48**, 277
86. Kondo T., Isogai A., Ishizu A., Nakano J.; *J. Appl. Polym. Sci.*; 1987, **34**, 55
87. Xiao Y., Ritcey A.M.; *Langmuir*; 2000; **16(9)**; 4252
88. LeNest J.F., Gandini A., Xu L., Schoenenberger C.; *Polym. Adv. Technol.*; 1993, **4**, 92
89. Schoenenberger C, Gandini A, LeNest J.F.; *Electrochim. Acta*; 1995, **40**, 2281
90. Schaub M., Fakirov C., Schmidt A., Lieser G., Wenz G., Wegner G., Albouy P.A., Wu H., Foster M.D., Majrkzak C., Satija A.; *Macromol.*; 1995, **28**, 1221
91. Basque P., de Gunzbourg A., Rondeau P., Ritcey A.M.; *Langmuir*; 1996, **12**, 5614
92. Duda G., Wegner G.; *Die Makromolekulare Chemie, Rapid Communications*; 1989, **9**, 495
93. Fischer P., Brooks C.F., Fuller G.G., Ritcey A.M., Xiao Y., Rahem T.; *Langmuir*; 2000, **16**, 726
94. Petrovic Z.S., MacKnight W.J., Koningsveld R., Dusek K.; *Macromol.*; 1987, **20**, 1088
95. Velazquez-Morales P., LeNest J-F., Gandini A.; *Electrochim. Acta*; 1998, **10-11**, 1275
96. Antonio J., O'Reilly T., Cavaille J.Y., Gandini A., *Cellulose*; 1997 – 1998, **4**, 305
97. Tambelli C.E., Donoso J.P., Regiani A.M., Pawlicka A., Gandini A., LeNest J-F.; *Electrochim. Acta*; 2001, **46**, 1665
98. Regiani A.M., Tambelli C.E., Pawlicka A., Curvelo A.S., Gandini A., LeNest J-F., Donoso J.P.; *Polym. Int.*; 2000, **49**, 960
99. Callens S., LeNest J.F., Gandini A., Armand M.; *Polym. Bull.*; 1991, **25**, 443
100. LeNest J.F., Callens S., Gandini A., Armand M.; *Electrochim. Acta*; 1992, **37**,1584
101. Schaub M.; *Dissertation*; Mainz; 1993
102. Seufert M.; *Dissertation*; Mainz; 1995
103. Sakellariou-Fragues R., Maurette M.T., Oliveros E., Riviere M., Lattes A., *Tetrahedron*; 1984, **40**, 2381

104. Gnanaguru K., Ramasubbu N., Venkatesan K., Ramamurthy V.; *J. Org. Chem.*; 1985, **50**, 2337
105. DeBoer C.D., Wwadsworth D.H., Perkins W.C.; *J. Am. Chem. Soc.*; 1973, **95**, 861
106. DeBoer C.D.; *J. Chem. Soc. Chemmical Communications*; 1972, 34, 377
107. Fishback T.L., Farona M.F., *Polym. Bull.*; 1994, **33**, 385
108. Endo T., Koizumi T., Tarata T., Chino K.; *J. Polym. Sci., Part A: Polym. Chem.*; 1995, **33**, 707
109. Fishback T.L., Farona M.F., *J. Polym. Sci., Part A: Polym. Chem.*; 1993, **31**, 2747
110. Deeken J.S., Farona M.F.; *Polym. Bull.*; 1992, **29**, 295
111. Canary S.A., Stevens M.P.; *J. Polym. Sci., Part A: Polym. Chem.*; 1992, **30**, 1755
112. Finter J., Widmer E., Zweifel H.; *Die Angewandte Makromolekulare Chemie*; 1984, **128**, 71
113. Moore J.A., Gamble D.R.; *Polym. Eng. Sci.*; 1992, **32**, 1642
114. Berger J.; *Polymer*; 1984, **25**, 1629
115. Tang W., Chang Y.,; Liu X.Y.; *Tetrahedron Lett.*; 1994, **35**, 6515
116. Rickert H.; *Angew. Chem.*; 1978, **90**, 38
117. Takahashi T.; *High Conductivity Solid Ionic Conductors*; World Scientific Publishinh; London 1989
118. Laskar A.L., Chandra S.; *Superionic Solid and Electrolytes*; Academic Press INC.; London 1989
119. Vincent C.A.; *Prog. Solid State Chem*; 1987, **17**, 145
120. Chung S.H., Jeffrey K.R., Stevens J.R.; *J. Chem. Phys.*; 1991, **94**, 1803
121. Panero S., Scrosati B., Greenbaum S.G.; *Electrochim. Acta*; 1992, **37**, 1533
122. Donoso J.P., Bonagamba T.J., Panepucci H.C., Oliveira L.N., Gorecki W., Berthier C., Armand M.; *J. Chem. Phys.*; 1993, **98**, 10026
123. Gorecki W., Jeanin M., Belorizky E., Roux C., Armand M.; *J. Phys.: Condens. Mater.*; 1995, **7**, 6823
124. Gorecki W., Andreani R., Berthier C., Armand M., Mali M., Roos J., Brinckmann D.; *Solid State Ionics*; 1986, **18–19**, 295
125. Johansson A., Tegenfeldt J.. *J. Chem. Phys.*; 1996, **104**, 5317
126. Geller S.; *Topics in Applied Physics: Solid Electrolytes*; Spriger-Verlag; Berlin 1977
127. Lee D-S., A.S. Perlin; *Carbohydr. Res.*; 1982, **106**, 1
128. Nagamoto T., Kakahati H., Ichikawa C., Omoto O.; *Jap. J. Appl. Phys.*; 1985, 24, 397
129. Nehls I., Wagenknecht W., Philipp B., Stscherbina D.; *Prog. Polym. Sci*.; 1994, **19**, 28
130. Myasoedova V.V.; *Physical Chemistry of Non-aqueous Solutions of Cellulose and Its Derivatives*; Wiley-VCH, Weinheim 2000
131. Bannister D.J., Davies G.R., Ward I.M., MacIntyre J.E.; *Polymer*; 1984, **25**, 1291
132. Fenton DE, Parker JM, Wright PV.; *Polymer*; 1973; **14**; 589
133. Armand M.B., Chabagno J.M., Duclot M.; *Second International Meeting on Solid Electrolytes*; St Andrews, Scotland, 1978
134. Armand M.B., Chabagno J.M., Duclot M. In: Vashisha P., Mundy J.N., Shenoy G.K., editors; *Fast IonTtransport in Solids*; New York: North Holland; 1979; 131
135. Zalewska A., Stygar J., Ciszewska E., Wiktorko M., Wieczorek W.; *J. Phys. Chem.*; 2001; **105** (25); 5847
136. Stygar J., Biernat A., Kwiatkowska A., Lewandowski P., Rusiecka A., Zalewska A., Wieczorek W.; *J. Phys. Chem.*; 2004; **108** (14); 4263
137. Cameron G.G., Ingram M.D., Sorrie G.A.; *J. Chem. Soc. Faraday Transactions 1*; 1987, **83**(11), 3345

138. Turi, E. A.; *Thermal Characterization of Polymeric Materials*; Academic Press; London 1997
139. http://composite.about.com
140. Craver C.D.; *Polymer Characterization*; American Chemical Society Washington 1983
141. Wunderlich, B.; *Thermal Analysis*; Academik Press Boston 1990
142. Mitchell J.; *Applied Polymer Analysis and Characterization*; Hanser Publishers Munich 1987
143. Mathot V.B.F.; *Thermochim. Acta – Thermal Analysis and Calorimetry in Polymer Physics*; Elsevier Science, Amsterdam 1994
144. Billmeyer F.W.; *Texrbook of Polymer Science*; John Wiley & Sons, Inc. New York 1984
145. Van Krevelen D.W.; *Propperties of Polymers*; Elsevier, Amsterdam 1990
146. Turturro A., Russo S., Antolini E., Cirafici S.; *Polymer*; **30** (1989) 1099
147. Williams G., Thomas D.K.; *Phenomenological and Molecular Theories of Dielectric and Electrical Relaxation of Materials*; Application Note Dielectric 3 – Novocontrol Technologies Company
148. Schönhals A.: *Dielectric Spectroscopy on the Dynamics of Amorphous Polymeric Systems*; Application Note Dielectric 1 - Novocontrol Technologies Company
149. Kremer F., Schönhals A.; *Broadband Dielectric Spectroscopy*; Springer, Berlin 2003
150. Runt J.P., Fitzgerald J.J.; *Dielectric Spectroscopy of Polymeric Materials*; Am.Chem. Soc., Washington 1997
151. Gray F.M.; *Polymer Electrolytes*; The Royal Society of Chemistry, Cambrige 1997
152. Sekhon S.S.; *Bull. Mater. Sci.*; **26**, (2003) 321
153. Tsuchida E., Ohno H., Kobayashi N., Ishizaka H.; *Macromol.*; 1989, **22**, 1771
154. Kobayashi N., Uchiyama M., Tsuchida E.; *Solid State Ionics*; 1985, **17**, 307
155. Owen J.; *Ionic Conductivity* in *Comprehensive Polymer Science*; Vol.2, Pergamon Press; Oxford 1989
156. Blythe A.R; *Electrical Properties of Polymers*; Cambridge University Press, Cambridge 1979
157. Sorensen P.R., Jacobsen T.; *Electrochim. Acta*; 1982, **27**, 1671
158. MacDonald J.R.; *J. Chem. Phys.*; 1973, **58**(**11**), 4982
159. MacDonald J.R.; *J. Chem. Phys.*; 1974, **61**(**10**), 3977
160. Ferloni P., Chiodelli G., Magistris A., Sanesi M.; *Solid State Ionics*; 1986, **18&19**, 265
161. Hardy L.C., Shriver D.F.; *J. Am. Chem. Soc.*; 1985, **107**, 3823
162. Dolle M., Orsini F., Gozdz A.S., Trascon J-M.; *J. Electrochem. Soc.*; 2001, **148**, A851
163. Clancy S., Shriver D. F., Ochrymowycz L. A.; *Macromol.*; 1986, **19**, 606

9. Glossary